Stable isotope geochemistry of light rare earth elements: technical development and isotope fractionation in nature

（軽希土類元素の安定同位体地球化学：
分析技術の開発と天然における同位体分別の研究）

WAKAKI, Shigeyuki

（若木　重行）

A dissertation for the degree of Doctor of Science
Department of Earth and Environmental Sciences,
Graduate School of Environmental Studies, Nagoya University
（名古屋大学大学院環境学研究科地球環境科学専攻　博士（理学））

2008

Stable isotope geochemistry of light rare earth elements: technical development and isotope fractionation in nature

WAKAKI, Shigeyuki

Department of Earth and Environmental Sciences,
Graduate School of Environmental Studies, Nagoya University

軽希土類元素の安定同位体地球化学：
分析技術の開発と天然における同位体分別の研究

名古屋大学大学院環境学研究科地球環境科学専攻

若木　重行

主論文

Stable isotope geochemistry of light rare earth elements: technical development and isotope fractionation in nature

（軽希土類元素の安定同位体地球化学：
分析技術の開発と天然における同位体分別の研究）

若木　重行

Abstract

Abundance of isotopes of an element is not a universal constant in nature. Every element suffers from isotope fractionation during a chemical reaction. Both equilibrium and kinetic chemical reactions fractionate isotopes of an element in a mass-dependent manner. Theoretical investigation on fractionation behavior of isotopes in equilibrium chemical reaction showed that isotope fractionation factor of an isotope exchange reaction is proportional to the relative mass difference between the isotopes of interest, to the inverse of the square of the temperature, and to the difference in strength of chemical bonding between two chemical species involved in the reaction.

Mass-dependent fractionation induced variations of isotope composition in nature have been studied widely on "light" elements such as H, O, C, N and S. Large difference of relative mass between isotopes in these elements leads to large and easily measurable variations in their isotope compositions. No natural variations in isotope compositions of high-atomic-number elements are expected beyond analytical error because of the small relative mass differences between isotopes in these elements. However, resent advance in mass spectrometry have opened the door to high-precision stable isotope analysis of intermediate to high-atomic number elements. Stable isotopes of the newly introduced intermediate to high-atomic number elements are referred as "non-traditional" stable isotopes. Studies of the non-traditional stable isotopes have showed that mass-dependent fractionation induced variations of isotope compositions in nature are measurable in every elements investigated.

This study has focused on rare earth elements (REEs) as a target for new non-traditional stable isotope study. Rare earth elements are one of the most useful elements in geochemistry. Elemental fractionation pattern of REEs is widely used in geochemical studies to constrain the origin of geological materials. Moreover, abundance of the radiogenic nuclide ^{143}Nd, product of the long-lived Sm-Nd radioactive decay system, provides chronological constraints of the sample. Combining stable isotopes with these two existing methodology, multiple information regarding the age, the origin and the process may be obtained from a single element (or a single group of elements) to constrain the history of geological materials. The target element of this study is set to two light REEs, Nd and Sm, to find out whether variation in stable isotopes of these elements can be used to trace various geochemical reactions.

Two mass spectrometric techniques are developed in this study to make high precision stable isotope analysis of REEs possible by thermal ionization mass spectrometry

(TIMS). The first technique is total evaporation normalization (TEN) method developed for the analysis of very small amount of Nd samples. It is a combination of two existing techniques: total evaporation technique and internal normalization technique. Total evaporation technique is developed and used primarily in nuclear industry. Internal normalization technique is used for instrumental mass-bias correction in conventional geochemical Nd isotope ratio measurements. Combination of these two existing techniques allows precise radiogenic Nd isotope ratio measurements of sub-ng Nd samples. The external precision of the $^{143}Nd/^{144}Nd$ ratio for 0.5 ng Nd sample was 140 ppm. This precision is order of magnitude smaller than that obtained by the conventional measurements. The precision achieved by the TEN method for the measurement of sub-ng Nd sample is sufficient for the application of $^{143}Nd/^{144}Nd$ ratio as a geochemical tracer.

The second technique developed in this study is a combined double-spike TIMS technique for high-precision stable isotope analysis of two REEs, Nd and Sm. Instrumental mass bias is inevitable in mass spectrometric isotope ratio measurements. Expected stable isotopic variation of Nd and Sm in nature is about an order of magnitude smaller than the possible instrumental mass bias effect. Rigorous instrumental mass bias correction is thus essential for stable isotope analysis of these elements. Small expected variations in isotope composition also requires very high precision in the analysis. The double-spike TIMS technique is a method of choice to meet these requirements. Several refinements in the double spike TIMS technique were made to minimize the introduction of possible error during deconvolution. Adjustment of free-parameters such as isotope composition of the double spike and sample-spike mixing ratio is important in double-spike analysis, because the degree of error magnification during the deconvolution process is considerably affected by these parameters. These parameters are optimized for Nd and Sm analyses by means of error propagation simulation. Precision of the developed technique is estimated from the analysis of in-house reference materials. The long-term reproducibility of the $\varepsilon^{146}Nd$ and $\varepsilon^{148}Sm$ values of the in-house reference materials were ± 0.2 (2SD, n = 44) and ± 1.2 (2SD, n = 44), respectively. This precision is sufficient for the investigation of the possible stable isotope variations in nature. Accuracy of the developed technique is confirmed from the analysis of isotope fractionation behavior during cation exchange chromatography for both elements. In addition, eleven commercial Nd oxide reagents were analyzed for their stable Nd isotope composition. The $\varepsilon^{146}Nd$ value (reference to the in-house reference material JNdi-1) of the 11 reagents ranges from -2.5 to +0.3. No correlation was found between $\varepsilon^{146}Nd$ value and the purity of the reagents. Therefore, it is not clear whether the observed stable isotopic variation among these reagents

reflects the difference of the degree of isotope fractionation during production and purification processes of these reagents or the difference of the isotope composition of their source materials.

Various terrestrial materials were analyzed for Nd stable isotopes by the developed double-spike TIMS technique. The stable Nd isotope composition of 8 igneous rocks (including 3 basalts, 2 granites and 3 rhyolites) agreed within analytical error. The average ε^{146}Nd value of the igneous rocks was –0.2 ± 0.4 (2SD). The consistency of stable Nd isotopes in igneous rocks suggests uniform stable Nd isotope composition of the mantle material since the effect of isotope fractionation is negligibly small in high-temperature reactions. Thus, the average Nd isotope composition of igneous rocks is a good estimate of the Nd isotope composition of the bulk silicate earth (BSE).

Stable isotope composition of Nd in the modern seawater is estimated from the analysis of Mn nodule and coral. The ε^{146}Nd value of Mn nodule and coral were 0.2 ± 0.2 (2SD, n = 2) and -0.2 ± 0.2 (2SE), respectively. REEs in Mn nodule and coral are of seawater origin. The consistency of the ε^{146}Nd values in Mn nodule and coral implies that no isotope fractionation took place during the REE incorporation from seawater into these materials: if isotope fractionation occurs, the degree of the fractionation will be different among different chemical compounds. Therefore, stable Nd isotope composition of the modern seawater is directly represented by Mn nodule and coral.

The theory of equilibrium isotope fractionation predicts a large isotope fractionation in low-temperature reactions. Marine carbonate rocks are good example of the materials formed in low-temperature environments. Large variation in Nd isotope composition was found among marine carbonate rocks: ε^{146}Nd values of 15 marine carbonate rocks range from –0.1 to +2.6. Difference of the REE concentrations between carbonate rocks and organic calcite, precursor material of the carbonate rocks, suggests that REE was concentrated in carbonate rocks via inorganic chemical reaction between calcite and seawater during diagenesis. REE concentration in most of the carbonate rock samples is consistent with the concentration of the calcite equilibrated with modern seawater. The stable isotope composition of Nd in carbonate rocks probably reflects equilibrium or near equilibrium isotope fractionation between seawater and inorganic calcite.

Acknowledgments

I am very grateful to Prof. T. Tanaka for his suggestions and for his kind support throughout this work. I have greatly benefited from discussion with Prof. I. Kawabe. Dr. K. Yamamoto, Dr. K. Mimura, Dr. M. Minami, Dr. Y. Asahara, Dr. R. Senda, Ms. M. Asahara, Dr. M. Tsuboi, Dr. A. Goto, Dr. M. Takebe, Dr. K. Tanaka, S. Shibata, Dr. T. Hayashi and all members of the geochemistry cosmochemistry laboratory are thanked for their assistance during analytical work, for their helpful suggestions on this work and for fruitful discussions. My gratitude goes to Dr. T. Hirata and Dr. T. Ohno of Tokyo institute of technology, for fruitful discussions, for providing me with their unpublished data, for helpful comments on this work and especially for their continuous encouragement. I express my thanks to Dr. K. Suzuki, Dr. T. Ishikawa, Dr. M. Tanimizu, Dr. Y. Hirahara of JAMSTEC for their advice on mass spectrometry, for discussions which improved this work and for their warm encouragement. K. Irisawa of Tokyo institute of technology, C. Okamoto, T. Murakami are thanked for providing me with intellectual stimulations and also for their friendship. Samples of kuzuu carbonate rocks are provided by Dr. T. Okai of GSJ via Prof. Tanaka. Carbonate rock samples from Ibuki, Ishimaki and Kasuga and cherts from Barberton Greenstone belt are provided by Dr. Minami, K. Suzuki, Prof. M. Enami and Dr. T. Hayashi, respectively. This work was supported in part by Research Fellowships for Young Scientists from the Japan Society for the Promotion of Science (17-7817).

Contents

Chapter 1

Introduction ……..1

Chapter 2

Isotope ratio measurements of trace Nd by the total evaporation normalization method……6

Chapter 3

Refined double spike-TIMS technique for stable isotope analysis of Nd and Sm……..25

Chapter 4

Stable isotope fractionation of Nd in nature……..55

Chapter 1

Introduction

Abundance of isotopes of an element is not a universal constant in nature. Two types of reaction can potentially change the isotopic composition of elements. One of the reactions is nuclear reaction, a reaction between nuclei and/or nuclear particles. Most of the nuclear reaction produces a particular nuclide as a product. Therefore, the resulting changes in the isotopic composition are non-mass-dependent. One example of a nuclear reaction is radioactive decay, which is a basis of the vast field of radiogenic isotope studies in geochemistry [1]. The other type of the reaction that can change the isotopic composition of elements is chemical reaction. Both equilibrium and kinetic chemical reactions fractionate isotopes of an element in a mass-dependent manner. Investigation on fractionation behavior of isotopes in equilibrium chemical reaction by Bigeleisen and Mayer [2] and Urey [3] theoretically showed that isotope fractionation factor of a reaction is proportional to the relative mass difference between the isotopes of interest, to the inverse of the square of the temperature, and to the difference in strength of chemical bonding between two chemical species involved in the reaction. Kinetic isotope fractionation arises from the difference in reaction rates between isotopes with distinct masses.

Mass-dependent fractionation induced variations of isotope composition in nature have been studied widely on "light" elements such as H, O, C, N and S [4]. Relative mass difference between isotopes is large in low-atomic-number elements leading to large and easily measurable variations in isotope compositions of these elements. In the case of high-atomic-number elements where the relative mass difference is small, early studies (e.g. [5]) have concluded that no measurable isotopic variation beyond analytical error exists for terrestrial materials. However, resent advance in mass spectrometry, particularly introduction of the multi-collector inductively coupled plasma mass spectrometry (MC-ICP-MS), opened the door to high-precision stable isotope analysis for almost all elements on the periodic table. MC-ICP-MS studies of the stable isotopes of intermediate to high-atomic number elements, so-called "non-traditional" stable isotopes, have revealed that mass-dependent fractionation induced variations of isotope ratios does exist in nature [6]. Non-traditional stable isotopes of biophile elements (e.g. Zn [7]) and redox-related elements (e.g. Fe [8]) have become an active field of research over the past eight years.

This study will focus on rare earth elements as a target for non-traditional stable isotope study. Rare earth elements (REEs) are one group of the most useful elements in geochemistry. They have similar chemical and physical properties while their ionic radius gradually changes with the increase of the atomic number causing a slight but systematic difference in their elemental

fractionation behavior during various geological processes. Relative difference in REE abundances, best illustrated by CI-chondrite normalized REE pattern, gives constraints about the origin of the sample. Rare earth elements also contain well-studied long-lived radioactive-decay system, ^{147}Sm-^{143}Nd system, from which age information can be obtained. Combining stable isotopes with these two existing methodology, multiple information regarding the age, the origin and process may be obtained from a single element (or a single group of elements) to constrain the history of geological materials. Pioneering work on stable isotopes of REEs was recently made by Ohno [9]. Ohno have studied stable isotopes of Nd and Ce by MC-ICP-MS, and found heavy isotope enrichment for both elements on one dolomite sample (GSJ reference rock JDo-1). Cerium is chosen in his study because it is sensitive to redox-condition changes: Ce can be both trivalent and tetravalent while most of the other REEs are trivalent. Large isotope fractionation is expected in redox reactions owing to the large difference in bonding powers between reactant and product species. However, Ohno [9] have found no evidence for redox-related isotope fractionation on Ce. The target element of this study is set to two light REEs, Nd and Sm, to find out whether variation in stable isotopes of these elements can be used to trace various geochemical reactions.

Developing a method for stable isotope analysis of REEs is an analytically challenging task. On of the existing problems in “stable” isotope ratio measurement is instrumental mass bias correction. Since mass spectrometry is the only choice for precise isotope analysis, all the mass spectrometric measurement suffers from large and variable instrumental mass bias. Rigorous correction of instrumental mass bias is essential, because the possible instrumental mass bias is order of magnitude larger than the expected stable isotopic variation in nature. The second problem is the sensitivity of the measurement. Abundance of REEs is quite high in evolved igneous rock, but is on the ppm order or less in other terrestrial rocks. Therefore, highly sensitive mass spectrometry is desired to cut down the sample amount required for the analysis to easily-handled level. The third problem is spectrometric interference during mass spectrometry. Many isobaric nuclides exist in the mass region of REEs. Oxides of REEs and Ba oxide are another source of isobaric interferences. Chemical purification can reduce the amount of unwanted elements, but perfect chemical purification is not possible. Isobaric interferences are serious in MC-ICP-MS measurements: high ionization efficiency of the Ar plasma ion source generates ions of all these nuclides and compounds. The conventional thermal ionization mass spectrometry (TIMS) has the advantage on this problem: the element of interest can be fractionated from unwanted elements according to the difference of the ionization potentials in the TIMS ion source. The TIMS method is also advantageous over MC-ICP-MS method on the sensitivity of the measurements of light REEs such

as Nd. Concerning these points, the method of choice for the analysis of Nd and Sm in this study is TIMS method rather than MC-ICP-MS.

Two mass spectrometric techniques are developed to overcome the first and the second problems and to make the high precision stable isotope analysis of REEs possible by TIMS. One of the techniques developed in this study is the total evaporation normalization (TEN) method. Precise radiogenic isotope ratio measurement of sub-nano-gram amounts of Nd was first made possible by TEN method. Lower limit of the amount of Nd required for precise isotope ratio measurement is reduced about an order of magnitude by introducing TEN method. Detailed description of the TEN method is given in chapter 2. Another technique developed in this study is a combined double-spike TIMS technique for high-precision stable isotope analysis of two REEs; Nd and Sm. The double-spike TIMS technique allows rigorous instrumental mass bias correction during isotope ratio measurement by TIMS method. Description of the double-spike TIMS method and the results of the stable isotope analysis of Nd and Sm is given in chapter 3.

The variation in Nd stable isotopic composition of terrestrial materials is studied by the double-spike TIMS technique (chapter 4). The theory of Bigeleisen and Mayer predicts a large isotope fractionation in low-temperature chemical reactions. Marine carbonate rocks are good example of the materials formed in low-temperature environments. Moreover, Ohno [9] have reported fractionated Nd isotopes on one dolomite sample. To confirm the result of the previous study and to investigate the possible mechanism causing isotope fractionation, stable isotope variations in marine carbonate rocks are studied in detail. In addition, the first estimation of the bulk earth Nd “stable” isotope composition is made in chapter 4. This dissertation represents the first detailed and systematic study of non-traditional stable isotopes of light REEs; Nd and Sm. The importance and the usefulness of non-traditional stable isotopes of REEs are clearly demonstrated by the course of studies described hereafter.

Reference

[1] A. P. Dickin, 1995, *Radiogenic Isotope Geology*, Cambridge University Press.

[2] J. Bigeleisen and M. G. Mayer, 1947, Calculation of equilibrium constants for isotopic exchange reactions. *J. Chem. Phys.* **15**, 261-267.

[3] H. C. Urey, 1947, The thermodynamic properties of isotopic substances. *J. Chem. Soc*. (London), 562-581.

[4] J. Hoefs, 1987, *Stable isotope geochemistry*, Springer-Verlag Berlin Heidelberg.

[5] O. Eugster, F. Tera amd G. J. Wasserburg, 1969, Isotopic analyses of barium in meteorites and in terrestrial samples. *J. Geophys Res*. **74**, 3897-3908.

[6] C. M. Johnson, B. L. Beard and F. Albarède, 2004, Overview and general concepts, *Rev. Mineral Geochem*. **55**, 1-24.

[7] C. N. Maréchal, P. Télouk and F. Albarède, 1999, Precise analysis of copper and zinc isotopic compositions by plasma-source mass spectrometry. *Chem. Geol.* **156**, 251-273.

[8] B. L. Beard and C. M. Johnson, 1999, High-precision iron isotope measurements of terrestrial and lunar materials. *Geochim. CosmoCim. Acta* **63**, 1653-1660.

[9] T. Ohno, 2006, Development of analytical methods for stable isotope geochemistry of non-traditional elements (Fe, Zn, Sr and REEs) using MC-ICPMS. Doctoral thesis, Tokyo Inst. Tech.

Chapter 2

Isotope ratio measurements of trace Nd by the total evaporation normalization method

2.1 Introduction

Isotope ratio of Nd can be measured very precisely by present-day thermal ionization mass spectrometry (TIMS). There are three essential points in achieving high precision in isotope ratio measurements. The first is the use of an internal normalization technique for instrumental mass fractionation correction. Instrumental mass fractionation is the primary source of imprecision in isotope ratio measurements, and normalization is known to be the best way to correct for it when the element under consideration has two or more nonradiogenic isotopes [1]. The second point is the high ion current during measurement to keep the signal-to-noise ratio of the faraday cup high. The third point is the long data acquisition time. Typical Nd isotopic measurements by TIMS require approximately 3 hours. Long data acquisition reduces random error due to ion counting statistics. The latter two points require large samples (e.g. 100-300 ng of Nd for a single measurement) to achieve good precision; decreasing the sample size decreases the ion current and shortens the data acquisition time. Thus, the precision of the measurement of a very small sample is usually poor compared to that obtained with large samples.

Many advances have been made in isotope geochemistry to improve analytical precision with very small samples. Many studies have focused on the enhancement of ionization efficiency to increase the sensitivity of elements in thermal ionization. For example, silica gel activator + phosphoric acid is known to improve the ionization efficiency of Pb [2], and Ta emitter is known to increase the sensitivity of Sr several-fold [3]. Neodymium is more efficiently ionized as the NdO^+ ion than as the Nd^+ ion. Thirlwall [4] reports that the silica gel + phosphoric acid technique promotes the ionization of NdO^+. However, NdO^+ measurement is not preferred because of the uncertainty in oxygen isotope ratio correction. To the best of our knowledge, no activator has yet been reported for Nd^+ ionization enhancement.

The total evaporation method [5], which is used primarily in nuclear industry, was developed as an instrumental mass fractionation correction technique for the measurement of U and Pu in which normalization cannot be applied. The principle of the total evaporation method is that no mass fractionation will occur if the entire sample is evaporated and ionized with a constant yield and the ion beams of the element are totally integrated [6]. The distinctive feature of the total evaporation method is the “burn out” of a very small amount of the sample in a very short time. There are a number of problems in applying the total evaporation method to geochemical isotope ratio measurements. First, the instrumental mass fractionation effect cannot

be totally eliminated because the ionization yield of an element is easily biased during the short measurement time by slight changes in the focus potential, by changes in the ionization efficiency of the oxide ions, etc [7]. Second, the observed isotope ratios are not coherent with that measured by the conventional normalization technique. Dubois et al. [8] measured 20 ng of Nd using the total evaporation method, obtaining a mean $^{146}Nd/^{144}Nd$ value of 0.72333, which is considerably distinct from the value 0.7219 [9] used for normalization in geochemical studies.

In seeking a new method for the isotopic measurement of very small Nd samples, we have experimented with the idea of combining the total evaporation method with the normalization technique. With the total evaporation normalization (TEN) method presented in this paper, small amounts of the sample are measured by a total evaporation procedure. The obtained isotope ratios subsequently undergo the normalization calculation to correct for relict instrumental mass fractionation and to obtain the "geochemically accurate" isotope ratio. This paper presents the procedure and the results of Nd isotope ratio measurement of very small samples (0.1-5 ng Nd) by the TEN method. The present results are compared with those obtained by conventional dynamic multi-collector thermal ionization mass spectrometry (MC-TIMS).

2.2 Materials and methods

2.2.1 Apparatus and reagents

Neodymium isotopic reference reagent JNdi-1 [10] dissolved in diluted HNO_3 was used as a sample. Nd was measured with triple Re filaments (one ionization filament and 2 evaporation filaments). Small amounts (0.1, 0.5, 1 and 5 ng Nd) of the JNdi-1 were loaded on one of the evaporation filaments with 1 ml 2M-H_3PO_4 and evaporated to dryness. Isotope ratio measurements were performed at Nagoya University on a VG Sector 54-30 equipped with seven faraday cups. Table 2-1 shows the configuration of the seven faraday cups.

2.2.2 Faraday cup efficiency calibration

Amplifier gains for the faraday cups were calibrated prior to each analytical session. In addition, efficiencies for faraday cups L1, Ax and H3 were calibrated relative to H1. Relative efficiency calibration for the other cups was not been carried out because the effect of the different efficiencies is negligible (L2 and H4) and because ^{145}Nd data is not used in $^{143}Nd/^{144}Nd$

ratio determination (H2). Efficiency factors for the faraday cups were measured by symmetrical peak jumping [11] using a ^{142}Nd ion beam with an intensity of 1V (10^{-11} A). Each calibration cycle consisted of 100 replicate measurements of the efficiency factors. Several calibration cycles were carried out each day, and the results were averaged to determine the efficiency factors for each analytical session. The results of the faraday cup efficiency calibration are shown in Table 2-2.

2.2.3 Mass spectrometry

Nd isotope ratios were measured using a total evaporation procedure. To the best of our knowledge, there is no software available for total evaporation measurements of Sector 54-30. Therefore, we controlled the filament current manually and used the software for dynamic measurement for the acquisition of "raw intensity data" during measurement.

Step 1: Adjustment phase

First, the ionization filament was heated to a filament current of 4.6 A and stabilized for approximately 10 minutes. The ion beam of ^{187}Re from the ionization filament was then used to optimize the focus settings of the ion source. The intensity of the ^{187}Re ion beam was around 10-100 mV, which corresponds to an ion beam current of 10^{-13}-10^{-12} A.

Next, evaporation filaments were slowly heated until the ion beam intensity of ^{142}Nd reached 1 mV. The evaporation filament current at this point was 1.6-1.7 A. Focus settings were optimized again using a ^{142}Nd ion beam. After the focus adjustment, the evaporation filament current was decreased to 1.0A to avoid consumption of the sample during baseline measurement.

Step 2: Data acquisition phase

The baseline was measured prior to the data acquisition. The integration time for the baseline was 30 seconds. The measured masses and corresponding collectors are shown in Table 1. Ion beam measurement was initiated immediately after baseline measurement. Ion beam integration of 8 seconds was repeated during measurement. As the data acquisition started, the evaporation filament current started to increase until the ion beam intensity of ^{144}Nd reached the target intensity. The target intensity of ^{144}Nd, which depended on the sample size, was 1 V, 500

mV and 100 mV, for 5 ng, 0.5 to 1 ng and 0.1 ng of Nd, respectively. The evaporation filament current was then controlled to keep the ion beam intensity constant. As the sample had been consumed, the evaporation filament current was finally raised to 4.4 A. When the ion beam intensity of ^{144}Nd had fallen below 1 mV, data acquisition was terminated. A typical time profile of a ^{144}Nd ion beam for a 5 ng sample is shown in Fig. 2-1; the intensity profiles of ^{140}Ce and ^{147}Sm ion beams are also plotted in mV scale. The typical data acquisition time was 15, 11, 7 and 4.5 minutes for 5 ng, 1 ng, 0.5 ng and 0.1 ng of Nd, respectively.

2.2.4 Data processing

The VG software outputs "raw intensity data" from which baseline are subtracted for each integration. For every isotope measured, "raw intensity data" were summed and converted to measured electric charge Q by

$$Q\ [C] = \Sigma\ I \times t \times R \qquad (2\text{-}1)$$

where I is the "raw intensity data" of a integration, t is the integration time (8 seconds) and R is the resistance of the faraday cup amplifier (10^{11} ohm). The isobaric interferences of Ce and Sm were corrected on Q (^{142}Nd) and Q (^{144}Nd), using Q (^{140}Ce) and Q (^{147}Sm) and the reported natural isotope ratios for Ce [12] and Sm [13], respectively. Raw isotope ratios of Nd were calculated from Q (Nd) with reference to ^{144}Nd.

$$^{i}Nd/^{144}Nd_{raw} = Q\ (^{i}Nd)/Q\ (^{144}Nd)\ (i = 142, 143, 145 \text{ and } 146) \qquad (2\text{-}2)$$

These raw isotope ratios were then corrected for instrumental mass fractionation by internal normalization using an exponential law [14] and the commonly used ratio ^{146}Nd/^{144}Nd = 0.7219 [9].

The error of the isotope ratio was estimated as follows. The number of ions counted in each faraday cup can be calculated from the measured electric charge Q:

$$N = Q \times N_A / F \qquad (2\text{-}3)$$

where N_A is the Avogadro's number and F is the Faraday constant. Applying the counting statistics, the standard deviation of N can be estimated:

$$\sigma N = \sqrt{N} \qquad (2\text{-}4)$$

The error of the normalized ^{143}Nd/^{144}Nd ratio can then be calculated by propagating the errors σN of isotopes ^{143}Nd, ^{144}Nd and ^{146}Nd.

2.3 Results and discussion

2.3.1 Results

The results of the Nd isotope ratios of 0.1-5 ng JNdi-1 samples measured by the TEN method are shown in Table 2-3 and Fig. 2-2. The raw isotope ratios $^{142}Nd/^{144}Nd_{raw}$, $^{143}Nd/^{144}Nd_{raw}$, $^{145}Nd/^{144}Nd_{raw}$ and $^{146}Nd/^{144}Nd_{raw}$ in which the ratio was not normalized to $^{146}Nd/^{144}Nd = 0.7219$, are also shown in Table 2-3. The raw $^{146}Nd/^{144}Nd$ ratio obtained in the present measurement is 0.7234 ± 15 (2SD, n = 38). Excluding the 3 obviously fractionated data (Fig. 2-3), average raw $^{146}Nd/^{144}Nd$ ratio in this study is 0.7232 ± 6 (2SD, n = 35). This is in agreement with the previously reported $^{146}Nd/^{144}Nd$ ratio of 0.72333 [8] measured by the total evaporation method. However, it differs significantly from the normalizing value 0.7219 used in geochemical studies (Fig. 2-3). The $^{146}Nd/^{144}Nd$ value of 0.7219, initially used by O'Nions et al. [9], is stated as the mean of large number of Nd analysis at that time [15]. Wasserburg et al. used $^{146}Nd/^{142}Nd = 0.636151$, which is mentioned as an average of 10 Nd mass spectrometric runs in 1976, for normalization in NdO^+ measurements and reported $^{146}Nd/^{144}Nd = 0.724134 \pm 0.000010$ [16] in that normalization scheme. Taking an average of a large number of measurements is not sufficient to eliminate the bias due to instrumental mass fractionation, leading to the inconsistent results between different laboratories. The value 0.7219 seems to be rather inaccurate estimation of $^{146}Nd/^{144}Nd$ ratio. However, despite the inaccuracy discussed above, we chose $^{146}Nd/^{144}Nd = 0.7219$ for normalization by convention.

The $^{143}Nd/^{144}Nd$ ratio obtained by the TEN method in the present study (0.51212 ± 0.00013 (2SD), n = 38) is consistent within analytical uncertainty with the ratio obtained at Nagoya University by the conventional dynamic MC-TIMS method (0.512101 ± 0.000012 (2SD), n = 37). The relative external precision of the $^{143}Nd/^{144}Nd$ ratio (0.025%, 2SD) is four times smaller than that of the raw $^{143}Nd/^{144}Nd$ ratio (0.107%, 2SD) in the same data set. The reproducibility of the measurement is improved significantly by the normalization procedure. The improvement of the reproducibility indicates that the continuation of the effect of instrumental mass fractionation on the raw data obtained by the total evaporation procedure (Fig. 2-3), and that the remaining instrumental mass discrimination is properly corrected by the normalization procedure.

The ionization efficiency of each sample (Table 2-3) can be calculated from the measured numbers of ions (Eq. 2-3) and the amount of sample loaded on the filament. The ionization

efficiencies of the 38 measurements in the present study vary largely from 0.06% to 1.52%. The measured numbers of ions do not correlate exactly with the sample amount because of the different ionization efficiency between different measurements. Therefore, in the present study, we grouped the data into 4 sections based on the measured electric charge Q instead of classifying the data by sample size (Table 2-3). The 4 sections, which have Q (^{143}Nd) ranges of 1-10 x 10^{-11}, 10-50 x 10^{-11}, 50-100 x 10^{-11} and 100-500 x 10^{-11} (Table 2-3) correspond roughly to Nd amounts of 0.1, 0.5, 1 and 5 ng, respectively.

The average ^{143}Nd/^{144}Nd ratios of the 4 sections are shown in Table 2-4; they do not differ significantly between the 4 sections and are consistent with the values obtained by the conventional method (Fig. 2-4). The external errors of the 4 sections shown in table 2-4 and Fig. 2-2 are about 1.3 to 7.5 times large as the internal errors of a single run in each section. It is likely that internal error of a run is underestimated since not all the possible sources of error (e.g. amplifier noise) are taken into account in our error estimation. Therefore, external error should be used as a representative of the uncertainty of the measurement. The external standard deviation for each section increases as the measured electric charge decreases. For sections (a) to (c), the external standard deviations (116-140 ppm) do not differ significantly despite the large difference in the measured electric charge and the sample size. The precision of these measurements shown by these external standard deviations corresponds to an uncertainty of 1.2-1.4 in epsilon scale (parts per 10^4) for the ^{143}Nd/^{144}Nd ratio. The precision of the measurements with Q (^{143}Nd) > 10 x 10^{-11}, corresponds roughly to Nd > 0.5 ng, is sufficient for the application of the ^{143}Nd/^{144}Nd ratio as a geochemical tracer. The external precision for section (d) (407 ppm) is 3 to 4 times larger than those of sections (a) to (c). Additionally, the internal errors of the samples in section (d) are larger than the external precisions of sections (a) to (c) (Tables 3 and 4). The precision of the 0.1 ng sample measurements is limited by the large error due to the small number of ions measured. The measured electric charge Q (^{143}Nd) = 10 x 10^{-11} is likely to be the lower limit of the range in which an external precision better than 140 ppm can be obtained. To measure the 0.1 ng sample with Q (^{143}Nd) > 10 x 10^{-11}, enhancement of the ionization efficiency of Nd to at least 1.3% is required.

2.3.2 Comparison with the conventional dynamic MC-TIMS technique

The data of the JNdi-1 measurements carried out at Nagoya University between July 2004 to May 2006 by conventional dynamic MC-TIMS using Sector 54-30 were compiled for

comparison (Table 2-5). The measured electric charge Q for the conventional measurements was estimated from the ion current and the average measurement time. Ion beam consumption during the filament warm-up procedure was not taken into consideration in the estimation of Q.

The relative external standard deviation of $^{143}Nd/^{144}Nd$ ratio measurements by dynamic MC-TIMS increased significantly as the measured electric charge decreased (Fig. 2-5). The increase of the uncertainty is likely to reflect a decrease in the signal-to-noise ratio of the faraday cups and an increase in the random error due to ion counting statistics. Only the measurement with a ^{144}Nd intensity over 0.05V, which corresponds to Q (^{143}Nd) > 236 x 10^{-11}, gives an external precision (2 SD) of approximately 100 ppm or better.

In contrast, the degradation of the relative external standard deviations by TEN is gradual. The precision of the TEN measurement for Q (^{143}Nd) values of less than 100 x 10^{-11} is remarkably better than that of the conventional measurement. The external precision of the TEN measurements is better than 140 ppm for Q (^{143}Nd) values as small as 10 x 10^{-11}.

2.4 Summary

The neodymium isotope ratio of very small samples (0.5-5 ng) was measured precisely by the proposed TEN method. The external precision achieved for measurements with Q (^{143}Nd) =100-500 x 10^{-11}, which corresponds to 5 ng samples, was 116 ppm (2 SD). Using our proposed method, samples as small as 0.5 ng can be measured with an external precision of 140 ppm (2 SD). Samples of 0.1 ng Nd can be measured with such precision if the ionization efficiency of Nd is over 1.3%. The precision of the total evaporation method is superior to that of the conventional method for isotope ratio measurements of samples smaller than 5 ng.

References

[1] I. T. Platzner, 1997, *Modern Isotope Ratio Mass Spectrometry*, John Wiley & Sons, Chichester.

[2] A. E. Cameron and D. H. Smith, R. L. Walker, 1969, Mass spectrometry of nanogram-size samples of lead, *Anal. Chem.* **41**, 525-526.

[3] J. L. Birck, 1986, Precision K-Rb-Sr isotopic analysis: application to Rb-Sr chronology, *Chem. Geol.* **56**, 73-83.

[4] M. F. Thirlwall, 1991, High-precision multicollector isotopic analysis of low levels of Nd as oxide, *Chem. Geol.* **94**, 13-22.

[5] M. Romkowski, S. Franzini and L. Koch, 1987, Mass-spectrometric analysis of sub-nanocurie samples of uranium and plutonium, in: *Proceedings of Eighth Annual ESARDA Symposium*, Commission European Comm., London, 1987, p. 12.

[6] E. L. Callis and R. M. Abernathey, 1991, High precision isotopic analysis of uranium and plutonium by total sample volatilization and signal integration, *Int. J. Mass Spectrom. Ion Processes* **103**, 93-105.

[7] S. Richter and S. A. Goldberg, 2003, Improved techniques for high accuracy isotope ratio measurements of nuclear materials using thermal ionization mass spectrometry, *Int. J. Mass Spectrom.* **229**, 181-197.

[8] J. C. Dubois, G. Retali and J. Cesario, 1992, Isotopic analysis of rare earth elements by total vaporization of samples in thermal ionization mass spectrometry, *Int. J. Mass Spectrom. Ion Processes* **120**, 163-177.

[9] R. K. O'Nions, P. J. Hamilton and N. M. Evensen, 1977, Variations in $^{143}Nd/^{144}Nd$ and $^{87}Sr/^{86}Sr$ ratios in oceanic basalts, *Earth Planet. Sci. Lett*. **34**, 13-22.

[10] T. Tanaka, S. Togashi, H. Kamioka, H. Amakawa, H. Kagami, T. Hamamoto, M. Yuhara, Y. Orihashi, S. Yoneda, H. Shimizu, T. Kunimaru, K. Takahashi, T. Yanagi, T. Nakano, H. Fujimaki, R. Shinjyo, Y. Asahara, M. Tanimizu and C. Dragusanu, 2000, JNdi-1: a neodymium isotopic reference in consistency with La Jolla neodymium, *Chem. Geol.* **168**, 279-281.

[11] K. L. Ramakumar and R. Fiedler, 1999, Calibration procedures for a multicollector mass spectrometer for cup efficiency, detector amplifier linearity, and isotope fractionation to evaluate the accuracy in the total evaporation method, *Int. J. Mass Spectrom.* **184**, 109-118.

[12] M. Tanimizu, T. Hayashi and T. Tanaka, 2004, Development of Ce isotope analysis for cosmochemistry using the dynamic multicollector technique, *J. Mass Spectrom. Soc. Jpn.* **52**, 177-181.

[13] H. Hidaka, M. Ebihara and M. Shima, 1995, Determination of the isotopic compositions of samarium and gadolinium by thermal ionization mass spectrometry, *Anal. Chem.* **67**, 1437-1441.

[14] W. A. Russell, D. A. Papanastassiou and T. A. Tombrello, 1978, Ca isotope fractionation of the earth and other solar system materials, *Geochem. Cosmochim. Acta* **42**, 1075-1090.

[15] R. K. O'Nions, S. R. Carter, N. M. Evensen and P. J. Hamilton, 1979, Geochemical and cosmochemical applications of Nd isotope analysis, *Ann. Rev. Earth Planet. Sci.* **7**, 11-38.

[16] G. J. Wasserburg, S. B. Jacobsen, D. J. DePaolo, M. T. McCulloch and T. Wen, 1981, Precise determination of Sm/Nd ratios, Sm and Nd isotopic abundances in standard solutions, *Geochem. Cosmochim. Acta* **45**, 2311-2323.

Table 2.1 Faraday cup configuration of the Sector 54-30.

Collector	L2	L1	Axial	H1	H2	H3	H4
Mass	140	142	143	144	145	146	147
Isotope	^{140}Ce	^{142}Ce + ^{142}Nd	^{143}Nd	^{144}Nd + ^{144}Sm	^{145}Nd	^{146}Nd	^{147}Sm
Baseline	139.5	141.5	142.5	143.5	144.5	145.5	146.5

Table 2.2 Results of the faraday cup efficiency calibration.

Session	L1	Axial	H1	H3	n
1	1.00014 ± 3	1.00025 ± 2	1	1.00005 ± 3	8
2	1.00038 ± 10	1.00032 ± 7	1	0.99994 ± 10	3
3	1.00034 ± 5	1.00038 ± 2	1	0.99996 ± 5	8

Errors are 2 SE.

Table 2.3 Results for the total evaporation normalization measurements of JNdi-1.

Sample size	$Q^{143}Nd^{*1}$ x 10^{11} [C]	Ionization efficiency [%]	$^{142}Nd/^{144}Nd_{raw}$ *2	$^{143}Nd/^{144}Nd_{raw}$ *2	$^{145}Nd/^{144}Nd_{raw}$ *2	$^{146}Nd/^{144}Nd_{raw}$ *2	$^{143}Nd/^{144}Nd$ normalized	2SD
(a)								
5 ng	491.3	1.26	1.1396	0.511601	0.348834	0.723244	0.512070	± 8
5 ng	468.6	1.34	1.1398	0.511698	0.348834	0.723211	0.512134	± 8
5 ng	441.3	1.14	1.1398	0.511679	0.348784	0.723079	0.512100	± 8
5 ng	267.2	0.69	1.1395	0.511634	0.348830	0.723190	0.512095	± 11
5 ng	263.1	0.68	1.1397	0.511671	0.348799	0.723113	0.512105	± 11
5 ng	200.3	0.52	1.1397	0.511784	0.348674	0.722943	0.512157	± 12
5 ng	191.6	0.49	1.1394	0.511578	0.348846	0.723403	0.512115	± 13
5 ng	177.5	0.46	1.1397	0.511761	0.348742	0.722993	0.512151	± 13
5 ng	174.2	0.45	1.1397	0.511646	0.348832	0.723132	0.512086	± 13
5 ng	164.0	0.42	1.1394	0.511595	0.348794	0.723271	0.512085	± 14
5 ng	154.4	0.40	1.1400	0.511778	0.348729	0.722921	0.512143	± 14
1 ng	117.8	1.52	1.1395	0.511610	0.348850	0.723222	0.512082	± 16
5ng	103.5	0.27	1.1404	0.511836	0.348621	0.722763	0.512145	± 17
(b)								
1 ng	82.9	1.07	1.1396	0.511631	0.348807	0.723196	0.512094	± 19
1 ng	79.2	1.02	1.1398	0.511671	0.348811	0.723048	0.512081	± 20
1 ng	74.3	0.96	1.1393	0.511539	0.348888	0.723367	0.512064	± 20
1 ng	66.0	0.85	1.1395	0.511669	0.348837	0.723225	0.512142	± 22
1 ng	65.9	0.85	1.1388	0.511542	0.348902	0.723490	0.512110	± 22
0.5ng	52.9	1.36	1.1403	0.511766	0.348817	0.722928	0.512133	± 24
(c)								
1 ng	47.5	0.61	1.1388	0.511629	0.348818	0.723406	0.512168	± 25
0.5 ng	42.4	1.09	1.1398	0.511681	0.348828	0.722993	0.512072	± 27
5 ng	33.1	0.09	1.1364	0.511010	0.349257	0.724999	0.512116	± 30
0.5 ng	26.9	0.69	1.1399	0.511681	0.348913	0.723249	0.512163	± 34
0.5 ng	17.5	0.45	1.1393	0.511651	0.348844	0.723330	0.512162	± 42
0.5 ng	14.1	0.36	1.1356	0.511475	0.348927	0.723708	0.512121	± 47
0.5 ng	12.9	0.33	1.1397	0.511742	0.348924	0.723072	0.512161	± 49
(d)								
0.5 ng	6.3	0.16	1.1372	0.510986	0.349157	0.724710	0.511989	± 70
0.1 ng	5.7	0.73	1.1394	0.511571	0.348904	0.723521	0.512150	± 74
0.1 ng	3.9	0.51	1.1397	0.511591	0.349139	0.723608	0.512202	± 89
0.1 ng	3.6	0.46	1.1394	0.511690	0.349011	0.723533	0.512274	± 92
0.1 ng	3.0	0.39	1.1410	0.511708	0.348891	0.722723	0.512003	± 100
0.1 ng	2.7	0.35	1.1396	0.511412	0.349322	0.724018	0.512169	± 106
0.1 ng	2.3	0.29	1.1374	0.511719	0.348865	0.723483	0.512285	± 117
0.5 ng	2.2	0.06	1.1320	0.510324	0.349912	0.726924	0.512113	± 117
0.1 ng	1.9	0.25	1.1398	0.511593	0.348650	0.722981	0.511979	± 127
0.1 ng	1.9	0.24	1.1394	0.511546	0.348758	0.723463	0.512104	± 128
0.1 ng	1.8	0.23	1.1409	0.511851	0.349009	0.722746	0.512153	± 132
0.1 ng	1.2	0.16	1.1388	0.511647	0.348982	0.722996	0.512039	± 159
	Average	0.61	1.1391	0.51158	0.34890	0.7234	0.51212	(n = 38)
	2SD		0.0032	0.00055	0.00045	0.0015	0.00013	
	2RSD		0.281	0.107	0.129	0.207	0.025	(%)

*1 These data are divided into 4 sections by means of integrated ^{143}Nd (see text).

*2 Isotope ratios obtained only by the total evaporation procedure.

Table 2.4 Average $^{143}Nd/^{144}Nd$ ratios measured by total evaporation normalization.

	$Q^{143}Nd$ x 10^{11} [C]	Average $^{143}Nd/^{144}Nd_{raw}$	2SD	2RSD (ppm)	Average $^{143}Nd/^{144}Nd_{normalized}$	2SD	2RSD (ppm)	n
(a)	100-500	0.51168	0.00017	327	0.512113	0.000060	116	13
(b)	50-100	0.51164	0.00017	337	0.512104	0.000061	118	6
(c)	10-50	0.51155	0.00051	991	0.512138	0.000072	140	7
(d)	1-10	0.51147	0.00084	1642	0.512122	0.000209	407	12

Fig. 2.1 Typical ion beam intensity profiles of ^{144}Nd, ^{140}Ce and ^{147}Sm during total evaporation normalization measurement plotted as a function of measurement time.

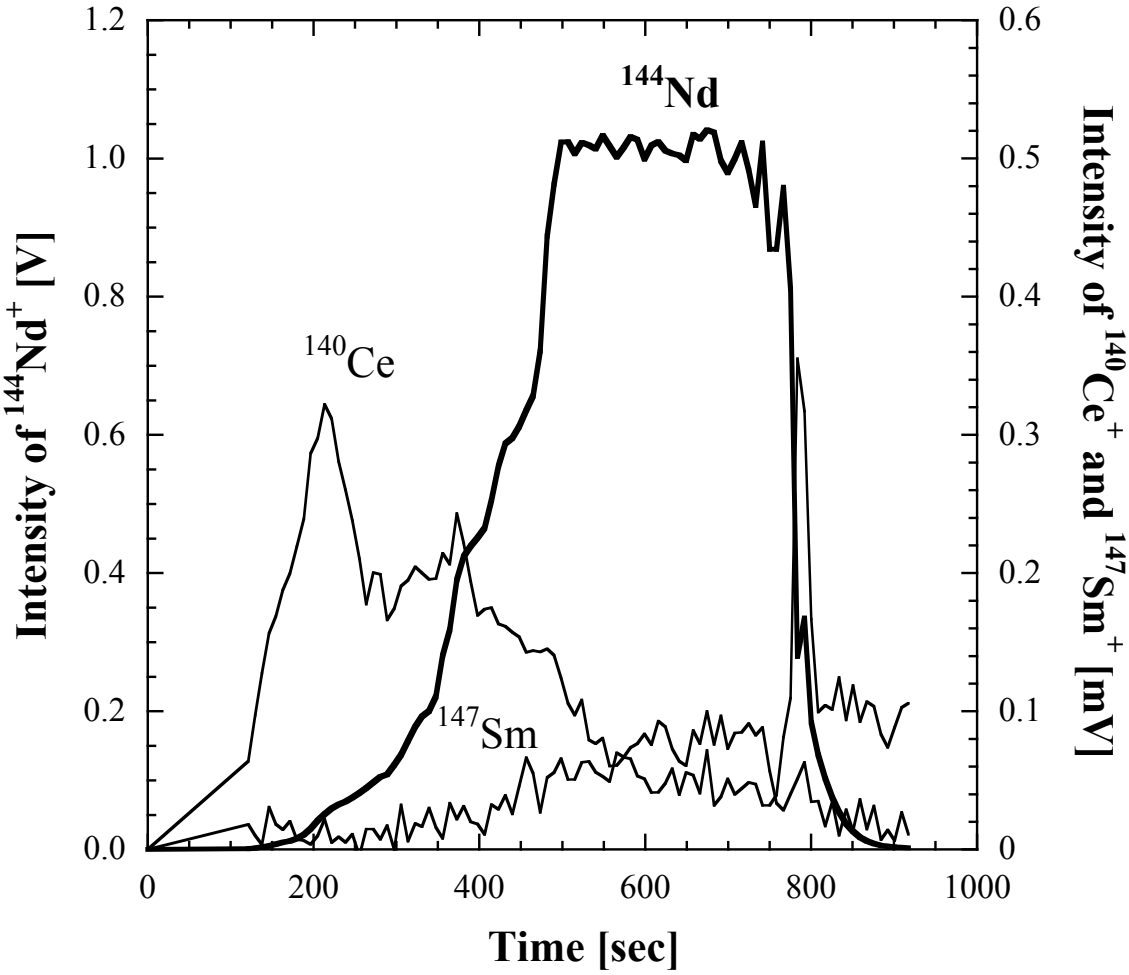

Fig. 2.2 Results of total evaporation normalization measurements of $^{143}Nd/^{144}Nd$ for samples of 0.1 to 5 ng JNdi-1. The horizontal axis shows the measured electric charge Q of ^{143}Nd in each run. The horizontal dashed line and the shaded area show the mean value and the reproducibility (0.512101 ± 0.000012 (2 SD), n = 37) of the large sample measurements of JNdi-1 by conventional dynamic MC-TIMS at Nagoya University.

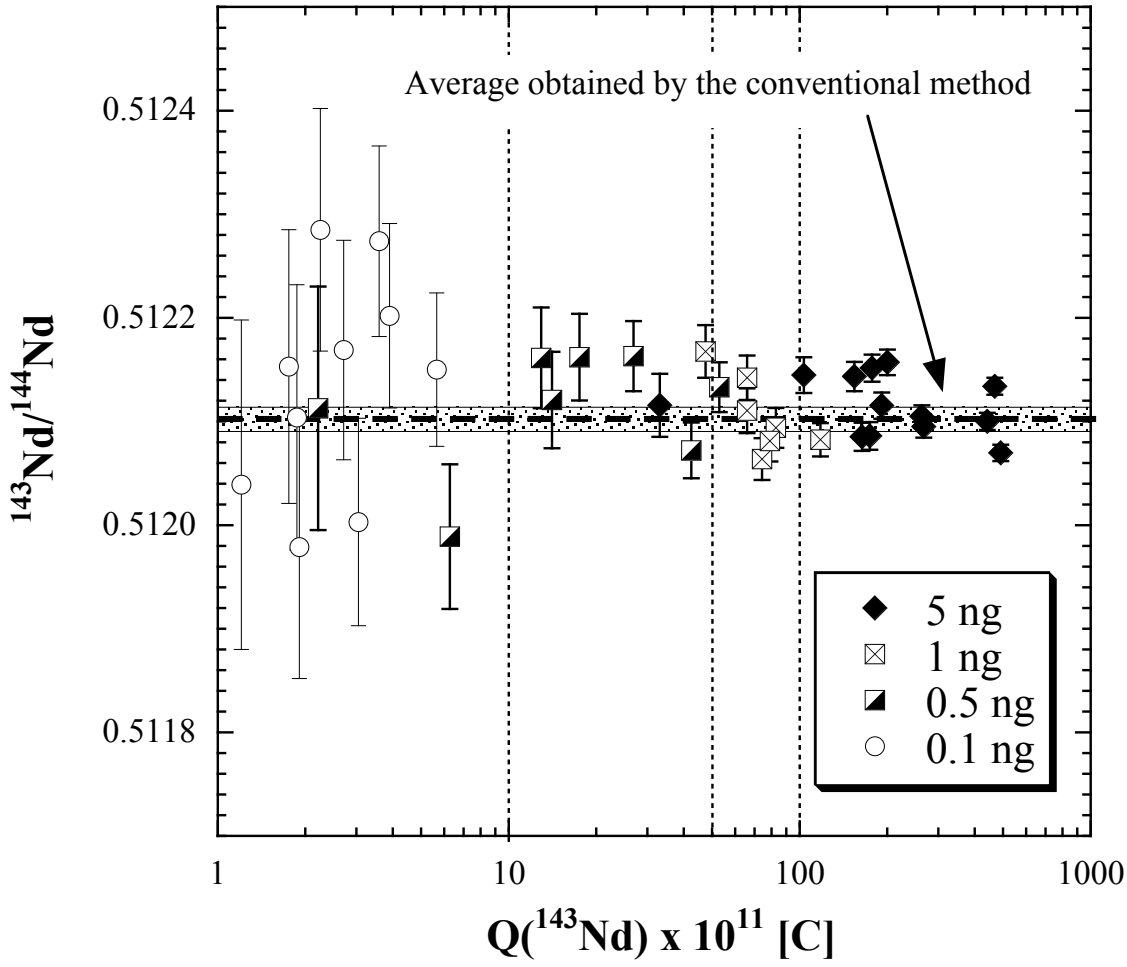

Fig. 2.3 Correlation plots of the raw $^{146}Nd/^{144}Nd$ and raw $^{143}Nd/^{144}Nd$ ratios of 0.1 to 5 ng JNdi-1 measurements, showing the remaining mass discrimination of the non-normalized isotope ratios. The diagonal dashed line indicates the theoretical mass fractionation trajectory. The vertical dashed line indicates the normalizing ratio $^{146}Nd/^{144}Nd = 0.7219$.

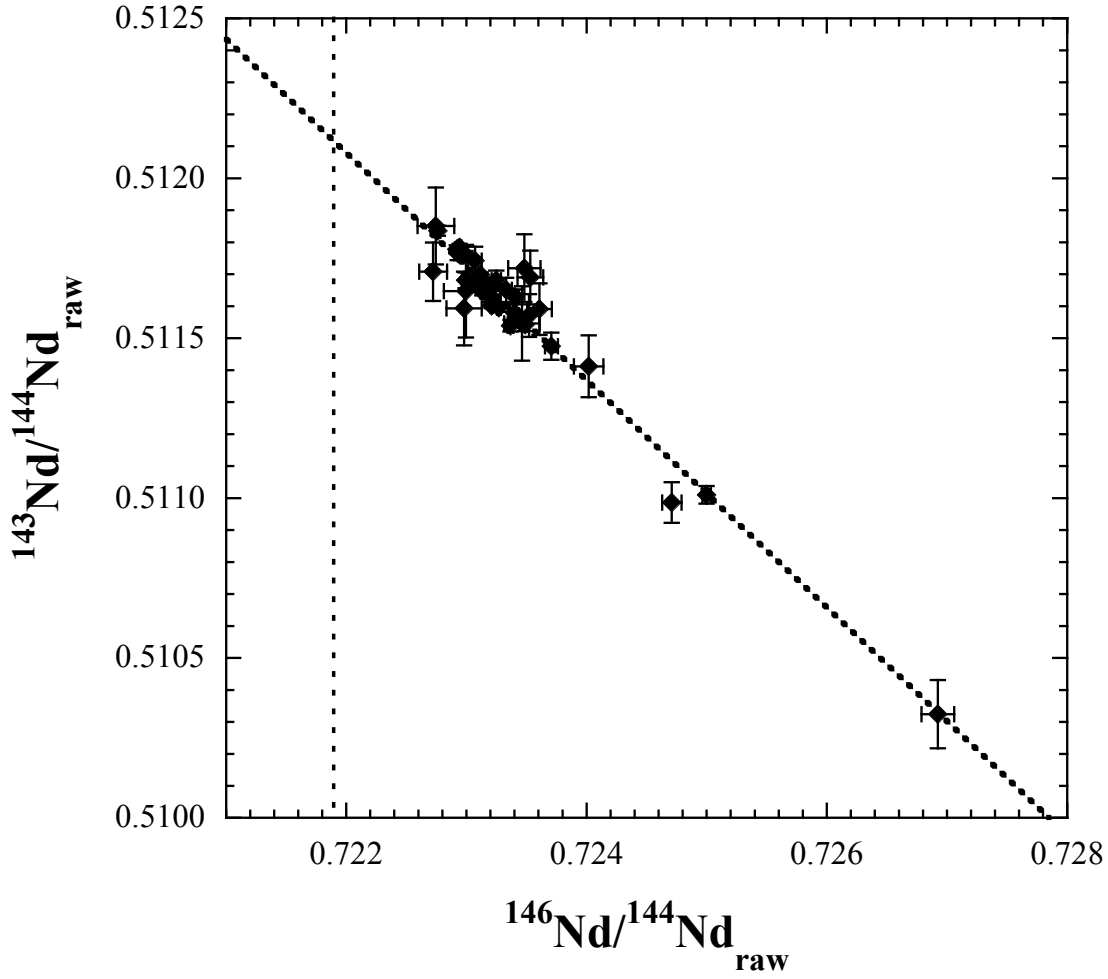

Fig. 2.4 Mean values (horizontal lines) and external standard deviations (shaded areas) of $^{143}Nd/^{144}Nd$ for 4 sections: (a) Q (^{143}Nd) = 100-500 x 10^{-11}, (b) Q (^{143}Nd) = 50-100 x 10^{-11}, (c) Q (^{143}Nd) = 10-50 x 10^{-11} and (d) Q (^{143}Nd) = 1-10 x 10^{-11}. The mean values and 2 SD of the dynamic MC-TIMS measurements are also plotted.

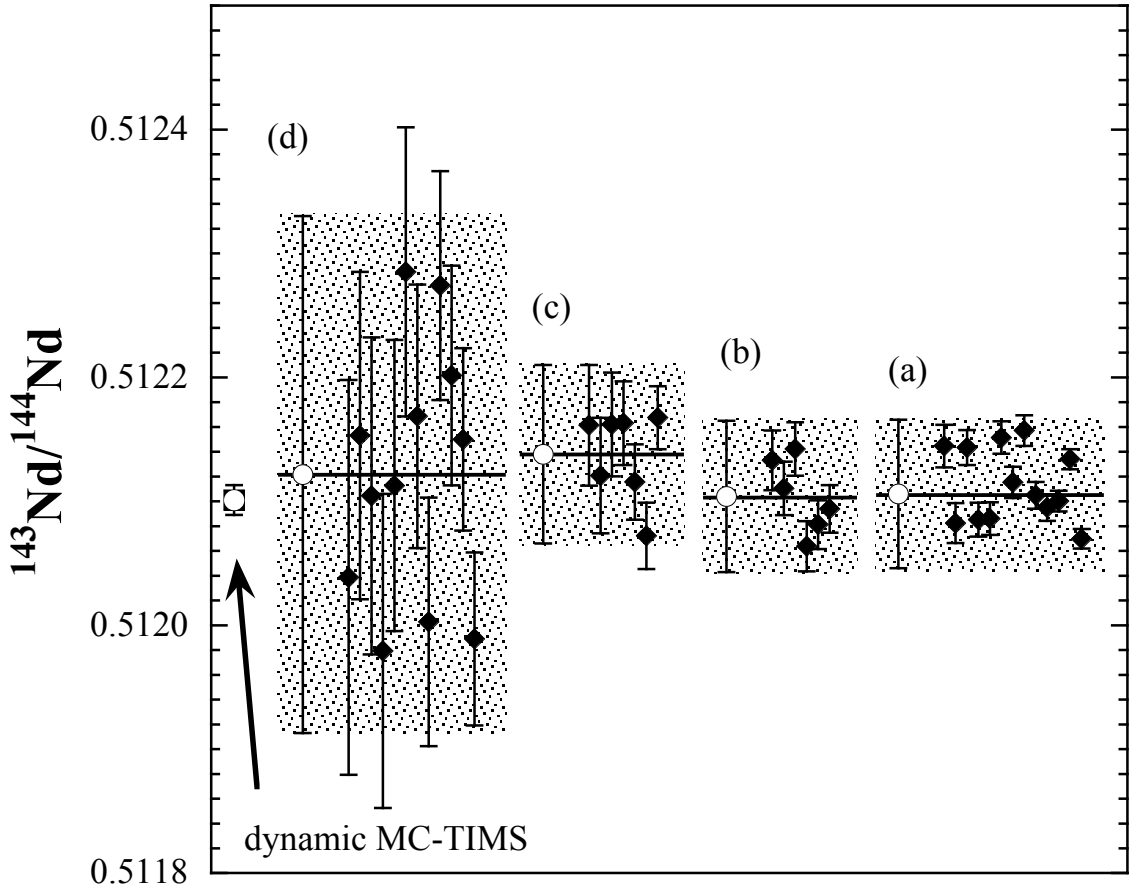

Fig. 2.5 Relative external standard deviations of the $^{143}Nd/^{144}Nd$ ratio by the total evaporation normalization measurements (diamonds) are compared with those of conventional dynamic MC-TIMS measurements (open circles).

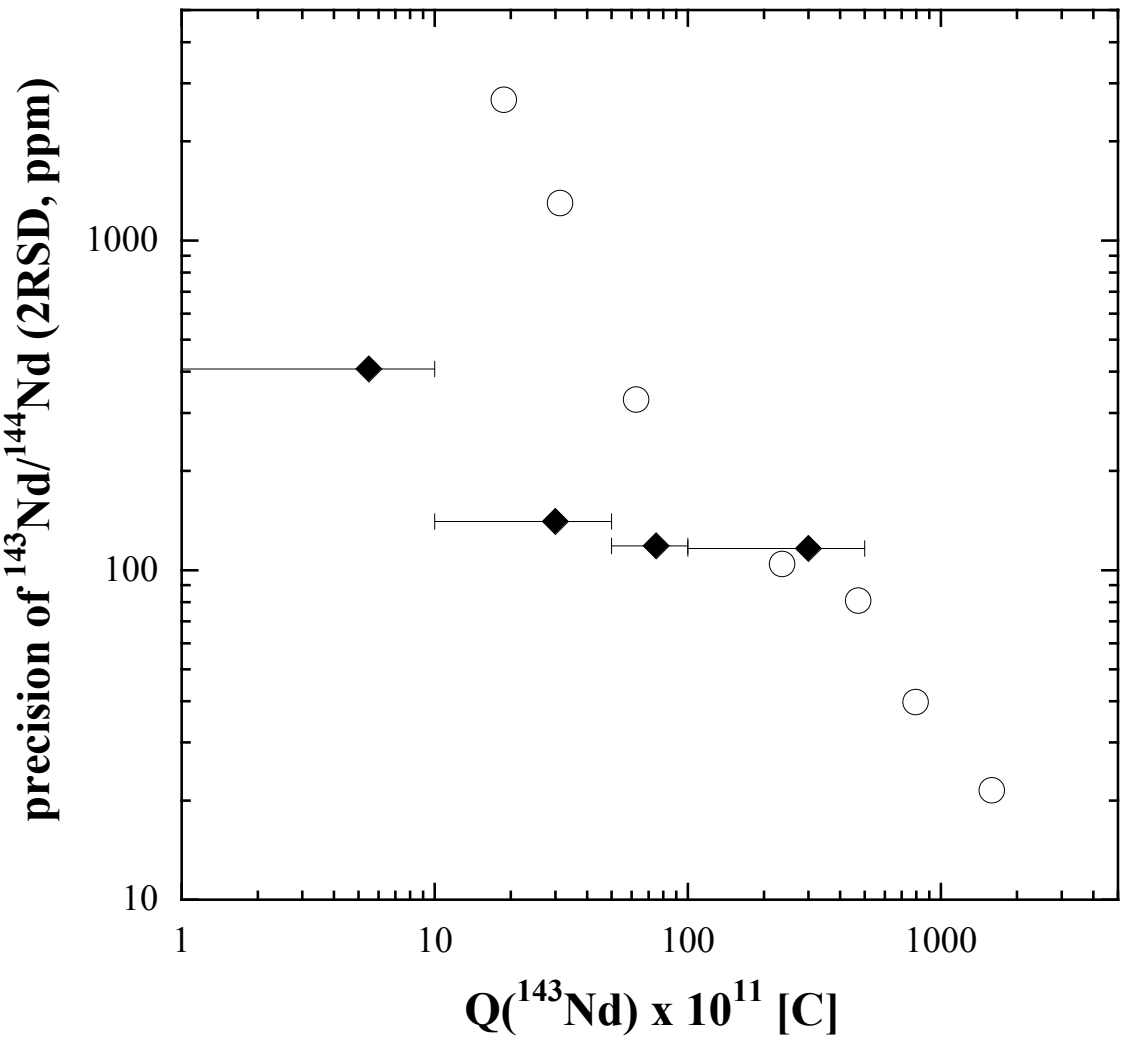

Chapter 3

Refined double spike-TIMS technique for stable isotope analysis of Nd and Sm

3.1 Introduction

Developing a method for stable isotope analysis of non-traditional high-atomic-number elements is an analytically challenging task. Mass spectrometry is the only choice for precise isotope analysis. All the mass spectrometric measurement suffers from large and variable instrumental mass bias. In the case of stable isotope analysis of "light" low-atomic-number elements, instrumental mass bias is not a serious problem because variation of stable isotope compositions in nature (e.g. of the order of % for C) is much larger than possible instrumental mass bias (several per mil). However, situation is very different for high-atomic-number elements: the expected stable isotopic variation in nature is order of magnitude smaller than the possible instrumental mass bias. Therefore, rigorous correction of instrumental mass bias is an essential requirement for stable isotope analysis of high-atomic-number elements.

Most of the recent studies of non-traditional stable isotopes of intermediate to high-atomic-number elements utilize multi-collector inductively coupled plasma mass spectrometry (MC-ICP-MS). MC-ICP-MS has several advantages over conventional thermal-ionization mass spectrometry (TIMS). First, the Ar plasma ion source has high ionization efficiency allowing high-precision measurement of the elements with high first ionization potential (e.g. Ni, Cu and Zn). Second, measurement time of a single sample is short. Typical measurement time for Nd isotopes is about 10 minutes [1] while TIMS measurement takes several hours long. The short measurement time leads to rapid sample throughput. Third, degree of the instrumental mass bias is quite constant during an analytical session. These characteristics allow the instrumental mass bias of MC-ICP-MS to be easily corrected by bracketing standards or by normalizing externally to another element of similar mass added before the measurement. However, MC-ICP-MS has several drawbacks compared to TIMS. First, high ionization efficiency ion source produces not only singly charged ions but doubly charged ions and molecular ions (e.g. oxides and argides). Mass spectrum will be complex and isobaric interferences will be a serious problem in REE measurement. Second, sensitivity of the measurement is lower compared to TIMS for TIMS-favorable elements such as Sm and Nd: although almost 100% ionization efficiency is achieved in Ar-plasma ion source most of the ions are lost in the plasma-mass spectrometer interface. Third, presence of the other elements in the analyte affects the instrumental mass bias of the element of interest. This is called the matrix effect. Matrix effect and relatively large instrumental mass bias causes the difficulty to assess the accuracy of the measurement.

An alternative technique for stable isotope analysis is the combined double-spike

TIMS technique. The double-spike technique is a complicated but a rigorous method to correct for the instrumental mass bias during isotope ratio measurement [2]. For the isotope measurement of Nd and Sm, TIMS has the advantage over MC-ICP-MS in sensitivity, less severe isobaric interferences and high precision. In this study, a procedure for high-precision stable isotope analyses of Nd and Sm is developed by optimizing the double-spike TIMS technique. The basis of the double-spike technique and the refinement of the technique for Nd and Sm analyses are described in detail. Finally, the precision and accuracy of the stable isotope analyses by the developed method will be demonstrated.

3.2 Double spike technique

Double spike technique first proposed by Dodson [2] is a rigorous method to correct for instrumental mass fractionation during mass spectrometry. Double spike technique allows direct determination of the instrumental mass fractionation factor of a mass spectrometric run of a sample after a second mass spectrometric measurement was performed on a "spiked" sample. Numerous approaches are demonstrated for the deconvolution of the double spike problem in the literature [3,4]. Among those, matrix method [5] described below gives the most simple and clear-cut solution.

When an isotope ratio $R_i = m_i / m_0$ of an "un-spiked" sample (natural) was measured on a mass spectrometer, the "measured" isotope ratio R_{in} is always deviated from the "true" isotope ratio R_{iN} by instrumental mass fractionation. The deviation of the measured isotope ratio from the true isotope ratio can be expressed in linear mass fractionation law:

$$R_{iN} = R_{in} \cdot (1 + \alpha \cdot \Delta m_i) \qquad (3\text{-}1)$$

where α is an instrumental mass fractionation factor per atomic mass unit and $\Delta m_i = m_i - m_0$. The "measured" isotope ratio of a mixture (i.e. "spiked" sample) R_{im} in the second mass spectrometric measurement is also deviated from its "true" value R_{iM}:

$$R_{iM} = R_{im} \cdot (1 + \alpha' \cdot \Delta m_i) \qquad (3\text{-}2)$$

where α' is an instrumental mass fractionation factor of the second measurement. The "true" isotope ratio of the mixture R_{iM} can also be expressed by the mixing equation between "true" isotope ratio of the natural sample R_{iN} and the isotope ratio of the double-spike R_{iS}:

$$R_{iN} - R_{iS} = q \cdot (R_{iM} - R_{iS}). \qquad (3\text{-}3)$$

The parameter q can be related to the mixing parameter Q for the denominator isotope by

$$Q = (q-1) / q. \qquad (3\text{-}4)$$

The mixing parameter Q is defined by

$$^0X_M = Q \cdot {}^0X_S + (1 - Q) \cdot {}^0X_N \quad (3\text{-}5)$$

where ^0X_M, ^0X_S and ^0X_N are amount of denominator isotope 0 in mixture, spike and natural, respectively.

Combining (3-1), (3-2) and (3-3) gives:

$$q \cdot (R_{iS} - R_{im}) - \alpha' \cdot q \cdot (\Delta m_i \cdot R_{im}) + \alpha \cdot (\Delta m_i \cdot R_{in}) = R_{iS} - R_{in} \quad (3\text{-}6)$$

Since three unknowns q, α and α', exists, system with three independent isotope ratios is required to solve the equation: application of the double spike technique is restricted to elements with four or more isotopes. Then, equation (3-6) of three isotope ratio of an element R_1, R_2 and R_3, can be expressed in terms of the matrix form:

$$A \cdot \begin{pmatrix} q \\ \alpha' \cdot q \\ \alpha \end{pmatrix} = b \quad (3\text{-}7)$$

where the matrix **A** and vector *b* are given by

$$A = \begin{pmatrix} R_{1s} - R_{1m} & -\Delta m_1 \cdot R_{1m} & \Delta m_1 \cdot R_{1n} \\ R_{2s} - R_{2m} & -\Delta m_2 \cdot R_{2m} & \Delta m_2 \cdot R_{2n} \\ R_{3s} - R_{3m} & -\Delta m_3 \cdot R_{3m} & \Delta m_3 \cdot R_{3n} \end{pmatrix} \quad (3\text{-}8)$$

and

$$b = \begin{pmatrix} R_{1S} - R_{1n} \\ R_{2S} - R_{2n} \\ R_{3S} - R_{3n} \end{pmatrix}. \quad (3\text{-}9)$$

Solution of eq. 3-7 will be given by

$$\begin{pmatrix} q \\ \alpha' \cdot q \\ \alpha \end{pmatrix} = A^{-1} \cdot b \quad (3\text{-}10)$$

where A^{-1} is the inverse matrix of A. The "true" isotope ratio of the sample R_{iN} can be finally calculated from the "measured" isotope ratio R_{in} and the calculated α by equation (3-1). The important requirements of the double spike technique are the knowledge of the isotope composition of the spike and existence of four or more isotopes in the element of interest.

3.3 Practical problems and refinement of the double spike technique

A couple of refinements are made on double-spike technique in order not to degrade the very high precision attainable by present-day TIMS measurements. In equations 3-1 and 3-2 above, liner mass fractionation law is used to relate the true and the measured isotope ratios. Liner law is the simplest one among various mass fractionation laws. Russell et al. [6] reported that exponential mass fractionation law best describes the instrumental mass fractionation effect during thermal ionization. The form of the exponential law is

$$R_{in} = R_{iN} \cdot \left(\frac{m_i}{m_0} \right)^{-\alpha \cdot m_0} \quad , \tag{3-11}$$

where α of the original equation by Russell et al. is replaced by $-\alpha$ in order to match the direction of the fractionation to that of eq. 3-1. Deviation of liner law from exponential law is large over range of fractionation factor as illustrated in fig.3.1. This will be a large error source in the double-spike deconvolution. The use of exponential law in place of liner law in equations 3-1 and 3-2 is not possible because the equations will be too complex to obtain a solution. Johnson and Beard [7] introduced a liner form exponential approximation law. Talor series expansion of the exponential law gives,

$$R_{iN} = R_{in} \cdot \left[1 + \alpha \cdot \Delta m_i - \alpha \cdot \frac{\Delta m_i^{\,2}}{2m_0} + \alpha^2 \cdot \frac{\Delta m_i^{\,2}}{2} + \cdots \right]. \tag{3-12}$$

Combining the first-order-term of the fractionation factor and ignoring high-order-terms, gives an approximation of the exponential law in liner form

$$R_{iN} = R_{in} \cdot \left[1 + \alpha \cdot \left(\Delta m_i - \frac{\Delta m_i^{\,2}}{2m_0} \right) \right]. \tag{3-13}$$

Introduction of liner form exponential approximation law to equations 3-1 and 3-2 reduces the possible error arises from the deviation from exponential law (or from the real mass fractionation behavior) by an order of magnitude (Fig. 3.1).

High-precision isotope ratio measurements on TIMS instruments is only possible when the instrumental mass bias is corrected by internal normalization. The measured ratios, R_{in} and R_{im}, in equation 3-1 and 3-2 should be obtained via internal normalization. An iterative calculation procedure is introduced in this study, which includes both internal normalization of the measured isotope ratio data and double-spike deconvolution, to minimize the introduction of possible error that may caused by large fractionation factor α as discussed above.

First, the "measured" isotope ratio of the sample R_{in} in eq. 3-1 is calculated by

internally normalizing "raw" isotope ratios of the sample measurement, $R_{i\cdot n\cdot raw}$, to the mean of one of the raw isotope ratio, $R_{1\ average}$, via exponential raw:

$$R_{i\cdot n} = R_{i\cdot n\cdot raw} \cdot \left[\frac{R_{1 average}}{R_{1\cdot n\cdot raw}} \right]^{\beta} \tag{3-14}$$

where $\beta = -\ln(m_i/m_0)/\ln(m_1/m_0)$. Since the "raw" isotope ratios distributes along a mass fractionation line on three-dimensional isotope space, this is equivalent to choosing an arbitrary point on the "measured" mass fractionation line. Similarly, the "measured" isotope ratio of the mixture R_{im} in eq. 3-2 is calculated by normalizing to an arbitrary value of R_1 from the "raw" isotope ratios of the mixture measurement, $R_{i\cdot m\cdot raw}$. Solving the double-spike equations with these calculated ratios, R_{in} and R_{im}, will give the first results on "true" isotope ratios for both the sample and the mixture, R_{iN} and R_{iM}. Then, the "measured" isotope ratios of the sample and the mixture are re-calculated by normalizing the "raw" isotope ratios to R'_{1N} and R'_{1M}:

$$R'_{i\cdot n} = R_{i\cdot n\cdot raw} \cdot \left[\frac{R_{1\cdot true}}{R_{1\cdot n\cdot raw}} \right]^{\beta} \tag{3-14'}$$

The double-spike spike equations are solved again with these calculated ratios, R'_{in} and R'_{im}, and the second results, R'_{iN} and R'_{iM}, will be obtained. This procedure is repeated until the calculated values of two fractionation factors, α and α', by eq. 3-10 became sufficiently small.

3.4 Optimization of analytical conditions by error propagation simulation

The importance of the optimization of some free-parameters in double-spike analysis is discussed in literature [8]. Parameters that may affect the error propagation in double-spike analysis are as follows: choice of the two spiked masses in the double-spike, composition of the double-spike, choice of the three isotope ratios to resolve equation 3-7 and spike-sample mixing ratio for the mixture run [7, 8]. These parameters have to be optimized for the analyses of Nd and Sm.

Error magnification factor of the double-spike calculation is a good indicator of the optimality of the parameters. Error magnification calculation was carried out to simulate the error propagation during the deconvolution. Error models for isotope ratios simulating mass spectrometry described by Galer [8] and error propagation calculation described by Hamelin et al. [5] are used in this study. Actually, the choice of the spiked masses is strongly limited by the availability of the spikes. Spikes available at the beginning of this study was ^{145}Nd, ^{150}Nd, ^{149}Sm, ^{150}Sm and ^{154}Sm. Therefore, only a possible combination of double-spikes are investigated.

An example of the calculation is shown in figure 3-2. The results of the optimal double spike compositions for stable isotope analyses of Nd and Sm are shown in table 3-1.

3.5 Experimental

3.5.1 Reagents

No common stable isotope reference material exists for Nd and Sm so far. In the case of Nd, two reagents, La Jolla [9] and JNdi-1 [10], are used as a reference material in radiogenic Nd isotope measurements. Since La Jolla is almost running out in many laboratories, JNdi-1 was chosen for an in-house reference material for stable isotopes in this study. In-house reference material for stable isotopes of Sm is prepared from a commercial Sm oxide reagent (Alfa Aesar, Sm_2O_3, 99.99%, Lot: P4362). Several commercial Nd oxide reagents are also prepared for stable isotope analysis. List of the analyzed reagents are given in table 3.2.

3.5.2 Mass spectrometry

Isotope ratios of Nd and Sm were measured at Nagoya University on a TIMS instrument (VG Sector 54-30) equipped with seven faraday cups.

Neodymium was measured in dynamic mode with reference to ^{144}Nd. Faraday cup configuration of the measurement is shown in table 3.3. In order to obtain radiogenic ^{143}Nd/^{144}Nd ratio in a conventional way, measured isotope ratios were initially normalized to ^{146}Nd/^{144}Nd = 0.7219 [11]. Ion beam intensity of ^{144}Nd was kept at 3V and 1-2 V for 4.5 hours for the measurement of natural and mixture, respectively. Approximately 700 ng Nd is required in total (for both natural and mixture measurements) to meet this condition. Isobaric interference of Ce and Sm were corrected on ^{142}Nd and $^{148, 150}$Nd, respectively, by the natural isotope ratios reported in literature for Ce [12] and Sm [13], respectively.

Samarium was measured with static mode with reference to ^{150}Sm. Table 3-3 shows the configuration of the seven faraday cups. Isotope ratios are normalized to ^{154}Sm/^{150}Sm. Condition of the measurement varied between different sessions but finally settled to ^{152}Sm ion beam intensity of 1V for 2 hours in both natural and mixture measurements. Approximately 300 ng Sm is required in total to meet this condition. Isobaric interference of Nd was corrected on ^{144}Sm, ^{148}Sm and ^{150}Sm by the natural isotope ratios, normalized to ^{146}Nd/^{144}Nd = 0.7219, measured in this study. Possible isobaric interference of CeO to ^{152}Sm and ^{154}Sm is monitored

on mass 156 ($^{140}Ce^{16}O$) but was always negligible. Isobaric interference of Gd to ^{152}Sm and ^{154}Sm is less likely because of the high first ionization potential of Gd.

Relative difference in isotope ratios of Nd and Sm are expressed in epsilon notation (parts par 10^4) relative to the in-house reference materials, JNdi-1 and Alfa Aesar Sm_2O_3 (99.999%):

$$\varepsilon^i Nd = \left(\frac{{}^i Nd/{}^{144}Nd_{sample}}{{}^i Nd/{}^{144}Nd_{JNdi-1}} - 1 \right) \times 10^4 \qquad (3\text{-}15)$$

and

$$\varepsilon^i Sm = \left(\frac{{}^i Sm/{}^{150}Sm_{sample}}{{}^i Sm/{}^{150}Sm_{Alfa \cdot Aesar \cdot Sm_2O_3}} - 1 \right) \times 10^4 . \qquad (3\text{-}16)$$

3.5.3 Preparation and calibration of the double-spike

Nd and Sm double spikes are prepared from two single spikes for each element, ^{145}Nd, ^{150}Nd, ^{150}Sm and ^{154}Sm. The compositions of the double spikes and optimized values of the parameters used in this study is shown in table 3.4. Accurate isotope compositions of the double spike is required to solve the double spike problem described above. Isotope compositions of the double spike, R_S (eq.3-3), is measured and calibrated by "inverse" double spike deconvolution technique, where the double spike is treated as a sample and the natural sample (JNdi-1 and Sm Standard) is treated as a double spike. This procedure requires a knowledge of the true isotope composition of the standards. Measured isotope composition of the standards normalized to $^{146}Nd/^{144}Nd = 0.7219$ and $^{154}Sm/^{150}Sm = 3.08267$ [13], were used as the true isotope composition in the spike calibration. Therefore, accuracy of the absolute values finally calculated from eq. 3-1, depends on the accuracy of the normalizing values used in the spike calibration described above. The accuracy of the relative epsilon values are discussed later.

3.6. Results and discussion

3.6.1 Reproducibility of the reference material analyses

The results of the replicate analysis of in-house Nd reference material, JNdi-1, are shown in table 3.5 and fig. 3.3. Precision of the stable isotope analysis of Nd, estimated from

the reproducibility of the reference material analysis, was ± 0.2 ε per atomic mass unit for all the isotope except for ε^{146}Nd where the precision was ± 0.2 (0.1 ε per atomic mass unit). Relatively high precision of ε^{146}Nd compared to the others can be explained by means of error propagation. Mass-spectrometrically measured "raw" ratios for all isotopes equally include a random statistical error. The "raw" ratios are transformed into "measured" ratios by internal normalization. Statistical error of the measurement included in the "raw" ^{146}Nd/^{144}Nd is completely transferred to all the other isotope ratios by this normalization procedure (eq. 3-14). This leads to the relatively high precision of ε^{146}Nd. Stable isotope fractionation of Nd will be discussed by the most-precise ε^{146}Nd hereafter.

The results of the replicate analysis of in-house Sm reference material are shown in table 3.6 and fig. 3.4. Precision of the stable isotope ratios were ± 0.4 ~ 0.8 ε per atomic mass unit. Alike the case of ε^{146}Nd, precision of ε^{154}Sm seems to be the highest among all Sm isotopes. However, the precision of the εSm values somewhat vary between isotopes and between sessions. Relatively low and variable precision of the Sm isotopes compared to that of Nd is caused by the difficulty in isotope ratio measurements of Sm by static mode. Use of the state-of-the-art TIMS instrument may improve the precision of Sm isotope measurements.

3.6.2 Isotope fractionation of Nd and Sm induced by cation exchange chromatography

Estimation of the accuracy of the stable isotope analyses of Nd and Sm is not straightforward since no certified reference material exists for these elements. In this study, accuracy of the analysis was estimated by measuring the isotope fractionation of Nd and Sm during cation exchange chromatography. Ion exchange chromatography is widely used to separate elements in wet chemistry. It is also known to separate isotopes of an element slightly causing a systematic isotope fractionation during the course of separation. Accuracy of the stable isotope analysis of Nd and Sm can be estimated by comparing the measured isotope fractionation behavior to the theoretical calculation.

Column with 1.4 mm and 6.0 mm in diameter are filled with cation exchange resin (Biorad AG 50W X8) to 90 mm and 120 mm in height, for Nd and Sm separation, respectively. Nd was separated into 7 fractions by 0.175M alpha-hydroxyisobutyric acid (HIBA) as an eluent (Fig. 3.5-a). Sm was separated into 8 fractions by 0.2M HIBA (Fig. 3.6-a).

Stable isotope composition of the eluted fractions of Nd and Sm are shown in table 3.7 and 3.8. The eluted fractions for both elements show systematic change in stable isotope

compositions from heavy-isotope enrichment to light-isotope enrichment. Theory of chromatography showed that isotope fractionation phenomena in chromatography are caused by slight difference in the elution band between isotopes, and liner relationship will be obtained when log of the isotope fractionation factor is plotted against the percentage of the eluted fraction on a probability scale [14, 15, 16]. Figures 3.5-b and 3.6-b shows that this is the case for both Nd and Sm. Batch isotope fractionation factor between cation exchange resin and the solute in this experimental condition may be calculated from the slope in figs. 3.5-b and 3.6-b. The batch isotope fractionation factor for $^{146}Nd/^{144}Nd$ and $^{148}Nd/^{150}Sm$ in this experiment was $\alpha_{146} = (^{146}Nd/^{144}Nd)_{resin}/(^{146}Nd/^{144}Nd)_{solute} = 0.999968 \pm 2$ and $\alpha_{148} = (^{148}Sm/^{150}Sm)_{resin}/(^{148}Sm/^{150}Sm)_{solute} = 1.000054 \pm 3$, respectively. The results of the fractionation behavior of Nd and Sm during column chromatography are fully consistent with theory and thus proving the accuracy of the stable isotope analyses in this study.

3.6.3 Variation of Nd stable isotopes among reagents

Stable isotope compositions of eleven commercial Nd oxide reagents and La Jolla are shown in table 3.9 and Fig. 3.7. The $\varepsilon^{146}Nd$ values of these reagents range from -2.5 to 0.3. Isotope fractionation effects recorded in these reagents are fully mass dependent (Fig 3.7 (c)). Five regents have Nd stable isotope composition indistinguishable from JNdi-1, while other reagents and La Jolla have light-isotope enriched stable isotopes. No correlation is found between the stable isotope composition and the purity of the reagents. Variation in radiogenic $^{143}Nd/^{144}Nd$ ratios among these reagents indicates that the source materials of these reagents are different. It is not clear whether the observed stable isotopic variation among these reagents reflects the difference of the degree of isotope fractionation during production and purification processes of these reagents or the difference of the stable isotope composition of their source materials.

3.6.4 Accuracy of the epsilon value

As noted earlier, the accuracy of the absolute isotope compositions obtained by the double spike technique depends on the accuracy of the isotope compositions of the double spike. The accuracy of the isotope compositions of the double spike depends on the accuracy of the assumption used in the double spike calibration, $^{146}Nd/^{144}Nd = 0.7219$ and $^{154}Sm/^{150}Sm =$

3.08267. To assess if the accuracy of the "relative" epsilon values were affected by the accuracy of the assumptions used in spike calibration, Nd isotope compositions of the column separation fractions and the reagents are recalculated using the double spike composition calibrated by assuming $^{146}Nd/^{144}Nd = 0.72333$. As clearly demonstrated by Fig. 3.8., epsilon values calculated by the two different spike calibrations completely agreed indicating that the inaccuracy of the spike composition does not affect the accuracy of the "relative" epsilon values.

3.7 Summary

Highly precise and accurate procedure for stable isotope analyses of Nd and Sm is developed by the combined double-spike TIMS technique. Iterative calculation is introduced in the deconvolution of the analysis to minimize the introduction of possible error due to the imperfect approximation of the instrumental mass bias correction in double-spike equations. The precision of the analyses of Nd and Sm is estimated from the reproducibility of the reference material analysis and was ± 0.2 and ± 1.2 for $\varepsilon^{146}Nd$ and $\varepsilon^{148}Sm$, respectively. The achieved precision is sufficient for the investigation of the possible stable isotope variations in nature. Isotope fractionation behavior during cation exchange chromatography is studied for both Nd and Sm to confirm the accuracy of the analysis.

References

[1] T. Ohno, 2006, Development of analytical methods for stable isotope geochemistry of non-traditional elements (Fe, Zn, Sr and REEs) using MC-ICPMS. Doctoral thesis, Tokyo Inst. Tech.

[2] M. H. Dodson, 1963, A theoretical study of the use of internal standards for precise isotopic analysis by the surface ionization technique: Part I-general first-order algebraic solutions, *J. Sci. Instrum*., **40**, 289-295.

[3] W. Compston and V. M. Oversby, 1969, Lead isotopic analysis using a double spike, *J. Geophys. Res*., **74**, 4338-4348.

[4] A. Hofmann, Fractionation corrections for mixed-isotope spikes of Sr, K, and Pb, *Earth Planet. Sci. Lett*., **10**, 397-402.

[5] B. Hamelin, G. Manhes, F. Albarede and C. J. Allegre, 1985, Precise lead isotope measurements by the double spike technique: a reconsideration, *Geochim. Cosmochim. Acta*, **49**, 173-182.

[6] W. A. Russell, D. A. Papanastassiou, T. A. Tombrello, 1978, Ca isotope fractionation on the earth and other solar system materials. *Geochem. Cosmochim. Acta,* **42**, 1075-1090.

[7] C. M. Johnson and B. L. Beard, 1999, Correction of instrumentally produced mass fractionation during isotopic analysis of Fe by thermal ionization mass spectrometry, *Int. J. Mass Spectrom*., **193**, 87-99.

[8] S. J. G. Galer, 1999, Optimal double and triple spiking for high precision lead isotopic measurement, *Chem. Geol.* **157**, 255-274.

[9] G. W. Lugmair and R. W. Carlson, 1978, The Sm-Nd history of KREEP, In *Proc. 9th Lunar Planet. Sci. Conf*., pp. 689-704.

[10] T. Tanaka, S. Togashi, H. Kamioka, H. Amakawa, H. Kagami, T. Hamamoto, M. Yuhara, Y.

Orihashi, S. Yoneda, H. Shimizu, T. Kunimaru, K. Takahashi, T. Yanagi, T. Nakano, H. Fujimaki, R. Shinjyo, Y. Asahara, M. Tanimizu, C. Dragusanu, 2000, JNdi-1: a neodymium isotopic reference in consistency with La Jolla neodymium, *Chem. Geol*. **168**, 279-281.

[11] R. K. O'Nions, P. J. Hamilton, N. M. Evensen, 1977, Variations in 143Nd/144Nd and 87Sr/86Sr ratios in oceanic basalts, *Earth Planet. Sci. Lett.*, **34**, 13-22.

[12] M. Tanimizu, T. Hayashi, T. Tanaka, 2004, Development of Ce isotope analysis for cosmochemistry using the dynamic multicollector technique, *J. Mass Spectrom. Soc. Jpn.,* **52**, 177-181.

[13] H. Hidaka, M. Ebihara, M. Shima, 1995, Determination of the isotopic compositions of Samarium and Gadolinium by thermal ionization mass spectrometry, *Anal. Chem.,* **67**, 1437-1441.

[14] E. Glueckauf, 1955, Theory of chromatography part 9. the "theoretical plate" concept in column separations, *Trans. Faraday Soc.,* **51**, 34-44.

[15] E. Glueckauf, 1956, Theory of chromatography part 11. enrichment of isotopes by chromatography, *Trans. Faraday Soc.,* **54**, 1203-1205.

[16] W. A. Russell and D. A. Papanastassiou, 1978, Calcium isotope fractionation in Ion-exchange chromatography, *Anal. Chem.,* **50**, 1151-1154.

[17] T. Tanaka, M. Tanimizu, Y. Asahara, C. Yonezawa, S. Togashi and H. Kamioka, 1996, A variety of 143Nd/144Nd ratios among six high purity neodymium oxide reagents, *J. Mass Spectrom. Soc. Jpn*. **44**, 79-83.

Table 3.1 Optimal double spike compositions for stable isotope analyses of Nd and Sm.

double-spike	denominator isotope	spike composition
^{145}Nd-^{150}Nd	^{144}Nd	^{150}Nd/^{145}Nd ~ 0.6
	^{145}Nd	^{150}Nd/^{145}Nd ~ 2.5
	^{150}Nd	^{150}Nd/^{145}Nd ~ 2.0
^{149}Sm-^{150}Sm	^{147}Sm	^{149}Sm/^{150}Sm > 10
	^{148}Sm	^{149}Sm/^{150}Sm ~ 6
	^{149}Sm	^{149}Sm/^{150}Sm ~ 1
	^{150}Sm	^{149}Sm/^{150}Sm ~ 1
	^{152}Sm	^{149}Sm/^{150}Sm > 10
	^{154}Sm	^{149}Sm/^{150}Sm > 10
^{149}Sm-^{154}Sm	^{147}Sm	^{149}Sm/^{154}Sm ~ 4
	^{148}Sm	^{149}Sm/^{154}Sm ~ 3
	^{149}Sm	^{149}Sm/^{154}Sm ~ 0.4
	^{150}Sm	^{149}Sm/^{154}Sm ~ 2
	^{152}Sm	^{149}Sm/^{154}Sm ~ 0.4
	^{154}Sm	^{149}Sm/^{154}Sm ~ 0.4
^{150}Sm-^{154}Sm	^{147}Sm	^{150}Sm/^{154}Sm < 0.1
	^{148}Sm	^{150}Sm/^{154}Sm < 0.1
	^{149}Sm	^{150}Sm/^{154}Sm < 0.1
	^{150}Sm	^{150}Sm/^{154}Sm ~ 0.4
	^{152}Sm	^{150}Sm/^{154}Sm < 0.1
	^{154}Sm	^{150}Sm/^{154}Sm ~ 0.4

Table 3.2 Neodymium oxide reagents analyzed in this study.

Abbreviation in the text	Product information	Purity
Wako	Wako Pure Chemical Ind., Ltd. Lot. No. EWE1348	99.9%
Kanto-A	Kanto Chemical Co., Inc. Lot. No. 712W2057	99.95%
Kanto-B	Kanto Chemical Co., Inc. Lot. No. 412C2029	99.0%
AA-99	Alfa Aesar Stock # 40252 Lot. # FA9802B	99%
AA-99.99	Alfa Aesar Stock # 11250 Lot. # F12R044	99.99%
JM*	Johnson Matthey Materials Technology Product No. 565041 Batch No. 75064	Grade 1
Mitsuwa*	Mitsuwa Chemical Co. Lot No.43541	99.99%
Merck*	MERCK Art. 12276 Lot No. 231 ZA 10351175	-
Spex*	SPEX Industries Catalog No. ND64-10 CAS No. 1313-97-9 Lot No. 08811	TMI-20
CERAC*	CERAC Inc. handled by Rare Metallic Co. Stock No. N-1097 Lot No. X 14066	99.999%

* The radiogenic $^{143}Nd/^{144}Nd$ ratio of these reagents are previously reported [17].

Table 3.3 Faraday cup configuration in Nd and Sm isotope ratio measurements.

sequence	faraday cups						
	L2	L1	Ax	H1	H2	H3	H4
Nd							
1	^{140}Ce		^{142}Nd	^{143}Nd	^{144}Nd	^{145}Nd	^{146}Nd
2	^{141}Pr	^{142}Nd	^{143}Nd	^{144}Nd	^{145}Nd	^{146}Nd	
3	^{142}Nd	^{143}Nd	^{144}Nd	^{145}Nd	^{146}Nd	^{147}Sm	^{148}Nd
4	^{143}Nd	^{144}Nd	^{145}Nd	^{146}Nd	^{147}Sm	^{148}Nd	
5	^{145}Nd	^{146}Nd	^{147}Sm	^{148}Nd		^{150}Nd	^{151}Eu
Sm							
1	^{144}Sm	^{147}Sm	^{148}Sm	^{149}Sm	^{150}Sm	^{152}Sm	^{154}Sm
2	^{144}Sm	^{147}Sm	^{148}Sm	^{149}Sm	^{150}Sm	^{152}Sm	^{154}Sm
3	^{144}Sm	^{147}Sm	^{148}Sm	^{149}Sm	^{150}Sm	^{152}Sm	^{154}Sm
4	^{144}Sm	^{147}Sm	^{148}Sm	^{149}Sm	^{150}Sm	^{152}Sm	^{154}Sm
5	^{145}Nd	^{148}Sm	^{149}Sm	^{150}Sm	^{151}Eu	^{153}Eu	^{155}Gd
6	^{146}Nd	^{149}Sm	^{150}Sm			^{154}Sm	^{156}CeO

Table 3.4 Double spike composition and other parameters used in this study.

double spike	denominator isotope	spike composition	optimal Q
^{145}Nd-^{150}Nd	^{144}Nd	^{145}Nd/^{144}Nd = 5.85	0.04
^{150}Sm-^{154}Sm	^{150}Sm	^{154}Sm/^{150}Sm = 3.80	0.75

Table 3.5 Results of replicate analysis of the reference material JNdi-1 in 6 analytical sessions.

Sample	n	ε^{142}Nd	ε^{145}Nd	ε^{146}Nd	ε^{148}Nd	ε^{150}Nd
session-1	11	0.0 ± 0.5	0.0 ± 0.2	0.0 ± 0.2	0.0 ± 0.6	0.0 ± 1.1
session-2	7	0.0 ± 0.5	0.0 ± 0.1	0.0 ± 0.2	0.0 ± 0.4	0.0 ± 1.2
session-3	3	0.0 ± 0.1	0.0 ± 0.1	0.0 ± 0.2	0.0 ± 0.5	0.0 ± 0.8
session-4	7	0.0 ± 0.7	0.0 ± 0.2	0.0 ± 0.3	0.0 ± 0.6	0.0 ± 1.3
session-5	9	0.0 ± 0.5	0.0 ± 0.1	0.0 ± 0.2	0.0 ± 0.7	0.0 ± 1.0
session-6	7	0.0 ± 0.5	0.0 ± 0.2	0.0 ± 0.4	0.0 ± 0.8	0.0 ± 1.3
total	44	0.0 ± 0.5	0.0 ± 0.2	0.0 ± 0.2	0.0 ± 0.6	0.0 ± 1.1

Errors are 2SD of the replicate analysis.

Table 3.6 Results of replicate analysis of the reference material of Sm in 5 analytical sessions.

Sample	n	Q	ε^{144}Sm	ε^{147}Sm	ε^{148}Sm	ε^{149}Sm	ε^{152}Sm	ε^{154}Sm
session-1	9	0.50	0.0 ± 3.7	0.0 ± 1.9	0.0 ± 2.1	0.0 ± 1.3	0.0 ± 1.6	0.0 ± 2.4
session-2	9	0.70	0.0 ± 1.0	0.0 ± 1.4	0.0 ± 0.7	0.0 ± 0.6	0.0 ± 0.7	0.0 ± 1.1
session-3	11	0.70	0.0 ± 1.5	0.0 ± 0.6	0.0 ± 0.8	0.0 ± 0.7	0.0 ± 1.3	0.0 ± 1.1
session-3	9	0.46	0.0 ± 1.7	0.0 ± 0.7	0.0 ± 0.3	0.0 ± 0.3	0.0 ± 0.9	0.0 ± 1.2
session-4	6	0.46	0.0 ± 4.8	0.0 ± 2.4	0.0 ± 1.3	0.0 ± 0.7	0.0 ± 0.7	0.0 ± 2.5
total	44		0.0 ± 2.9	0.0 ± 1.5	0.0 ± 1.2	0.0 ± 0.8	0.0 ± 1.3	0.0 ± 1.9

Errors are 2SD of the replicate analysis.

Table 3.7 Results of stable isotope analysis on fractions obtained by cation exchange chromatography. of Nd

Sample	eluted volume [ml]	Nd [ng]	[%]	ε^{142}Nd	ε^{143}Nd	ε^{145}Nd	ε^{146}Nd	ε^{148}Nd	ε^{150}Nd
0903-01	4 - 8	64599	17.22	-5.1 ± 0.2	-2.4 ± 0.1	2.4 ± 0.1	4.6 ± 0.2	9.3 ± 0.4	12.5 ± 0.6
0903-02	8 - 9	112823	30.07	-2.0 ± 0.2	-1.0 ± 0.1	1.0 ± 0.1	1.8 ± 0.2	3.7 ± 0.4	5.0 ± 0.7
0903-03	9 - 9.5	70381	18.76	0.4 ± 0.2	0.2 ± 0.1	-0.3 ± 0.1	-0.6 ± 0.2	-1.3 ± 0.4	-2.5 ± 0.7
0903-04	9.5 - 10.5	96684	25.77	2.3 ± 0.2	1.2 ± 0.1	-1.2 ± 0.1	-2.4 ± 0.2	-4.9 ± 0.4	-7.6 ± 0.7
0903-05	10.5 - 11	20612	5.49	5.4 ± 0.2	2.7 ± 0.1	-2.7 ± 0.1	-5.3 ± 0.2	-10.6 ± 0.4	-15.6 ± 0.6
0903-06	11 - 12	9426	2.51	7.1 ± 0.3	3.5 ± 0.1	-3.5 ± 0.1	-6.9 ± 0.3	-13.6 ± 0.6	-20.1 ± 0.8
0903-07	12 - 16	676	0.18	9.5 ± 0.3	4.8 ± 0.1	-4.8 ± 0.1	-9.4 ± 0.3	-18.4 ± 0.5	-27.5 ± 0.8

Errors are 2SE of a single analysis.

Table 3.8 Results of stable isotope analysis on fractions obtained by cation exchange chromatography of Sm.

Sample	eluted volume [ml]	Sm [ng]	[%]	$\varepsilon^{144}Sm$	$\varepsilon^{147}Sm$	$\varepsilon^{148}Sm$	$\varepsilon^{149}Sm$	$\varepsilon^{152}Sm$	$\varepsilon^{154}Sm$
0715-02	19 -29	335	0.28	-61.1 ± 7.7	-32.4 ± 5.2	-21.0 ± 4.4	-9.8 ± 3.7	20.9 ± 2.1	66.5 ± 2.5
0715-03	29-31	1337	1.10	-39.9 ± 1.6	-20.0 ± 0.6	-13.8 ± 0.8	-6.7 ± 0.7	11.2 ± 1.3	24.3 ± 1.1
0715-04	31-32	1632	1.35	-34.2 ± 1.6	-17.1 ± 0.6	-11.8 ± 0.8	-5.4 ± 0.7	10.5 ± 1.3	21.8 ± 1.1
0715-05	32-36	23216	19.16	-22.8 ± 1.6	-11.1 ± 0.6	-7.5 ± 0.8	-3.7 ± 0.7	6.9 ± 1.3	14.3 ± 1.1
0715-06	36-37	11505	9.50	-15.0 ± 1.6	-7.0 ± 0.6	-4.6 ± 0.8	-2.3 ± 0.7	4.1 ± 1.3	8.3 ± 1.1
0715-07	37-39	26793	22.11	-5.0 ± 1.6	-2.4 ± 0.6	-1.2 ± 0.8	-0.7 ± 0.7	1.8 ± 1.3	3.6 ± 1.1
0715-08	39-41	25487	21.03	6.2 ± 1.6	3.3 ± 0.6	1.6 ± 0.8	0.9 ± 0.7	-2.3 ± 1.3	-4.3 ± 1.1
0715-09	41-49	30862	25.47	19.3 ± 1.6	10.6 ± 0.6	7.3 ± 0.8	3.6 ± 0.7	-7.6 ± 1.3	-15.4 ± 1.1

Errors are 2SD of the replicated STD analysis except for 0715-02 where errors are 2SE of a single analysis.

Table 3.9 Results of stable isotope analysis and radiogenic isotope measurement on 10 commercial Nd_2O_3 reagents and two isotope reference materials, La Jolla and JNdi-1.

Sample	n	$\varepsilon^{142}Nd$	$\varepsilon^{145}Nd$	$\varepsilon^{146}Nd$	$\varepsilon^{148}Nd$	$\varepsilon^{150}Nd$	$^{143}Nd/^{144}Nd$
Wako	4	0.3 ± 0.8	-0.1 ± 0.3	-0.1 ± 0.5	-0.1 ± 0.8	-0.1 ± 1.9	0.512202 ± 5
Kanto-A	1	0.8 ± 0.2	-0.2 ± 0.1	-0.7 ± 0.2	-1.6 ± 0.5	-2.3 ± 0.7	0.51221 ± 2
Kanto-B	1	0.4 ± 0.3	-0.3 ± 0.1	-0.6 ± 0.3	-1.3 ± 0.5	-2.1 ± 0.7	0.51220 ± 1
AA-99	8	-0.1 ± 0.5	-0.1 ± 0.1	0.0 ± 0.2	0.0 ± 0.7	-0.4 ± 1.1	0.512147 ± 9
AA-99.99	10	0.9 ± 0.5	-0.4 ± 0.2	-0.9 ± 0.3	-1.7 ± 1.0	-3.0 ± 1.4	0.511560 ± 9
JM	3	0.5 ± 0.3	-0.2 ± 0.2	-0.6 ± 0.2	-1.2 ± 0.4	-2.5 ± 1.0	0.512241 ± 5
Mitsuwa	2	0.1 ± 0.8	0.1 ± 0.5	0.2 ± 0.9	0.3 ± 1.6	0.6 ± 3.3	0.511476 ± 8
Merck	4	-0.2 ± 0.4	0.2 ± 0.4	0.3 ± 0.7	0.6 ± 1.2	1.3 ± 2.8	0.511471 ± 3
SPEX	4	2.5 ± 0.2	-1.3 ± 0.1	-2.4 ± 0.1	-4.5 ± 0.6	-6.8 ± 0.6	0.511716 ± 5
CERAC	3	0.0 ± 0.5	0.0 ± 0.2	0.1 ± 0.3	0.3 ± 0.5	0.4 ± 0.3	0.512122 ± 7
LaJolla	2	2.1 ± 0.1	-1.0 ± 0.2	-2.0 ± 0.3	-3.8 ± 0.8	-5.5 ± 1.2	0.511850 ± 7
JNdi-1[*1]	37	0.0 ± 0.5	0.0 ± 0.2	0.0 ± 0.2	0.0 ± 0.5	0.0 ± 1.0	0.512105 ± 9

Errors are 2SD except for Kanto-A and Kanto-B where represented errors are 2SE of measurement.

[*1] Epsilon values of average JNdi-1 are 0 by definition.

Fig. 3.1 Calculated deviation of liner and liner form exponential approximation law from exponential law in $^{146}Nd/^{144}Nd$.

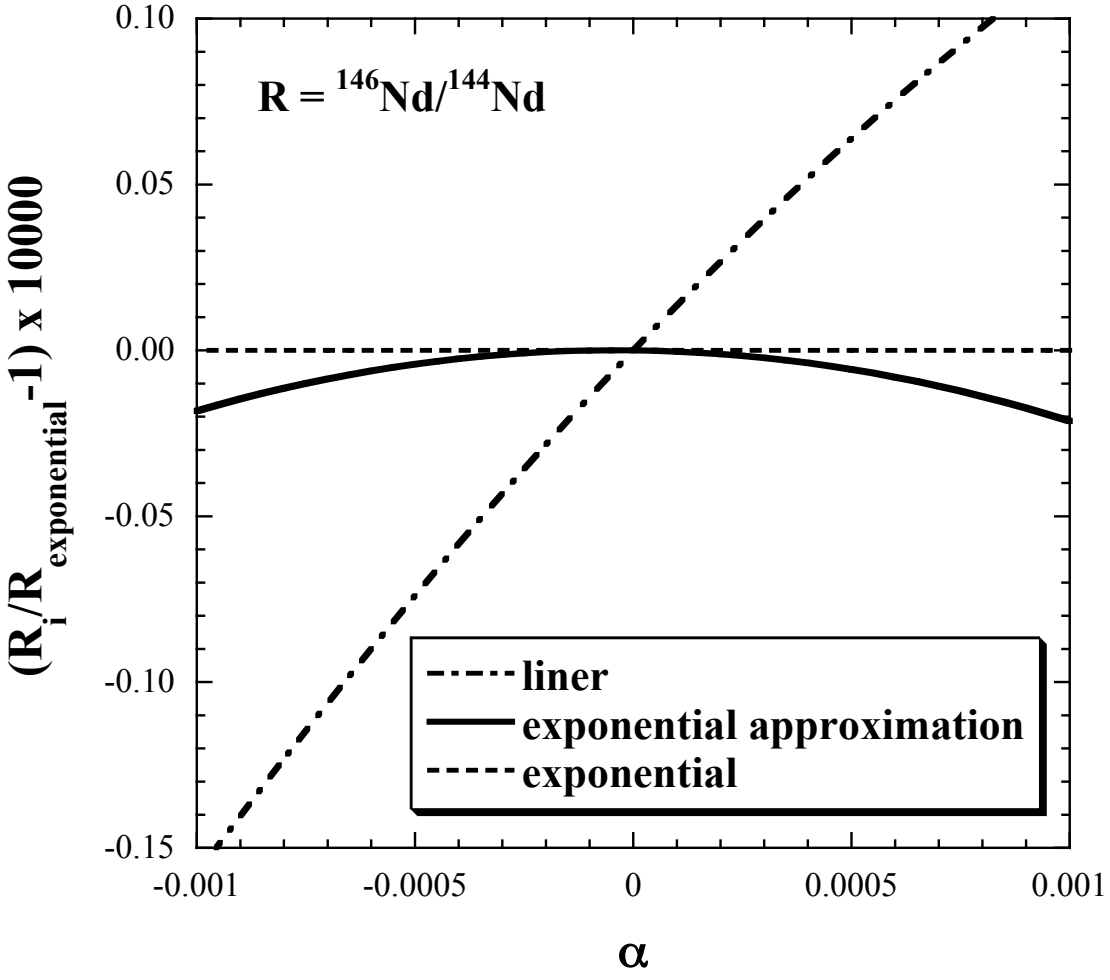

Fig. 3.2 Example of the results of error propagation simulation. Calculated error magnification factor of $^{149}Sm/^{150}Sm$ ratio is plotted against the spike composition of a ^{150}Sm-^{154}Sm double spike. Five curves corresponds to five different choices of the three isotope ratios used in the double spike deconvolution.

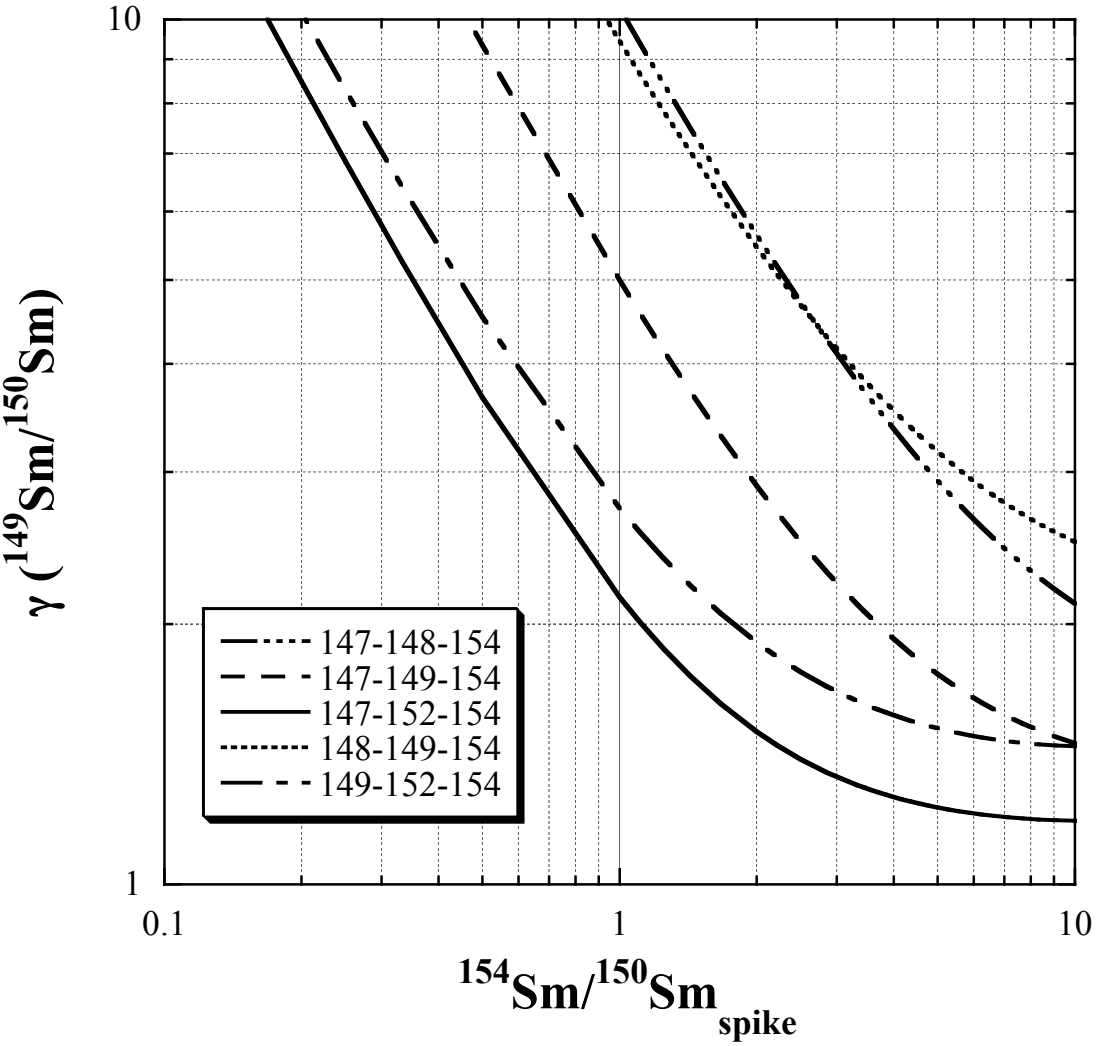

Fig. 3.3 (a) Neodymium isotope composition of 11 replicate analysis of in-house Nd reference material, JNdi-1, in a single analytical session. Red lines show the 2SD range. (b) Epsilon ^{146}Nd values of JNdi-1 for six analytical sessions showing long term reproducibility of this number.

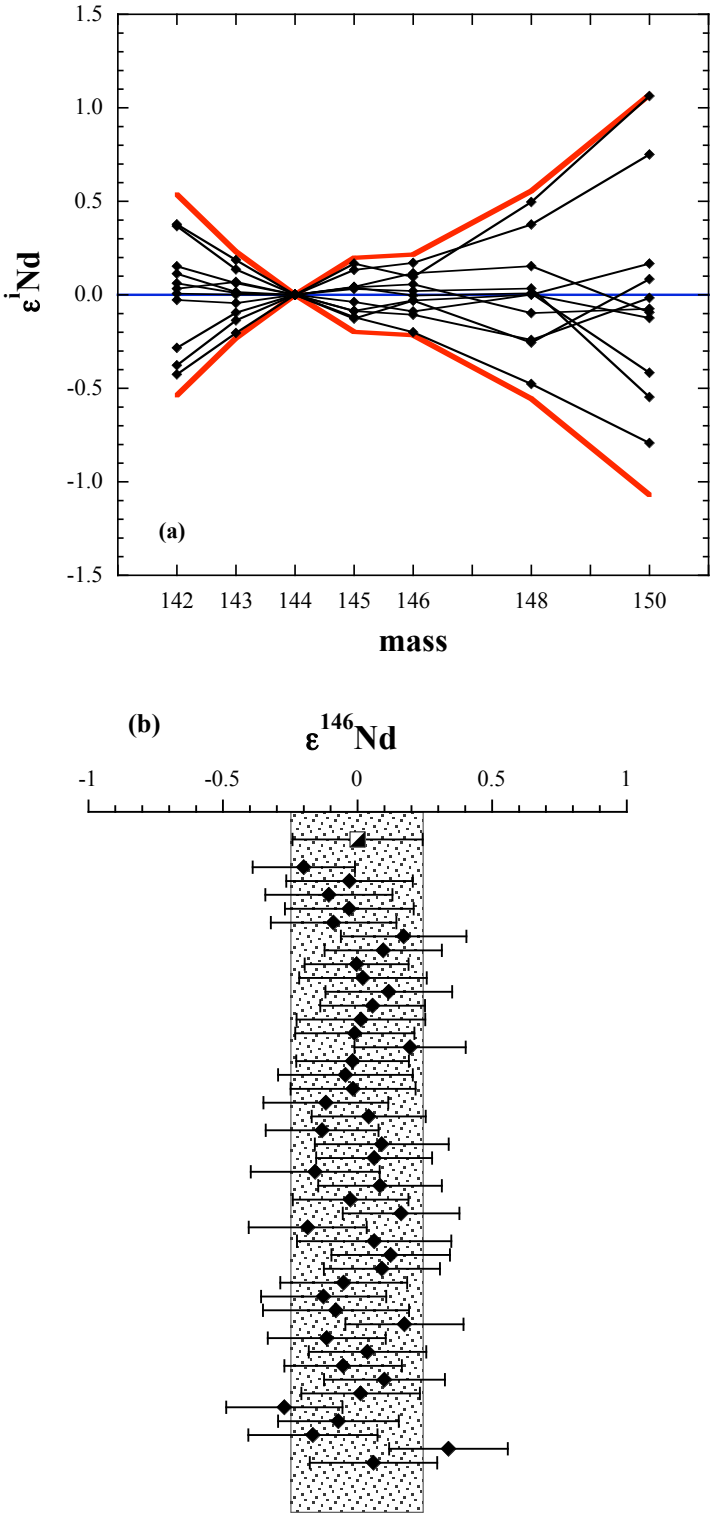

Fig. 3.4 (a) Samarium isotope composition of 11 replicate analysis of in-house Sm reference material in a single analytical session. Red lines show the 2SD range. (b) Epsilon ^{148}Sm values of in-house Sm reference material for 4 analytical sessions.

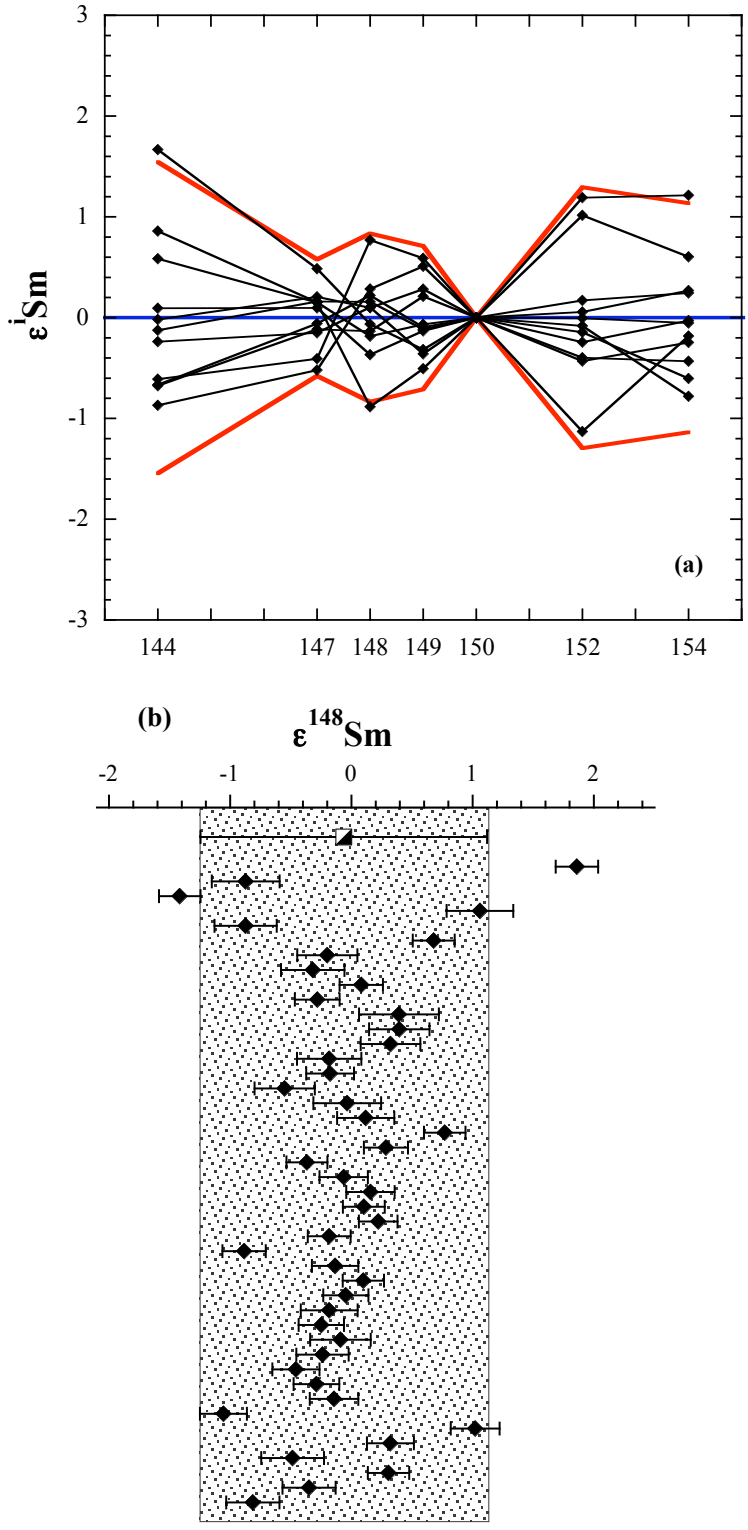

Fig. 3.5 Isotope fractionation behavior of Nd during cation exchange column chromatography. (a) Elution curve of Nd. (b) Stable isotope compositions of 7 eluted fractions are plotted against the percentage of Nd in probability scale.

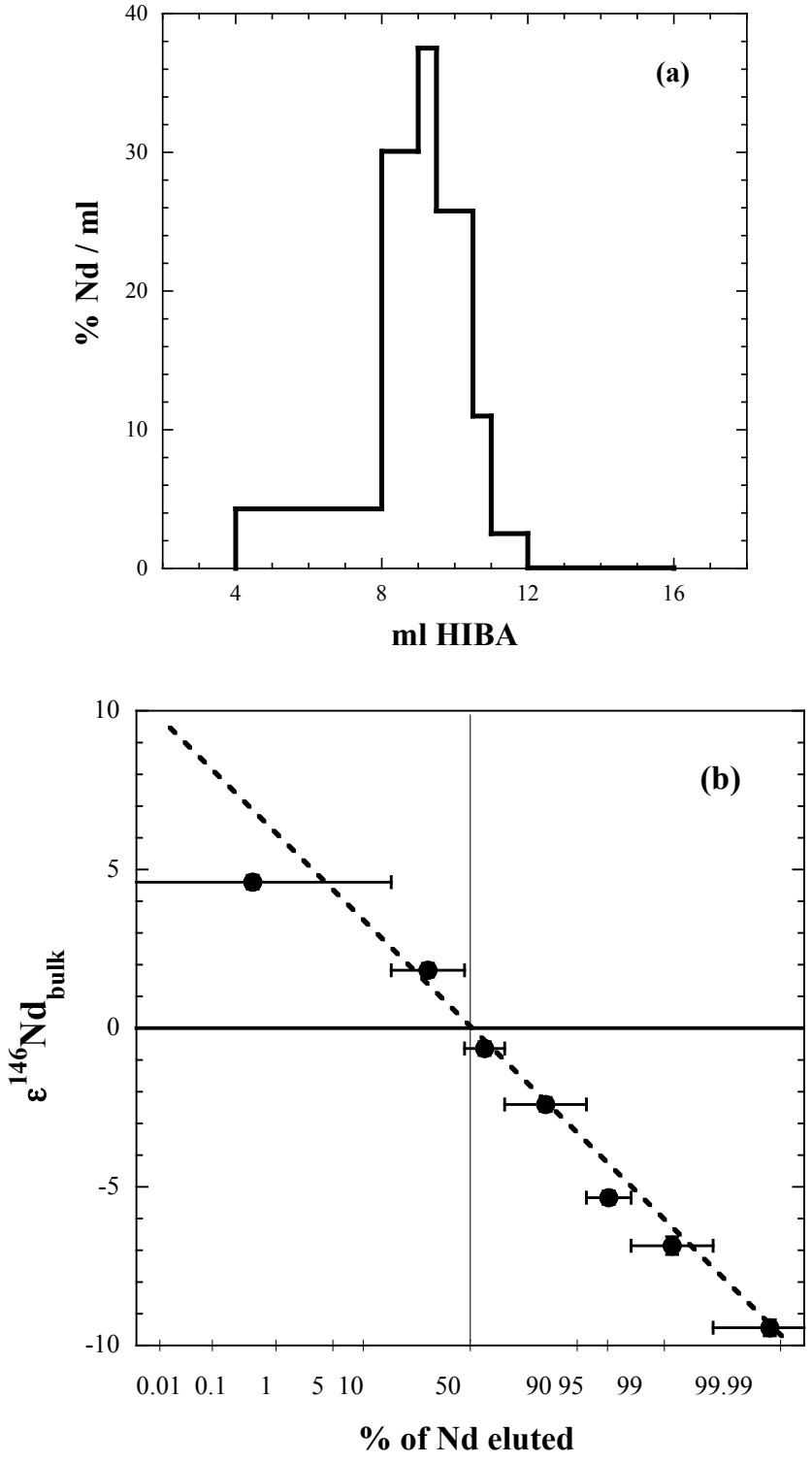

Fig. 3.6 Isotope fractionation behavior of Sm during cation exchange column chromatography. (a) Elution curve of Sm. (b) Stable isotope compositions of 8 eluted fractions are plotted against the percentage of Sm in probability scale.

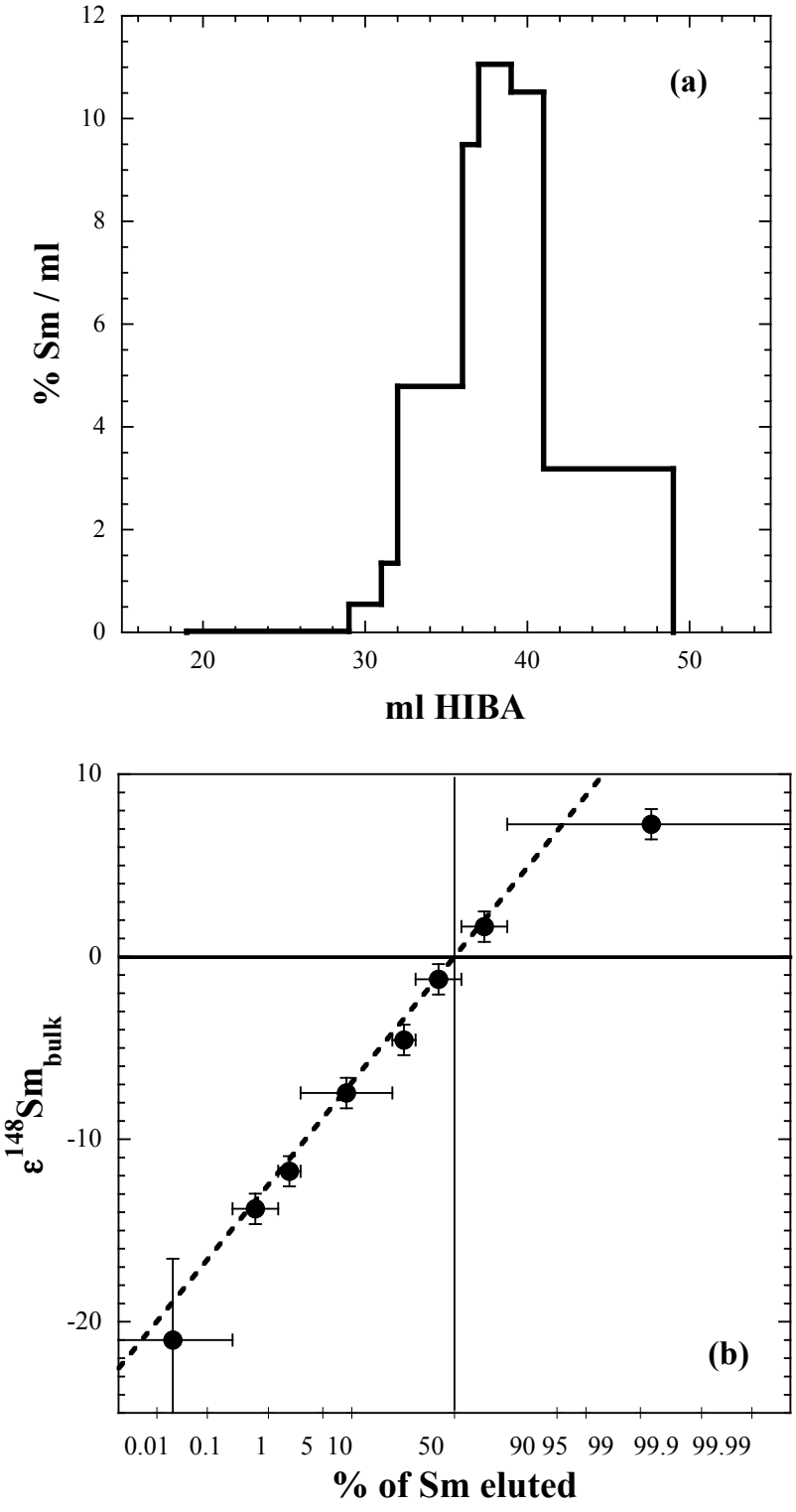

Fig. 3.7 Stable isotope composition of 10 commercial Nd_2O_3 reagents and two isotope reference materials, La Jolla and JNdi-1. (a) Epsilon ^{146}Nd, (b) Epsilon ^{148}Nd and (c) correlation of epsilon ^{146}Nd and Epsilon ^{148}Nd. Bold line shows mass dependent fractionation curve.

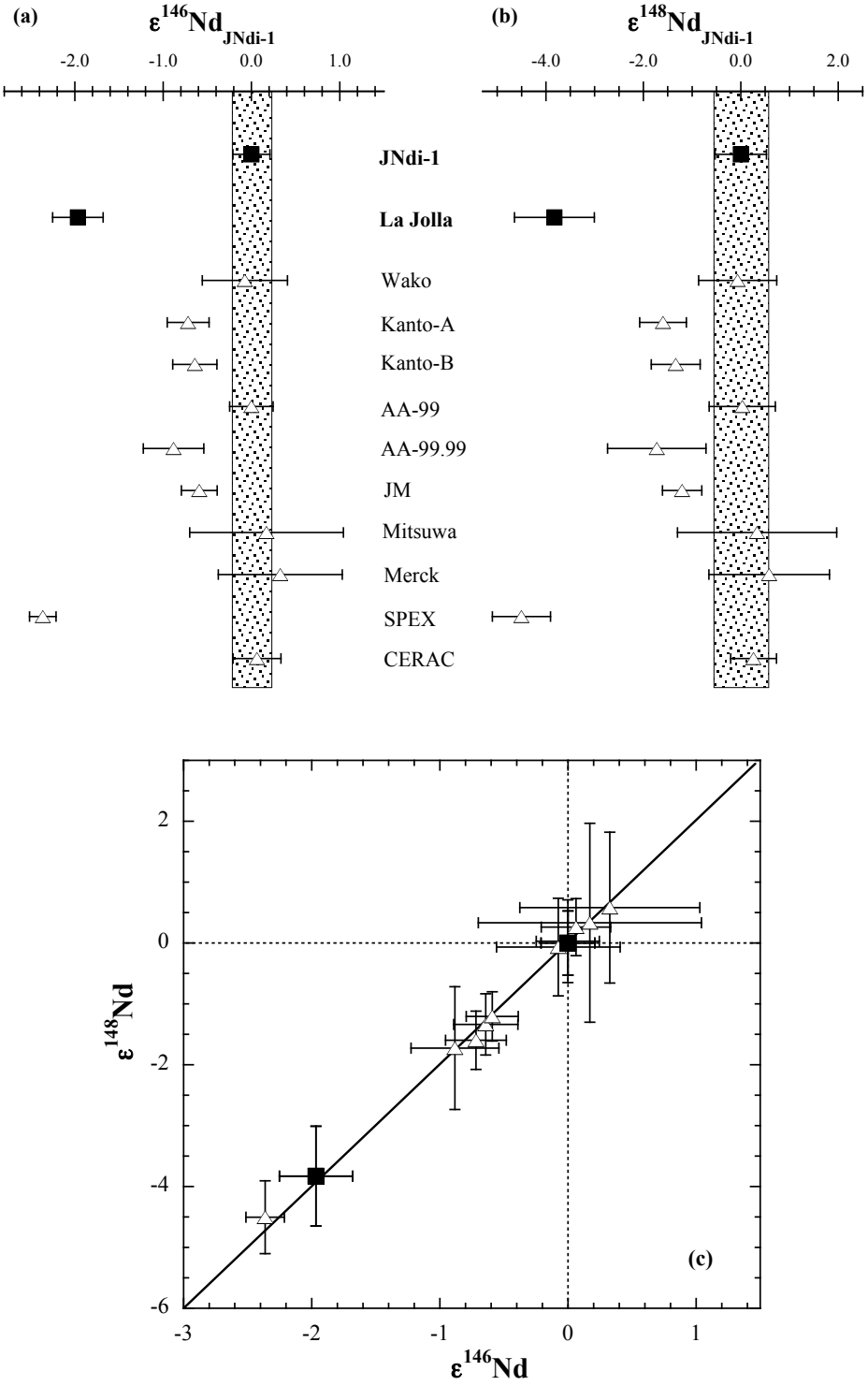

Fig. 3.8 Epsilon ^{146}Nd values of reagents (open triangles) and column separated fractions (filled circle) calculated by different spike calibration schemes.

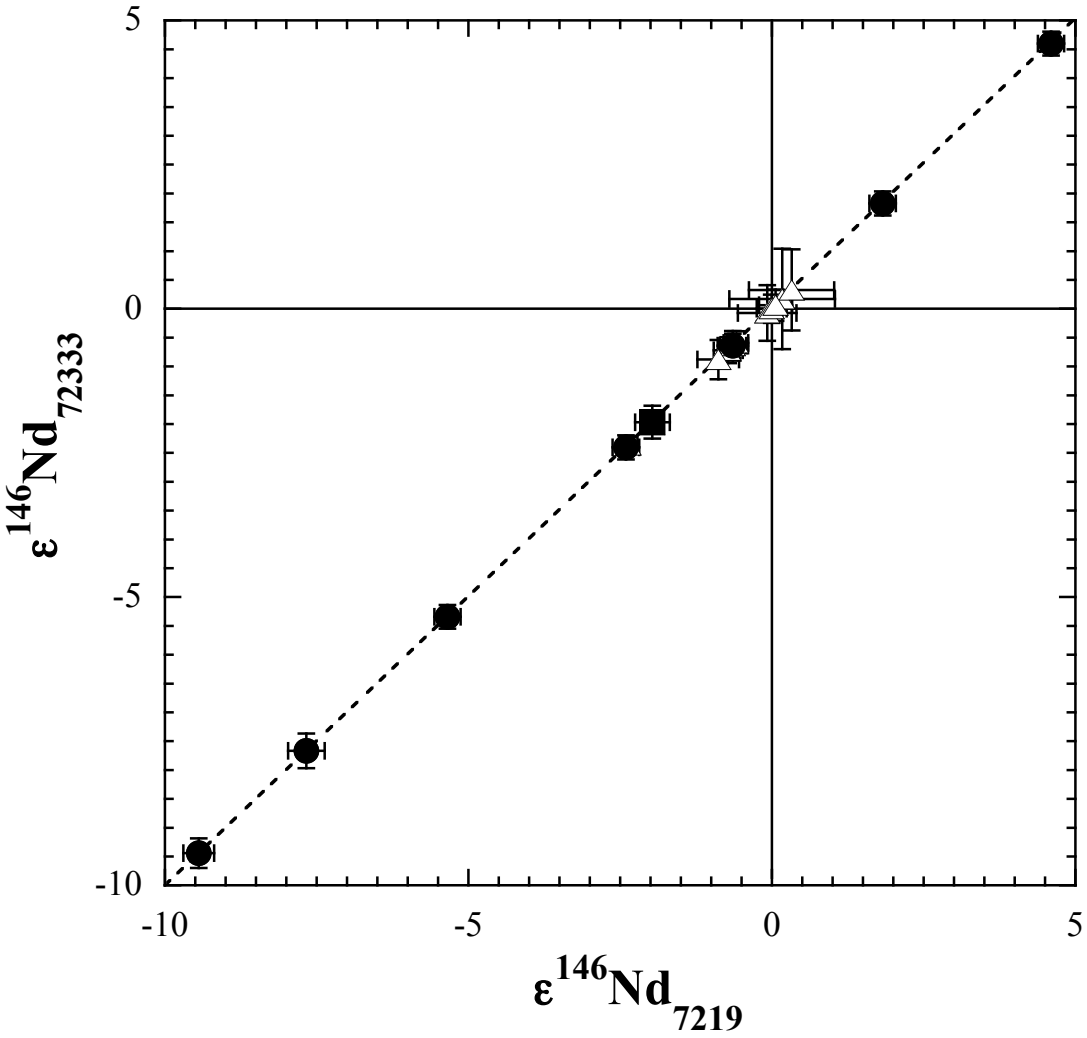

Chapter 4

Stable isotope fractionation of Nd in nature

4.1 Introduction

Fractionation of the non-traditional stable isotopes (i.e. stable isotopes of intermediate- to high-atomic number elements) in nature is acquiring special interest in geochemistry. As analogous to the conventional stable isotopes, mass-dependent fractionation of the non-traditional stable isotopes by both equilibrium and kinetic chemical reactions generates natural variations in stable isotope composition of these elements among various geological materials. Conventional stable isotopes are probed to be a useful tool for tracing geological events or chemical reactions, which the sample had under went in its history. Studies of non-traditional stable isotopes on some elements, thoroughly reviewed in [1], showed that non-traditional stable isotopes could also be used to trace a history of geological matter. Every element in a geological sample have different histories: different sources, different reaction pathways, etc.. Therefore, stable isotopes of different elements likely to contain clues for various events which the sample has underwent. It is worth studying stable isotopes of multiple elements in a given sample to figure out its history.

Neodymium is a forth element in group of rare earth elements (REEs). Variations in the $^{143}Nd/^{144}Nd$ isotopic ratio produced by the radioactive decay of ^{147}Sm to ^{143}Nd, with a half-life of 106 billion years (Gy), is widely studied among various geological materials for dating purposes or to constrain the origin and history of the material [2]. The elemental fractionation pattern of REEs is also a widely used geochemical tool, which gives constraints about the origin of the sample. Study of the stable isotopes of Nd, in systematic combination with the two existing methodologies, radiogenic Nd isotope and the elemental fractionation pattern of REEs, may be a powerful geochemical tool providing multi-dimensional and consistent information regarding the age, the origin and the history of the sample. Ohno [3] have recently studied stable isotopes of Nd and Ce by MC-ICP-MS, and found heavy isotope enrichment for both elements on one dolomite sample (GSJ reference rock JDo-1). However, detailed studies on natural variation of stable Nd (and Ce) isotopes are not yet made.

This chapter will provide the first detailed and systematic investigation on stable isotopes of Nd in various geological materials to demonstrate whether variation in stable isotopes of Nd can be used to trace various geochemical reactions. The theory of equilibrium isotope fractionation by Bigeleisen and Mayer predicts a large isotope fractionation in low-temperature environments. Marine carbonate rocks are good examples of a product of low-temperature chemical reactions. Stable isotope variations in marine carbonate rocks are studied

in detail to investigate the possible mechanism causing isotope fractionation. Igneous rocks are also studied to estimate the bulk earth stable isotopic composition.

4.2 Samples

Samples are selected to cover a wide range of terrestrial materials. Eleven samples are reference rocks of the geological survey of Japan, which includes two basalts (JB-1b and JB-2), two granites (JG-1a and JG-2), three rhyolites (JR-1, JR-2 and JR-3), Fe-Mn nodule from central pacific (JMn-1), limestone (JLs-1), dolomite (JDo-1) and coral (JCp-1). Other silicate rocks analyzed are chert (SH) and banded ferruginous chert (FBC) from the Barberton Greenstone belt [4], Columbia River flood basalt (USGS reference rock, BCR-1) and rhyoritic welded tuff from the Nohi Rhyorite complex (AWT) [5]. Thirteen marine-carbonate rocks are from Akiyoshi (96-1 and 96-5), France(chalk), Ibuki (Ibuki-Cal.-1 and Ibuki-Cal.-2), Ishimaki (Ishimaki-1), kuzuu (kuzuu-d, kuzuu-6, kuzuu-39, kuzuu-45, kuzuu-55 and kuzuu-64) and torinosu (96-2). One sample, kuzuu-d, is dolomite and two samples chalk and 96-2 are continental platform type limestone. Other samples are seamount type limestone. Detail geological descriptions and major element data of Kuzuu samples are previously reported by Fujinuki et al. [6]. Dolomite sample from kasuga (kasuga-b) have underwent severe metamorphism. Three non-marine dolomites are from Bamle, Telemark, Norway (telemark); Brumado, bahia, Brazil (bahia); Eugui, Navarra, Spain (spain). The later two samples was dolomite crystal. Branchs of a bamboo (*Phyllostachys nigra Munro var. henonis Stapf*) collected in the campus of Nagoya University is also analyzed.

4.3 Experimental

Samples were decomposed by standard techniques: silicate samples were decomposed with mixed HF-$HClO_4$-HNO_3, Fe-Mn nodule was decomposed by 6M-HCl with small quantities of H_2O_2 and carbonate samples were leached by 6M-HCl. Residues of the leached carbonate samples, which probably include silicate and organic matter, were removed from the solution prior to the following chemical treatment. An aliquot of the sample was spiked with REE spikes just after sample decomposition for isotope dilution analysis.

Neodymium was separated from the other elements by four-step cation exchange column chromatography. First, REEs were separated from major elements with HCl media. Some of the large carbonate samples were split into several fractions not to exceed the cation

exchange capacity of the column. Neodymium was then separated from the other REEs with alpha-hydroxyisobutyric acid (HIBA) media. As demonstrated in chapter 3, preferential loss of the early or the late eluted fractions of Nd in this separation step might cause serious artificial isotope fractionation. To avoid this situation, care was taken to keep the column yield as high as possible. This step was repeated to purify the Nd fraction. Final step was made with HCl media to remove HIBA from the Nd fraction. An aliquot of the Nd fraction was finally spiked with Nd double-spike. Details of mass spectrometry and stable isotope analysis are given in chapter 3. Results of the stable isotope analysis of Nd are expressed in epsilon notation (parts par 10^4) relative to JNdi-1:

$$\varepsilon^{i}Nd = \left(\frac{{}^{i}Nd/{}^{144}Nd_{sample}}{{}^{i}Nd/{}^{144}Nd_{JNdi-1}} - 1 \right) \times 10^{4}. \qquad (4\text{-}1)$$

The value of radiogenic $^{143}Nd/^{144}Nd$ is normalized to $^{146}Nd/^{144}Nd = 0.7219$ [7] and reported in a conventional manner. Abundance of Ca, Mg and Fe in carbonate samples are measured by atomic absorption spectrometry.

4.4 Results and discussion

4.4.1 Igneous rocks

Results of the stable Nd isotope analysis of igneous rocks are shown in table 4.1 and Fig 4.1. Analyzed igneous rock samples, basalts granites and rhyolites, show no variation in Nd stable isotopes beyond analytical error. The average of the analyzed igneous rocks overlaps the "epsilon zero" which is the average of the in-house reference material JNdi-1 by definition. However, small difference does exists between average igneous rocks and average JNdi-1 when considering standard error of the mean for these numbers: $\varepsilon^{146}Nd$ of the average igneous rock is -0.2 ± 0.1 (2SE, n = 11), $\varepsilon^{146}Nd$ of the average JNdi-1 is 0 ± 0.04 (2SE, n = 44). This difference has to be taken in to account when discussing small numbers of εNd.

4.4.2 Carbonate rocks

The stable isotope compositions of Nd on marine carbonate rocks and non-marine dolomites are given in table 4.2 and Fig 4.2. The analyzed marine carbonate rocks show large and significant variations in $\varepsilon^{146}Nd$ values from -0.1 to 2.6. The result of GSJ reference rock JDo-1 (dolomite) is $\varepsilon^{146}Nd = 1.5 \pm 0.8$. This value is in agreement with the value previously

reported by Ohno [3]. Non-marine dolomites also shows significant variations in ε^{146}Nd values. A metamorphosed marine dolomite sample, kasuga-b, have the Nd isotope composition identical to the igneous rocks. The analyzed carbonate portion corresponds to only 50% of this sample: residue of the HCl-leach was 52.3% of the original sample. Moreover, Nd abundance in kasuga-b is 4 ~ 10 times higher than the other marine carbonate rocks analyzed in this study. These observation suggests that large part of Nd in this sample have been acquired during high-temperature metamorphic process from the co-existing silicates, which have Nd isotope composition indistinguishable from the igneous rocks, diluting the original nature of the seawater-derived Nd. The other dolomite sample bamle shows slight heavy isotope enrichment (ε^{146}Nd = 0.5). Two crystalline dolomites, burumado and eugui show very different Nd isotope compositions. The ε^{146}Nd value of eugui is 4.0 which is the heaviest Nd isotope composition measured so far. Burumado has Nd isotope composition indistinguishable from the igneous rocks. Since these samples are crystalline and high-temperature origin, difference of the Nd isotope composition are probably inherited from there source materials.

4.4.3 Mn nodule, coral, cherts and bamboo

The results of the stable Nd isotope compositions of Mn nodule, coral, cherts and bamboo are given in table 4.3 and Fig 4.3. Stable Nd isotope composition of Mn nodule, coral and bamboo agrees with the igneous rock average within analytical error. One chert sample, FBC, shows slight enrichment of the heavy Nd isotopes.

4.4.4 Variation of Nd stable isotopes in nature

The ε^{146}Nd values of all the sample analyzed in this study are summarized in fig. 4-4. The ε^{146}Nd of samples analyzed so far, including the samples measured by [3], varies from -0.5 to 4.0. Epsilon level variation of stable Nd isotope composition does exists in nature. The variation of Nd isotope composition is characterized by the heavy isotope enrichment of sedimentary rocks, especially marine carbonates rocks, and by the consistency of the igneous rocks. Samples enriched in light Nd isotopes (relative to igneous rocks) have not been found at this point.

4.4.5 Estimation of Nd stable isotope composition of the bulk silicate earth

Theoretical studies predict no or very small isotope fractionation in high-temperature chemical reactions. Since igneous rocks are formed at very high-temperature, isotope fractionation effect in igneous rock forming process is likely to be negligible. Consistency of the stable isotope composition among igneous rocks with different rock types and different sources implies that the source materials of these rocks, probably mantle material, have uniform Nd stable isotope composition. Stable Nd isotope composition of the bulk silicate earth (BSE), as analogous to radiogenic Nd isotope composition, probably represented by chondritic uniform reservoir (CHUR). Since mantle differentiation takes place at very high-temperature, isotope fractionation during mantle differentiation will be negligible and stable isotope composition of the differentiated mantle and that of the undifferentiated mantle is likely to be identical. Therefore, the consistent Nd stable isotope composition of igneous rocks will be a good estimation of the Nd stable isotope composition of the BSE.

4.4.6 Estimation of Nd stable isotope composition of the modern seawater

Both Mn nodule and coral are generated in marine environment. Neodymium in these materials are derived from seawater. Large difference in Nd concentration of these materials clearly indicates that the affinity of REEs for Fe-Mn oxide and biogenic carbonate is very different. The chemical characteristics of these two materials are also very different. These conditions predict that the equilibrium isotope-fractionation factor between seawater and Fe-Mn oxide differs from that between seawater and biogenic carbonate. Therefore, the consistency of Nd stable isotope composition of these two materials implies that isotope fractionation did not occur during the incorporation of REEs into these materials: if fractionation takes place, it will fractionate Nd isotopes in different degree between two materials. Consequently, these two materials can be considered as a proxy of seawater regarding stable Nd isotope composition. The estimation of the stable isotope composition of modern seawater in this study is $\varepsilon^{146}Nd$ = 0.2, which is an average of the measured stable isotope ratios of Fe-Mn nodule and coral.

4.4.7 Isotope fractionation of Nd during carbonate rock formation process

Large variation found in stable Nd isotope composition of the marine carbonate rocks implies that isotope fractionation of Nd took place during carbonate rock forming process. Most of the marine carbonate rocks analyzed in this study is a seamount type limestones and dolomites. Seamount-type carbonate rocks are formed in a pelagic zone with almost no input of terrigenous materials. Thus, REEs in seamount-type carbonate rocks are of seawater origin with no or negligible terrigenous contamination. This is demonstrated by the typical seawater-like REE fractionation pattern of kuzuu carbonate rocks with negative Ce and Eu anomalies and concave tetrad-effects [8].

Formation process of the seamount-type carbonate rocks can be modeled as follows: 1) biogenic carbonates (aragonite and/or calcite) are formed on a top of a seamount by some living organisms, 2) biogenic carbonates turn into limestone (inorganic calcite) by diagenetic process, 3) dolomitization of limestone took place for dolomite samples. Incorporation of REEs from seawater into carbonate rocks and also isotope fractionation of Nd should have taken place in one of these processes. The third process, dolomitization, could not be a major process for Nd isotope fractionation, because heavy-isotope enrichment was found not only in dolomites but also in limestones. Moreover, Miura et al. [8] have studied REE fractionation pattern of limestones and dolomites in the kuzuu carbonate rock complex and concluded that dolomitization of the kuzuu dolomites did not affect the REE features of the precursor limestone. Biological intake of REEs into limestone precursor biogenic carbonate is also unlikely to be a major process for Nd isotope fractionation. REE abundances of present-day biogenic carbonates are about three orders of magnitude lower than the typical REE abundance found in the analyzed seamount-type carbonate rocks [9]. To account for ε^{146}Nd values of 2.0, for example, in a limestone only by the biological intake, ε^{146}Nd values of about 200 is required for the biogenic carbonate. This value is clearly impractical.

The difference of REE abundances between limestones and biogenic carbonates indicate that limestones have concentrated its Nd content in diagenetic process. During diagenesis, biogenic carbonate reacts with seawater to form inorganic calcite. This inorganic reaction between seawater and calcite is most likely to be responsible for Nd isotope fractionation. Heavy isotope enrichment in limestones compared to the estimated modern seawater indicates that Nd forms stiffer bond in $CaCO_3$ structure than forming a complex in the seawater. Nd isotope composition of seawater do not need to change if the amount of seawater

is large enough to buffer the fractionation effect of calcite precipitation.

Experimentally determined distribution coefficients for REEs between calcite and synthetic seawater [10, 11] suggests that if the calcite is in equilibrium with seawater, Nd/Ca molar ratio in calcite will be 1000 to 20000 times enriched from that of seawater. Nd/Ca molar ratios in most of the analyzed carbonate rocks and the range of Nd concentrations in modern seawater indicates that these carbonate rocks are close to the equilibrium concentration of the reaction between modern-seawater (Fig. 4.5.). This implies that the reaction between paleo-seawater and limestone reached or nearly reached the equilibrium condition. Since isotope exchange reaction is part of a chemical reaction, equilibrium condition for a chemical reaction is linked with equilibrium condition for isotope exchange reaction. Consequently, stable Nd isotope composition of marine carbonate rocks probably records equilibrium or near equilibrium condition of the isotope exchange reaction between seawater and inorganic calcite.

4.5 Conclusion

Stable isotope compositions of Nd in various terrestrial materials are studied in detail by double spike TIMS technique. No variation in stable Nd isotopes is found among igneous rocks analyzed so far. The consistency of stable Nd isotopes in igneous rocks suggests uniform stable Nd isotope composition of the mantle material. The ε^{146}Nd value of the BSE and the modern-seawater was estimated as = -0.1 and 0.3, respectively. Large variation in Nd isotope composition was found in marine carbonate rocks. Equilibrium or near equilibrium condition of the isotope exchange reaction between seawater and inorganic calcite is probably responsible for the variation found in marine carbonate rocks.

References

[1] C. M. Johnson, B. L. Beard and F. Albarède, 2004, Overview and general concepts, *Rev. Mineral Geochem*. **55**, 1-24.

[2] A. P. Dickin, 1995, *Radiogenic Isotope Geology*, Cambridge University Press.

[3] T. Ohno, 2006, Development of analytical methods for stable isotope geochemistry of non-traditional elements (Fe, Zn, Sr and REEs) using MC-ICPMS. Doctoral thesis, Tokyo Inst. Tech.

[4] T. Hayashi, T. Tanimizu and T. Tanaka, 2004, Origin of negative Ce anomalies in Barberton sedimentary rocks, deduced from La-Ce and Sm-Nd isotope systematics, *Precambrian Res*. **135**, 345-357.

[5] S. Wakaki and T. Tanaka, 2005, Single mineral Rb-Sr isochron dating applied to the Nohi Rhyorite and a quartz porphyry dyke, central Japan, *Geochem. J.* **39**, 21-28.

[6] T. Fujinuki, T. Igarashi and C. Hosogoe, 1982, Geochemical study of the Permian carbonate rocks from the Kuzuu district, Tochigi prefecture, central Japan, *Bull. Geol. Surv. Japan*, **33**, 187-206.

[7] R. K. O'Nions, P. J. Hamilton and N. M. Evensen, 1977, Variations in $^{143}Nd/^{144}Nd$ and $^{87}Sr/^{86}Sr$ ratios in oceanic basalts, *Earth Planet. Sci. Lett*. **34**, 13-22.

[8] N. Miura, Y. Asahara and I. Kawabe, 2004, Rare earth element and Sr isotopic study of the Middle Permian limestone-dolostone sequence in Kuzuu area, central Japan: Seawater tetrad effect and Sr isotopic signatures of seamount-type carbonate rocks, *J. Earth Planet. Sci. Nagoya Univ.* **51**, 11-35.

[9] H. F. Shaw and G. J. Wasserburg, 1985, Sm-Nd in marine carbonates and phosphates: Implications for Nd isotopes in seawater and crustal ages, *Geochim. Cosmochim. Acta* **49**, 503-518.

[10] K. Tanaka and I. Kawabe, 2006, REE abundances in ancient seawater inferred from marine limestone and experimental REE partition coefficients between calcite and aqueous solution, *Geochem. J.* **40**, 425-435.

[11] S. Zhong and A. Mucci, 1995, Partitioning of rare earth elements (REEs) between calcite and seawater solutions at 25˚C and 1 atm, and high dissolved REE concentrations, *Geochim. Cosmochim. Acta* **59**, 443-453.

[12] D. J. Piepgras and S. B. Jacobsen, 1992, The behavior of rare earth elements in seawater: Precise determination of variations in the North Pacific water column, *Geochim. Cosmochim. Acta* **56**, 1851-1862.

[13] N. Imai, S. Terashima, S. Itoh and A. Ando, 1996, 1996 compilation of analytical data on nine GSJ geochemical reference samples, "sedimentary rock series", *Geostandards and Geoanalytical Res.* **20**, 165-213.

Table 4.1 Stable and radiogenic Nd isotope compositions of igneous rocks.

Sample	Nd [ppm]	ε^{142}Nd ± 2SE	ε^{145}Nd ± 2SE	ε^{146}Nd ± 2SE	ε^{148}Nd ± 2SE	ε^{150}Nd ± 2SE	^{143}Nd/^{144}Nd ± 2SE
basalt							
JB-1b	26.2	0.5 ± 0.2	-0.1 ± 0.1	-0.5 ± 0.2	-0.9 ± 0.4	-1.7 ± 0.6	0.512777 ± 2
JB-2	6.28	-0.1 ± 0.2	0.0 ± 0.1	-0.2 ± 0.2	-0.2 ± 0.4	-0.5 ± 0.6	0.513090 ± 2
	6.25	0.1 ± 0.3	0.2 ± 0.2	-0.1 ± 0.3	-0.1 ± 0.6	-0.4 ± 0.9	0.513089 ± 3
	6.19	0.0 ± 0.3		-0.1 ± 0.2	-0.2 ± 0.5	-0.8 ± 0.7	0.513104 ± 3
	6.20	0.4 ± 0.3	0.1 ± 0.1	-0.3 ± 0.3	-0.2 ± 0.6	-0.3 ± 0.8	0.513104 ± 3
BCR-1	28.7	-0.2 ± 0.2	0.0 ± 0.1	-0.1 ± 0.2	0.0 ± 0.5	-1.0 ± 0.7	0.512635 ± 2
		-0.5 ± 0.2	0.0 ± 0.1	0.0 ± 0.2	0.3 ± 0.5	-0.7 ± 0.7	0.512637 ± 3
		0.2 ± 0.3	-0.2 ± 0.1	-0.4 ± 0.3	-0.8 ± 0.5	-1.4 ± 0.8	0.512631 ± 2
Average basalts		0.1 ± 0.6	0.1 ± 0.5	-0.2 ± 0.3	-0.3 ± 0.8	-0.9 ± 1.0	(2SD, n = 8)
granite							
JG-1a	20.4	0.0 ± 0.2	0.0 ± 0.1	-0.3 ± 0.2	-0.6 ± 0.4	-0.9 ± 0.5	0.512365 ± 2
	19.7	0.4 ± 0.2	-0.1 ± 0.1	-0.5 ± 0.2	-1.0 ± 0.4	-2.0 ± 0.7	0.512375 ± 2
JG-2	24.1	0.4 ± 0.2	0.0 ± 0.1	-0.3 ± 0.2	-0.7 ± 0.4	-1.7 ± 0.5	0.512219 ± 1
rhyolite							
JR-1	22.9	-0.3 ± 0.2	0.2 ± 0.1	0.3 ± 0.2	0.3 ± 0.4	-0.2 ± 0.6	0.512905 ± 2
JR-3	98.5	0.6 ± 0.2	-0.2 ± 0.1	-0.4 ± 0.2	-0.9 ± 0.4	-1.8 ± 0.6	0.512673 ± 1
		0.2 ± 0.2	-0.1 ± 0.1	-0.3 ± 0.2	-0.4 ± 0.4	-1.1 ± 0.7	0.512677 ± 2
AWT	33.2	0.3 ± 0.2	0.0 ± 0.1	-0.3 ± 0.2	-0.5 ± 0.4	-1.1 ± 0.7	0.512241 ± 2
Average Igneous rocks		0.1 ± 0.6	0.0 ± 0.4	-0.2 ± 0.4	-0.4 ± 0.9	-1.0 ± 1.1	(2SD, n = 11)

Table 4.2 Stable and radiogenic Nd isotope compositions of marine carbonate rocks.

Sample	CaO	MgO	Fe_2O_3	Nd	Sm	$\varepsilon^{142}Nd$	$\varepsilon^{145}Nd$	$\varepsilon^{146}Nd$	$\varepsilon^{148}Nd$	$\varepsilon^{150}Nd$	$^{143}Nd/^{144}Nd$
	[%]	[%]	[%]	[ppm]	[ppm]	± 2SE	± 2SE	± 2SE	± 2SE	± 2SE	± 2SE
Marine limestone											
96-1	56.0	0.45	0.01	1.19	0.266	-2.9 ± 0.2	0.5 ± 0.1	2.6 ± 0.2	5.3 ± 0.4	7.2 ± 0.6	0.512282 ± 2
96-5	53.4	0.41	0.18	1.67	0.324	-0.2 ± 0.2	0.5 ± 0.1	0.6 ± 0.2	1.4 ± 0.5	1.9 ± 0.7	0.512528 ± 2
chalk-l	55.7	0.39	0.07	2.09	0.409	-0.6 ± 0.3	0.3 ± 0.1	0.3 ± 0.3	0.7 ± 0.5	0.7 ± 0.8	0.512303 ± 2
IbukiCal.-1	56.0	0.57	0.04	2.26	0.402	-1.2 ± 0.2	0.8 ± 0.1	1.5 ± 0.2	3.1 ± 0.4	4.6 ± 0.7	0.512229 ± 2
IbukiCal.-2	55.9	0.25	0.02	0.659	0.139	-2.1 ± 0.2	1.0 ± 0.1	1.9 ± 0.2	3.7 ± 0.4	5.6 ± 0.6	0.512277 ± 2
Ishimaki-1	55.6	0.22	0.04	3.33	0.477	-0.8 ± 0.2	0.5 ± 0.1	0.9 ± 0.2	1.9 ± 0.4	2.2 ± 0.6	0.512308 ± 2
JLs-1	55.1[*1]	0.61[*1]	0.02[*1]	0.081	0.018	-0.9 ± 0.4		0.5 ± 0.4	-0.1 ± 0.8	0.5 ± 1.1	0.51224 ± 1
				0.081	0.018	0.3 ± 0.5		-0.1 ± 0.4	0.2 ± 0.9	1.4 ± 1.3	0.512264 ± 4
kuzuu- 6	55.17[*2]	0.76[*2]	0.17[*2]	1.53	0.266	-2.2 ± 0.2	1.1 ± 0.1	1.9 ± 0.2	3.9 ± 0.4	5.1 ± 0.7	0.512337 ± 2
kuzuu-39	48.40[*2]	6.21[*2]	0.15[*2]	2.49	0.394	-2.1 ± 0.3	0.8 ± 0.1	1.7 ± 0.3	3.9 ± 0.5	3.8 ± 0.8	0.512313 ± 4
kuzuu-45	44.80[*2]	9.37[*2]	0.12[*2]	2.36	0.392	-2.0 ± 0.2	1.1 ± 0.1	2.1 ± 0.3	4.1 ± 0.5	6.1 ± 0.7	0.512229 ± 3
kuzuu-55	55.90[*2]	0.58[*2]	0.05[*2]	1.73	0.282	-1.9 ± 0.2	0.9 ± 0.1	1.8 ± 0.3	3.5 ± 0.4	4.7 ± 0.6	0.512278 ± 2
kuzuu-64	52.29[*2]	2.28[*2]	0.43[*2]	3.41	0.593	-0.8 ± 0.2	0.4 ± 0.1	0.6 ± 0.3	1.2 ± 0.4	0.9 ± 0.6	0.512366 ± 2
96-2	56.1	0.26	0.19	8.03	1.73	-0.7 ± 0.2	0.5 ± 0.1	0.9 ± 0.2	1.9 ± 0.4	2.6 ± 0.6	0.512209 ± 2
				7.98	1.72	-1.4 ± 0.2	0.6 ± 0.1	1.1 ± 0.2	2.2 ± 0.4	2.3 ± 0.7	0.512196 ± 2
Marine dolomite											
JDo-1[*3]	34.1[*1]	18.7[*1]	0.01[*1]	4.16	0.710	-1.5 ± 0.8	0.9 ± 0.4	1.5 ± 0.8	3.0 ± 1.4	4.6 ± 2.6	0.512256 ± 8
kuzuu-d	34.1	18.7	0.02	3.95	0.634	-1.6 ± 0.2	1.0 ± 0.1	1.8 ± 0.2	3.8 ± 0.5	5.4 ± 0.7	0.512237 ± 2
				3.93	0.638	-2.0 ± 0.2	0.9 ± 0.1	1.4 ± 0.2	2.5 ± 0.4	3.1 ± 0.5	0.512224 ± 2
Non-marine dolomite											
kasuga-b	45.0	7.6	5.90	13.5	2.50	0.1 ± 0.2	-0.1 ± 0.1	-0.2 ± 0.2	-0.2 ± 0.4	-0.3 ± 0.6	0.512463 ± 2
				13.7	2.48	0.3 ± 0.2		0.1 ± 0.2	-0.3 ± 0.5	0.6 ± 0.7	0.512461 ± 2
burumado	29.7	20.3	0.05	0.326	0.122	0.4 ± 0.3		-0.3 ± 0.3	-0.5 ± 0.6	-0.7 ± 0.9	0.512578 ± 3
eugui	31.2	20.3	1.69	0.136	0.240	-3.9 ± 0.3		4.0 ± 0.3	8.3 ± 0.5	12.4 ± 0.9	0.512506 ± 4
bamle	30.6	17.8	3.65	6.92	3.62	-0.6 ± 0.3		0.5 ± 0.3	1.1 ± 0.6	0.8 ± 0.8	0.513466 ± 4

[*1] Data from Imai et al. (1996) [13].

[*2] Data from Fujinuki et al. (1982) [6].

[*3] Average and 2SD of 9 replicate analysis

Table 4.3 Stable and radiogenic Nd isotope compositions of Mn nodule, coral, cherts and bamboo.

Sample	Nd [ppm]	ε^{142}Nd ± 2SE	ε^{145}Nd ± 2SE	ε^{146}Nd ± 2SE	ε^{148}Nd ± 2SE	ε^{150}Nd ± 2SE	^{143}Nd/^{144}Nd ± 2SE
Mn nodule							
JMn-1	119	-0.3 ± 0.2	0.1 ± 0.1	0.3 ± 0.2	0.4 ± 0.4	0.4 ± 0.6	0.512346 ± 2
	118	-0.1 ± 0.2	0.1 ± 0.1	0.1 ± 0.2	0.3 ± 0.4	0.4 ± 0.5	0.512348 ± 2
coral							
JCp-1	0.0337	0.2 ± 0.3		-0.2 ± 0.2	-0.3 ± 0.5	-0.2 ± 0.7	0.512483 ± 2
Average		-0.1 ± 0.5	0.12 ± 0.03	0.1 ± 0.5	0.1 ± 0.8	0.2 ± 0.7	(2SD, n = 3)
chert							
FBC	3.62	-1.3 ± 0.3		1.0 ± 0.3	1.9 ± 0.5	3.1 ± 0.8	0.511224 ± 2
	-	-0.6 ± 0.2	0.2 ± 0.1	0.6 ± 0.2	1.4 ± 0.5	2.1 ± 0.7	0.511227 ± 3
	3.79	-0.7 ± 0.2	0.5 ± 0.1	0.4 ± 0.2	1.0 ± 0.4	0.7 ± 0.7	0.511251 ± 2
SH	3.29	-0.5 ± 0.2	0.3 ± 0.1	0.3 ± 0.2	0.7 ± 0.6	0.5 ± 0.7	0.511610 ± 2
bamboo							
bamboo-5	0.807	-0.2 ± 0.2		0.0 ± 0.2	0.1 ± 0.4	-0.2 ± 0.7	0.512211 ± 2
bamboo-6	0.830	0.7 ± 0.3	-0.1 ± 0.1	-0.5 ± 0.3	-0.9 ± 0.5	-1.3 ± 0.8	0.512207 ± 2

Fig. 4.1 Stable Nd isotope composition of igneous rocks. open squares, open diamonds, open triangles and open inverted triangles represent average igneous rocks, basalts, granites and rhyolites, respectively. Plotted errors are 2SD for the average igneous rocks and 2SE of the measurement for the rest of the sample.

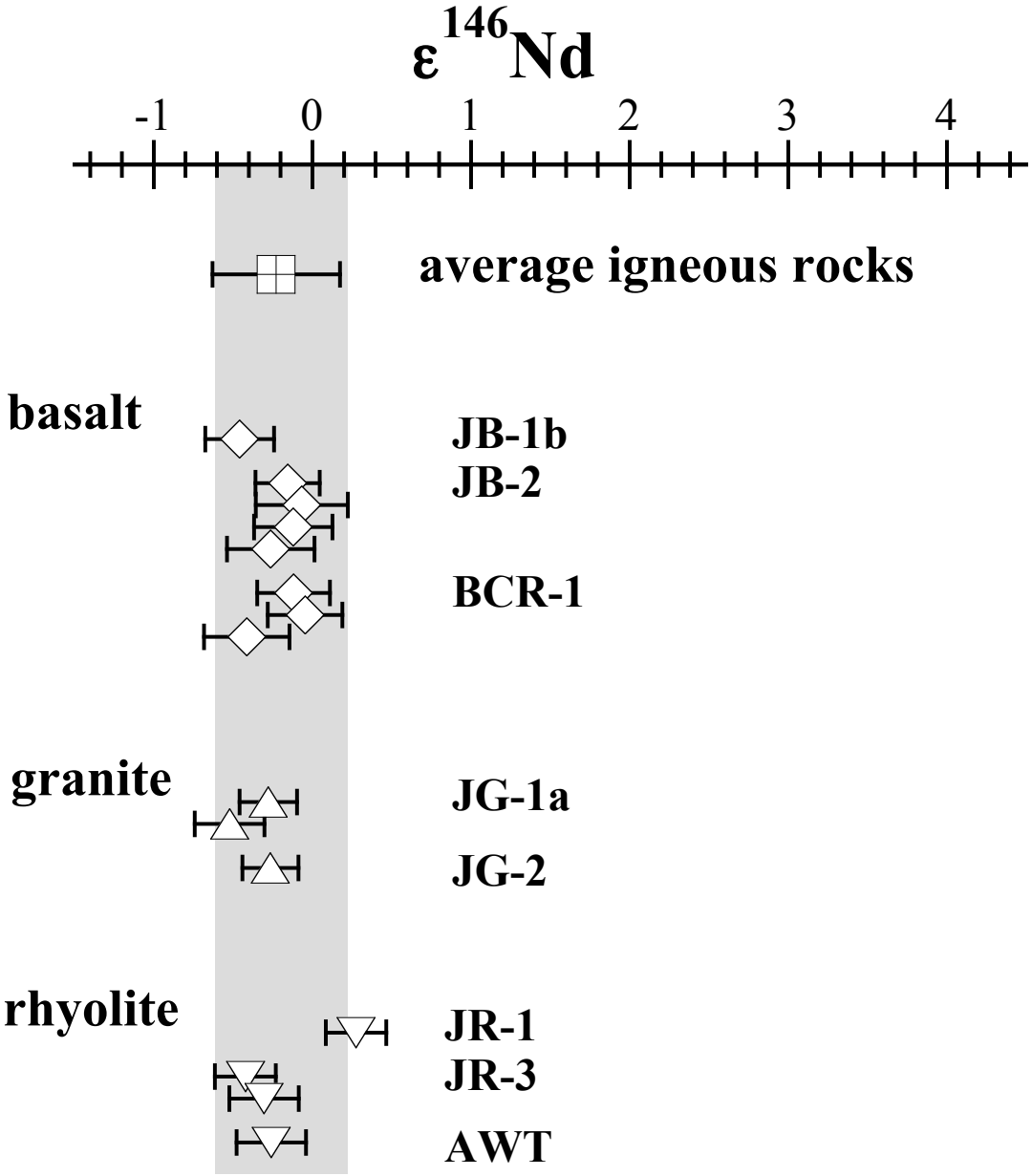

Fig. 4.2 Stable Nd isotope composition of marine carbonate rocks and non-marine dolomites. Filed squares and half-filed squares represent limestones and dolomites, respectively. Shaded area shows the range of the average igneous rocks. Plotted errors are 2SE of the measurement except for JDo-1 where 2SD uncertainties of nine replicate analysis are plotted.

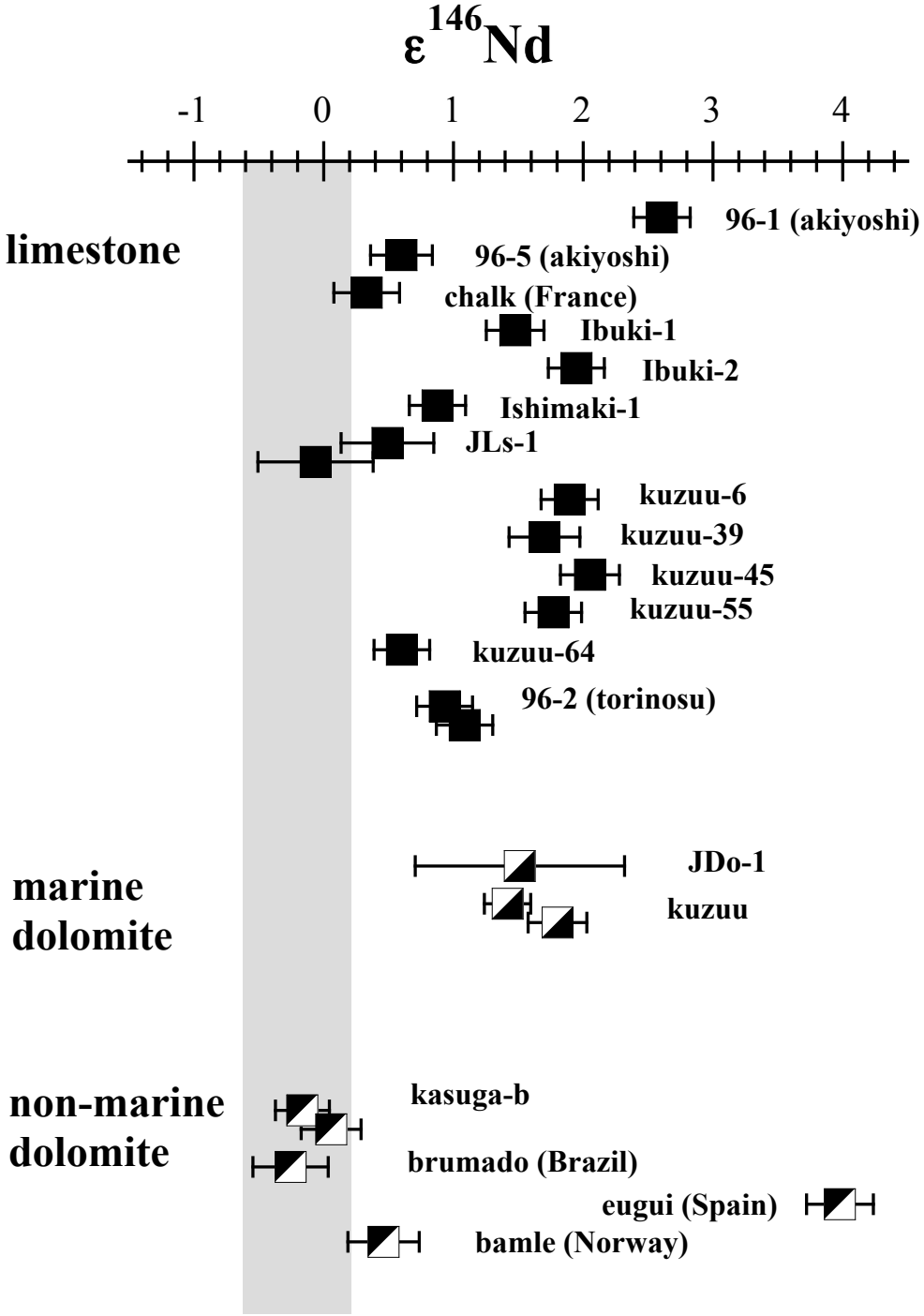

Fig. 4.3 Stable Nd isotope composition of Mn-nodule, coral, cherts and bamboo. Filled circles, open circle, open squares and cross marks represent Mn-nodules, coral, cherts and bamboos, respectively. Shaded area shows the range of the average igneous rocks. Plotted errors are 2SE of the measurement.

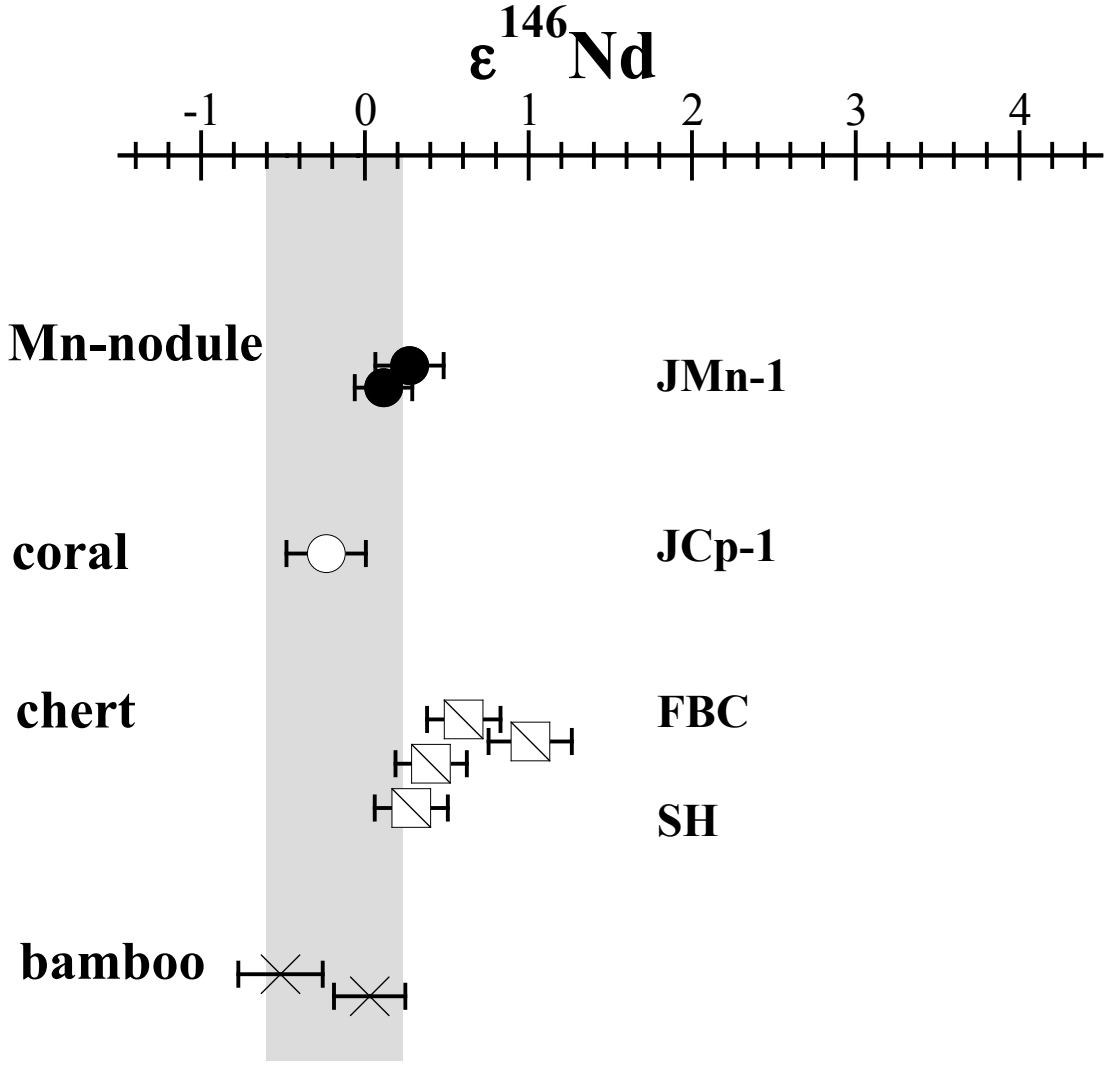

Fig. 4.4 Summary of the stable Nd isotope compositions of all samples analyzed in this study.

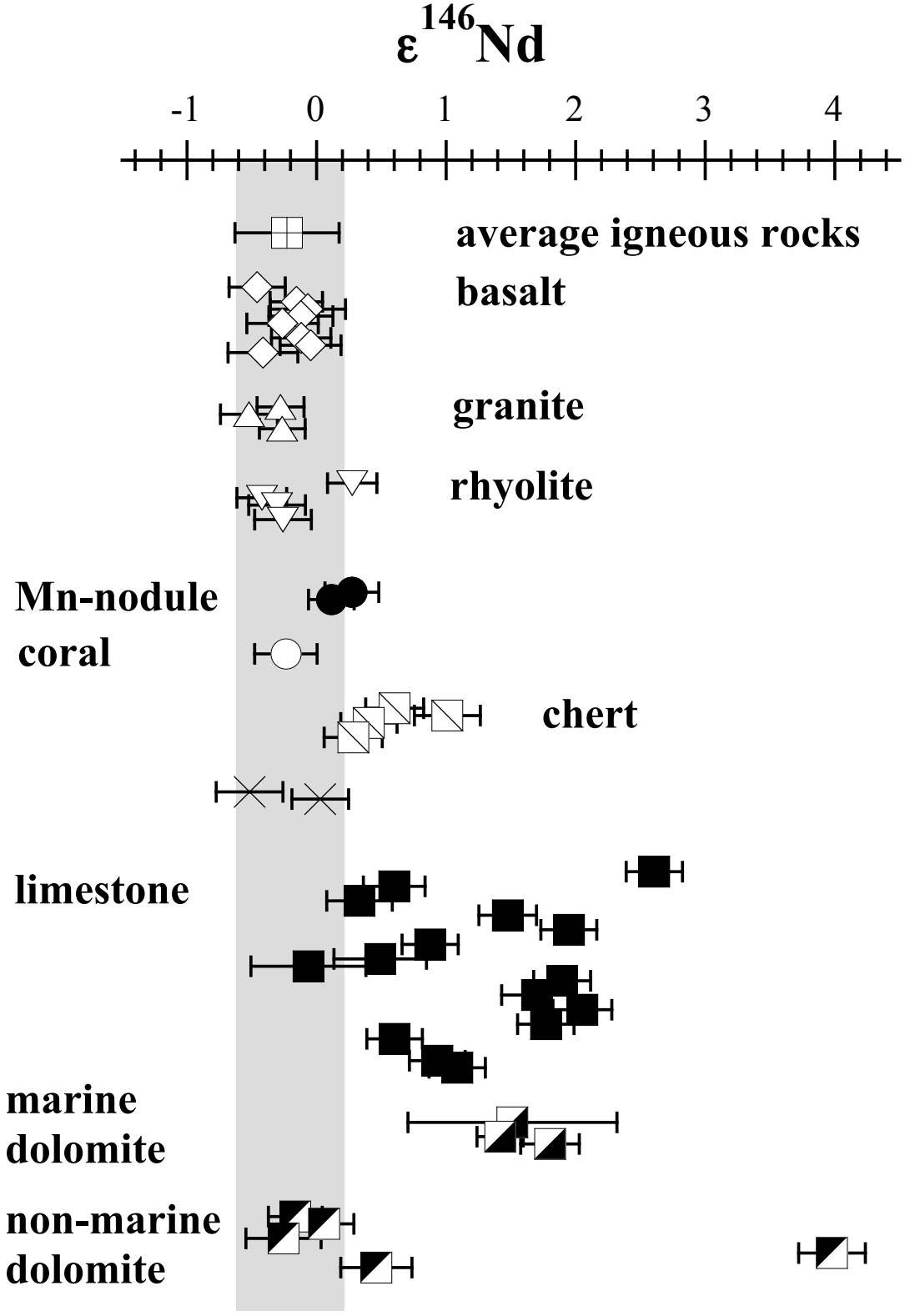

Fig. 4.5 Correlation between Nd and major cation (Ca and Mg) molar ratio and stable isotope composition of Nd in marine carbonate rocks. Large filed squares, small filed squares, half-filed squares and open circle represent seamount type limestones, continental platform type limestones, dolomites and modern-coral, respectively. Shaded area shows the range of the modern seawater. Nd concentration data in modern seawater were taken from [12]. Concentration range of biogenic carbonate calculated from [9] is also shown. Plotted errors are 2SE of the measurement.

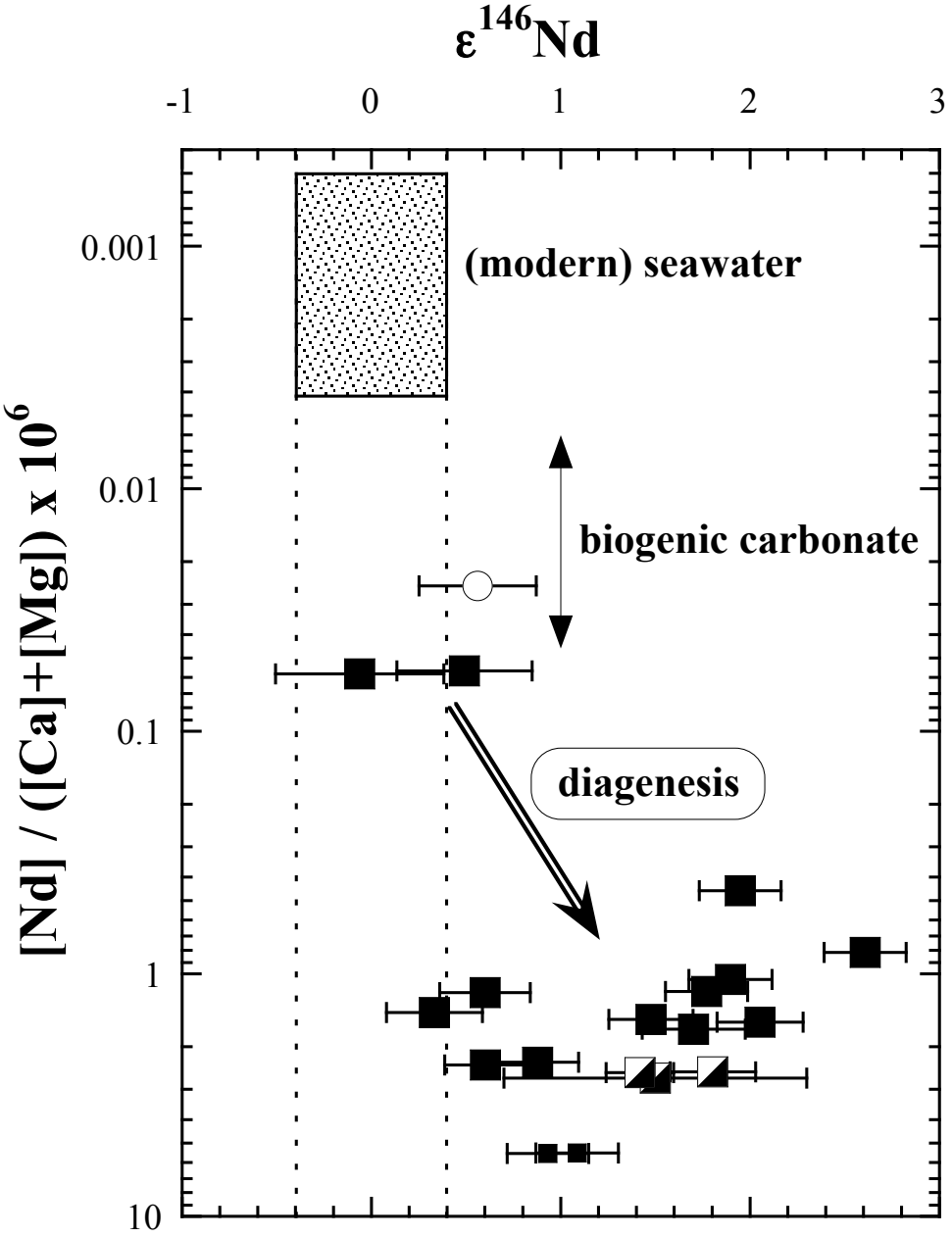

副論文

Isotope ratio measurements of trace Nd by the total evaporation normalization (TEN) method in thermal ionization mass spectrometry.

S. Wakaki, S. Shibata and T. Tanaka

International Journal of Mass Spectrometry **264**, 157-163 (2007).

（表面電離質量分析における TEN 法による微量 Nd の同位体比測定）

Available online at www.sciencedirect.com
ScienceDirect
International Journal of Mass Spectrometry 264 (2007) 157–163
International Journal of Mass Spectrometry
www.elsevier.com/locate/ijms

Isotope ratio measurements of trace Nd by the total evaporation normalization (TEN) method in thermal ionization mass spectrometry

Shigeyuki Wakaki *, Shin-Nosuke Shibata, Tsuyoshi Tanaka

Department of Earth and Planetary Sciences, Nagoya University, Chikusa, Nagoya 464-8601, Japan

Received 27 December 2006; received in revised form 6 April 2007; accepted 6 April 2007
Available online 12 April 2007

Abstract

Isotope ratios of very small Nd samples (0.1–5 ng) are measured by the total evaporation normalization (TEN) method. Samples as small as 0.5 ng can be measured with an external precision of 140 ppm by this method. The average $^{143}Nd/^{144}Nd$ ratio of the samples with the measured electric charge Q (^{143}Nd) = 10–50 × 10^{-11} corresponds roughly to 0.5 ng JNdi-1, is 0.51214 ± 0.00007 (n = 7) and is coherent with the values obtained by conventional dynamic multi-collection thermal ionization mass spectrometric measurements. The precision of 0.5 ng Nd measurements is sufficient for the application of the $^{143}Nd/^{144}Nd$ ratio as a geochemical tracer. The precision of TEN measurements for samples smaller than 5 ng is superior to that of the conventional method.

Keywords: Total evaporation normalization; Nd isotope ratio; Thermal ionization mass spectrometry; Small sample; High precision

1. Introduction

The samarium–neodymium isotope system is widely used in geochemical and cosmochemical studies. The radioactive decay of ^{147}Sm to ^{143}Nd, with a half-life of 106 billion years (Gy), produces variations in the $^{143}Nd/^{144}Nd$ isotopic ratio. The isotopic ratio of Nd can be measured very precisely by present-day thermal ionization mass spectrometry (TIMS). There are three essential points in achieving high precision in isotope ratio measurements. The first is the use of an internal normalization technique for instrumental mass fractionation correction. Instrumental mass fractionation is the primary source of imprecision in isotope ratio measurements, and normalization is known to be the best way to correct for it when the element under consideration has two or more nonradiogenic isotopes [1]. The second point is the high ion current during measurement to keep the signal-to-noise ratio of the faraday cup high. The third point is the long data acquisition time. Typical Nd isotopic measurements by TIMS require approximately 3 h. Long data acquisition reduces random error due to ion counting statistics. The latter two points require large samples (e.g., 100–300 ng of Nd for a single measurement) to achieve good precision; decreasing the sample size decreases the ion current and shortens the data acquisition time. Thus, the precision of the measurement of a very small sample is usually poor compared to that obtained with large samples.

Many advances have been made in isotope geochemistry to improve analytical precision with very small samples. Many studies have focused on the enhancement of ionization efficiency to increase the sensitivity of elements in thermal ionization. For example, silica gel activator + phosphoric acid is known to improve the ionization efficiency of Pb [2], and Ta emitter is known to increase the sensitivity of Sr severalfold [3]. Neodymium is more efficiently ionized as the NdO^+ ion than as the Nd^+ ion. Thirlwall [4] reports that the silica gel + phosphoric acid technique promotes the ionization of NdO^+. However, NdO^+ measurement is not preferred because of the uncertainty in oxygen isotope ratio correction. To the best of our knowledge, no activator has yet been reported for Nd^+ ionization enhancement.

The total evaporation method [5], which is used primarily in nuclear industry, was developed as an instrumental mass fractionation correction technique for the measurement of U and Pu

* Corresponding author. Tel.: +81 52 789 2530; fax: +81 52 789 3033.
E-mail address: wakaki@gcl.eps.nagoya-u.ac.jp (S. Wakaki).

1387-3806/$ – see front matter © 2007 Elsevier B.V. All rights reserved.
doi:10.1016/j.ijms.2007.04.006

Table 1
Faraday cup configuration of the Sector 54-30

Collector	L2	L1	Axial	H1	H2	H3	H4
Mass	140	142	143	144	145	146	147
Isotope	^{140}Ce	^{142}Ce + ^{142}Nd	^{143}Nd	^{144}Nd + ^{144}Sm	^{145}Nd	^{146}Nd	^{147}Sm
Baseline	139.5	141.5	142.5	143.5	144.5	145.5	146.5

in which normalization cannot be applied. The principle of the total evaporation method is that no mass fractionation will occur if the entire sample is evaporated and ionized with a constant yield and the ion beams of the element are totally integrated [6]. The distinctive feature of the total evaporation method is the "burn out" of a very small amount of the sample in a very short time. There are a number of problems in applying the total evaporation method to geochemical isotope ratio measurements. First, the instrumental mass fractionation effect cannot be totally eliminated because the ionization yield of an element is easily biased during the short measurement time by slight changes in the focus potential, by changes in the ionization efficiency of the oxide ions, etc [7]. Second, the observed isotope ratios are not coherent with that measured by the conventional normalization technique. Dubois et al. [8] measured 20 ng of Nd using the total evaporation method, obtaining a mean ^{146}Nd/^{144}Nd value of 0.72333, which is considerably distinct from the value 0.7219 [9] used for normalization in geochemical studies.

In seeking a new method for the isotopic measurement of very small Nd samples, we have experimented with the idea of combining the total evaporation method with the normalization technique. With the total evaporation normalization (TEN) method presented in this paper, small amounts of the sample are measured by a total evaporation procedure. The obtained isotope ratios subsequently undergo the normalization calculation to correct for relict instrumental mass fractionation and to obtain the "geochemically accurate" isotope ratio. This paper presents the procedure and the results of Nd isotope ratio measurement of very small samples (0.1–5 ng Nd) by the TEN method. The present results are compared with those obtained by conventional dynamic multi-collector thermal ionization mass spectrometry (MC-TIMS).

2. Materials and methods

2.1. Apparatus and reagents

Neodymium isotopic reference reagent JNdi-1 [10] dissolved in diluted HNO_3 was used as a sample. Nd was measured with triple Re filaments (one ionization filament and two evaporation filaments). Small amounts (0.1, 0.5, 1 and 5 ng Nd) of the JNdi-1 were loaded on one of the evaporation filaments with 1 μl 2 M-H_3PO_4 and evaporated to dryness. Isotope ratio measurements were performed at Nagoya University on a VG Sector 54-30 equipped with seven faraday cups. Table 1 shows the configuration of the seven faraday cups.

2.2. Faraday cup efficiency calibration

Amplifier gains for the faraday cups were calibrated prior to each analytical session. In addition, efficiencies for faraday cups L1, Ax and H3 were calibrated relative to H1. Relative efficiency calibration for the other cups was not been carried out because the effect of the different efficiencies is negligible (L2 and H4) and because ^{145}Nd data is not used in ^{143}Nd/^{144}Nd ratio determination (H2). Efficiency factors for the faraday cups were measured by symmetrical peak jumping [11] using a ^{142}Nd ion beam with an intensity of 1V (= 10^{-11} A). Each calibration cycle consisted of 100 replicate measurements of the efficiency factors. Several calibration cycles were carried out each day, and the results were averaged to determine the efficiency factors for each analytical session. The results of the faraday cup efficiency calibration are shown in Table 2.

2.3. Mass spectrometry

Nd isotope ratios were measured using a total evaporation procedure. To the best of our knowledge, there is no software available for total evaporation measurements of Sector 54-30. Therefore, we controlled the filament current manually and used the software for dynamic measurement for the acquisition of "raw intensity data" during measurement.

2.3.1. Step 1: adjustment phase

First, the ionization filament was heated to a filament current of 4.6 A and stabilized for approximately 10 min. The ion beam of ^{187}Re from the ionization filament was then used to optimize the focus settings of the ion source. The intensity of the ^{187}Re ion beam was around 10–100 mV, which corresponds to an ion beam current of 10^{-13} to 10^{-12} A.

Table 2
Results of the faraday cup efficiency calibration

Session	L1	Axial	H1	H3	*n*
1	1.00014 ± 3	1.00025 ± 2	1	1.00005 ± 3	8
2	1.00038 ± 10	1.00032 ± 7	1	0.99994 ± 10	3
3	1.00034 ± 5	1.00038 ± 2	1	0.99996 ± 5	8

Errors are 2S.E.

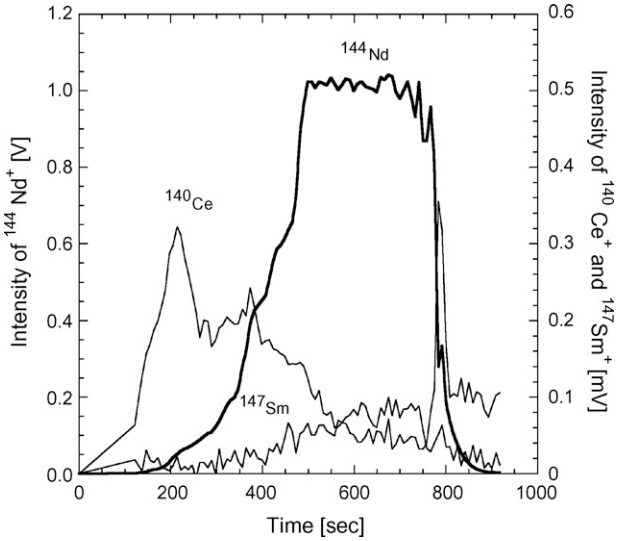

Fig. 1. Typical ion beam intensity profiles of ^{144}Nd, ^{140}Ce and ^{147}Sm during total evaporation normalization measurement plotted as a function of measurement time.

Next, evaporation filaments were slowly heated until the ion beam intensity of ^{142}Nd reached 1 mV. The evaporation filament current at this point was 1.6–1.7 A. Focus settings were optimized again using a ^{142}Nd ion beam. After the focus adjustment, the evaporation filament current was decreased to 1.0 A to avoid consumption of the sample during baseline measurement.

2.3.2. Step 2: data acquisition phase

The baseline was measured prior to the data acquisition. The integration time for the baseline was 30 s. The measured masses and corresponding collectors are shown in Table 1. Ion beam measurement was initiated immediately after baseline measurement. Ion beam integration of 8 s was repeated during measurement. As the data acquisition started, the evaporation filament current started to increase until the ion beam intensity of ^{144}Nd reached the target intensity. The target intensity of ^{144}Nd, which depended on the sample size, was 1 V, 500 mV and 100 mV, for 5, 0.5–1 and 0.1 ng of Nd, respectively. The evaporation filament current was then controlled to keep the ion beam intensity constant. As the sample had been consumed, the evaporation filament current was finally raised to 4.4 A. When the ion beam intensity of ^{144}Nd had fallen below 1 mV, data acquisition was terminated. A typical time profile of a ^{144}Nd ion beam for a 5 ng sample is shown in Fig. 1; the intensity profiles of ^{140}Ce and ^{147}Sm ion beams are also plotted in mV scale. The typical data acquisition time was 15, 11, 7 and 4.5 min for 5, 1, 0.5 ng and 0.1 ng of Nd, respectively.

2.4. Data processing

The VG software outputs "raw intensity data" from which baseline are subtracted for each integration. For every isotope measured, "raw intensity data" were summed and converted to measured electric charge Q by

$$Q[C] = \Sigma I \times t \times R \quad (1)$$

where I is the "raw intensity data" of a integration, t the integration time (8 s) and R is the resistance of the faraday cup amplifier ($\times 10^{11}$ Ω). The isobaric interferences of Ce and Sm were corrected on Q (^{142}Nd) and Q (^{144}Nd), using Q (^{140}Ce) and Q (^{147}Sm) and the reported natural isotope ratios for Ce [12] and Sm [13], respectively. Raw isotope ratios of Nd were calculated from Q (Nd) with reference to ^{144}Nd:

$$^{i}\mathrm{Nd}/^{144}\mathrm{Nd}_{\mathrm{raw}} = Q(^{i}\mathrm{Nd})/Q(^{144}\mathrm{Nd})$$
$$(i = 142, 143, 145 \text{ and } 146) \quad (2)$$

These raw isotope ratios were then corrected for instrumental mass fractionation by internal normalization using an exponential law [14] and the commonly used ratio ^{146}Nd/^{144}Nd = 0.7219 [9].

The error of the isotope ratio was estimated as follows. The number of ions counted in each faraday cup can be calculated from the measured electric charge Q:

$$N = Q \times N_{\mathrm{A}}/F \quad (3)$$

where N_{A} is the Avogadro's number and F is the Faraday constant. Applying the counting statistics, the standard deviation of N can be estimated:

$$\sigma N = \sqrt{N}/N \quad (4)$$

The error of the normalized ^{143}Nd/^{144}Nd ratio can then be calculated by propagating the errors σN of isotopes ^{143}Nd, ^{144}Nd and ^{146}Nd.

3. Results and discussion

3.1. Results

The results of the Nd isotope ratios of 0.1–5 ng JNdi-1 samples measured by the TEN method are shown in Table 3 and Fig. 2. The raw isotope ratios ^{142}Nd/^{144}Nd$_{\mathrm{raw}}$, ^{143}Nd/^{144}Nd$_{\mathrm{raw}}$, ^{145}Nd/^{144}Nd$_{\mathrm{raw}}$ and ^{146}Nd/^{144}Nd$_{\mathrm{raw}}$ in which the ratio was not normalized to ^{146}Nd/^{144}Nd = 0.7219, are also shown in Table 3. The raw ^{146}Nd/^{144}Nd ratio obtained in the present measurement is 0.7234 ± 15 (2S.D., n = 38). Excluding the three obviously fractionated data (Fig. 3), average raw ^{146}Nd/^{144}Nd ratio in this study is 0.7232 ± 6 (2S.D., n = 35). This is in agreement with the previously reported ^{146}Nd/^{144}Nd ratio of 0.72333 [8] measured by the total evaporation method. However, it differs significantly from the normalizing value 0.7219 used in geochemical studies (Fig. 3). The ^{146}Nd/^{144}Nd value of 0.7219, initially used by O'Nions et al. [9], is stated as the mean of large number of Nd analysis at that time [15]. Wasserburg et al. used ^{146}Nd/^{142}Nd = 0.636151, which is mentioned as an average of 10 Nd mass spectrometric runs in 1976, for normalization in NdO^+ measurements and reported ^{146}Nd/^{144}Nd = 0.724134 ± 0.000010 [16] in that normalization scheme. Taking an average of a large number of measurements is not sufficient to eliminate the bias due to instrumental mass fractionation, leading to the inconsistent results between different laboratories. The value 0.7219 seems to be rather inaccurate

Table 3
Results for the total evaporation normalization measurements of JNdi-1

Sample size	$Q^{143}Nd$[a] × 10^{11} (C)	Ionization efficiency (%)	$^{142}Nd/^{144}Nd_{raw}$[b]	$^{143}Nd/^{144}Nd_{raw}$[b]	$^{145}Nd/^{144}Nd_{raw}$[b]	$^{146}Nd/^{144}Nd_{raw}$[b]	$^{143}Nd/^{144}Nd$ normalized	2S.D.
(a)								
5 ng	491.3	1.26	1.1396	0.511601	0.348834	0.723244	0.512070	±8
5 ng	468.6	1.34	1.1398	0.511698	0.348834	0.723211	0.512134	±8
5 ng	441.3	1.14	1.1398	0.511679	0.348784	0.723079	0.512100	±8
5 ng	267.2	0.69	1.1395	0.511634	0.348830	0.723190	0.512095	±11
5 ng	263.1	0.68	1.1397	0.511671	0.348799	0.723113	0.512105	±11
5 ng	200.3	0.52	1.1397	0.511784	0.348674	0.722943	0.512157	±12
5 ng	191.6	0.49	1.1394	0.511578	0.348846	0.723403	0.512115	±13
5 ng	177.5	0.46	1.1397	0.511761	0.348742	0.722993	0.512151	±13
5 ng	174.2	0.45	1.1397	0.511646	0.348832	0.723132	0.512086	±13
5 ng	164.0	0.42	1.1394	0.511595	0.348794	0.723271	0.512085	±14
5 ng	154.4	0.40	1.1400	0.511778	0.348729	0.722921	0.512143	±14
1 ng	117.8	1.52	1.1395	0.511610	0.348850	0.723222	0.512082	±16
5 ng	103.5	0.27	1.1404	0.511836	0.348621	0.722763	0.512145	±17
(b)								
1 ng	82.9	1.07	1.1396	0.511631	0.348807	0.723196	0.512094	±19
1 ng	79.2	1.02	1.1398	0.511671	0.348811	0.723048	0.512081	±20
1 ng	74.3	0.96	1.1393	0.511539	0.348888	0.723367	0.512064	±20
1 ng	66.0	0.85	1.1395	0.511669	0.348837	0.723225	0.512142	±22
1 ng	65.9	0.85	1.1388	0.511542	0.348902	0.723490	0.512110	±22
0.5ng	52.9	1.36	1.1403	0.511766	0.348817	0.722928	0.512133	±24
(c)								
1 ng	47.5	0.61	1.1388	0.511629	0.348818	0.723406	0.512168	±25
0.5 ng	42.4	1.09	1.1398	0.511681	0.348828	0.722993	0.512072	±27
5 ng	33.1	0.09	1.1364	0.511010	0.349257	0.724999	0.512116	±30
0.5 ng	26.9	0.69	1.1399	0.511681	0.348913	0.723249	0.512163	±34
0.5 ng	17.5	0.45	1.1393	0.511651	0.348844	0.723330	0.512162	±42
0.5 ng	14.1	0.36	1.1356	0.511475	0.348927	0.723708	0.512121	±47
0.5 ng	12.9	0.33	1.1397	0.511742	0.348924	0.723072	0.512161	±49
(d)								
0.5 ng	6.3	0.16	1.1372	0.510986	0.349157	0.724710	0.511989	±70
0.1 ng	5.7	0.73	1.1394	0.511571	0.348904	0.723521	0.512150	±74
0.1 ng	3.9	0.51	1.1397	0.511591	0.349139	0.723608	0.512202	±89
0.1 ng	3.6	0.46	1.1394	0.511690	0.349011	0.723533	0.512274	±92
0.1 ng	3.0	0.39	1.1410	0.511708	0.348891	0.722723	0.512003	±100
0.1 ng	2.7	0.35	1.1396	0.511412	0.349322	0.724018	0.512169	±106
0.1 ng	2.3	0.29	1.1374	0.511719	0.348865	0.723483	0.512285	±117
0.5 ng	2.2	0.06	1.1320	0.510324	0.349912	0.726924	0.512113	±117
0.1 ng	1.9	0.25	1.1398	0.511593	0.348650	0.722981	0.511979	±127
0.1 ng	1.9	0.24	1.1394	0.511546	0.348758	0.723463	0.512104	±128
0.1 ng	1.8	0.23	1.1409	0.511851	0.349009	0.722746	0.512153	±132
0.1 ng	1.2	0.16	1.1388	0.511647	0.348982	0.722996	0.512039	±159
Average		0.61	1.1391	0.51158	0.34890	0.7234	0.51212 (n = 38)	
2S.D.			0.0032	0.00055	0.00045	0.0015	0.00013	
2R.S.D.			0.281	0.107	0.129	0.207	0.025 (%)	

[a] These data are divided into four sections by means of integrated ^{143}Nd (see text).
[b] Isotope ratios obtained only by the total evaporation procedure.

estimation of $^{146}Nd/^{144}Nd$ ratio. However, despite the inaccuracy discussed above, we chosed $^{146}Nd/^{144}Nd = 0.7219$ for normalization by convention.

The $^{143}Nd/^{144}Nd$ ratio obtained by the TEN method in the present study (0.51212 ± 0.00013 (2S.D.), $n = 38$) is consistent within analytical uncertainty with the ratio obtained at Nagoya University by the conventional dynamic MC-TIMS method (0.512101 ± 0.000012 (2S.D.), $n = 37$). The relative external precision of the $^{143}Nd/^{144}Nd$ ratio (0.025%, 2S.D.) is four times smaller than that of the raw $^{143}Nd/^{144}Nd$ ratio (0.107%, 2S.D.) in the same data set. The reproducibility of the measurement is improved significantly by the normalization procedure. The improvement of the reproducibility indicates that the continuation of the effect of instrumental mass fractionation on the raw data obtained by the total evaporation procedure (Fig. 3), and that the remaining instrumental mass discrimination is properly corrected by the normalization procedure.

The ionization efficiency of each sample (Table 3) can be calculated from the measured numbers of ions (Eq. (3)) and the amount of sample loaded on the filament. The ionization

Table 4
Average $^{143}Nd/^{144}Nd$ ratios measured by total evaporation normalization

$Q^{143}Nd \times 10^{11}$ (C)	Average $^{143}Nd/^{144}Nd_{raw}$	2S.D.	2R.S.D. (ppm)	Average $^{143}Nd/^{144}Nd_{normalized}$	2S.D.	2R.S.D. (ppm)	n
(a) 100–500	0.51168	0.00017	327	0.512113	0.000060	116	13
(b) 50–100	0.51164	0.00017	337	0.512104	0.000061	118	6
(c) 10–50	0.51155	0.00051	991	0.512138	0.000072	140	7
(d) 1–10	0.51147	0.00084	1642	0.512122	0.000209	407	12

efficiencies of the 38 measurements in the present study vary largely from 0.06% to 1.52%. The measured numbers of ions do not correlate exactly with the sample amount because of the different ionization efficiency between different measurements. Therefore, in the present study, we grouped the data into four sections based on the measured electric charge Q instead of classifying the data by sample size (Table 3). The four sections, which have Q (^{143}Nd) ranges of 1–10 $\times 10^{-11}$, 10–50 $\times 10^{-11}$, 50–100 $\times 10^{-11}$ and 100–500 $\times 10^{-11}$ (Table 3) correspond roughly to Nd amounts of 0.1, 0.5, 1 and 5 ng, respectively.

The average $^{143}Nd/^{144}Nd$ ratios of the four sections are shown in Table 4; they do not differ significantly between the four sections and are consistent with the values obtained by the conventional method (Fig. 4). The external errors of the four sections shown in Table 4 and Fig. 2 are about 1.3–7.5 times large as the internal errors of a single run in each section. It is likely that internal error of a run is underestimated since not all the possible sources of error (e.g., amplifier noise) are taken into account in our error estimation. Therefore, external error should be used as a representative of the uncertainty of the measurement. The external standard deviation for each section increases as the measured electric charge decreases. For sections (a)–(c), the external standard deviations (116–140 ppm) do not differ significantly despite the large difference in the measured electric charge and the sample size. The precision of these measurements shown by these external standard deviations corresponds to an uncertainty of 1.2–1.4 in epsilon scale (parts per 10^4) for the $^{143}Nd/^{144}Nd$ ratio. The precision of the measurements with Q (^{143}Nd) >10 $\times 10^{-11}$, corresponds roughly to Nd > 0.5 ng, is sufficient for the application of the $^{143}Nd/^{144}Nd$ ratio as a geochemical tracer. The external precision for section (d) (407 ppm) is three to four times larger than those of sections (a) to (c). Additionally, the internal errors of the samples in section (d) are larger than the external precisions of sections (a) to (c) (Tables 3 and 4). The precision of the 0.1 ng sample measurements is limited by the large error due to the small number of ions measured. The measured electric charge Q (^{143}Nd) = 10 $\times 10^{-11}$ is likely to be the lower limit of the range in which an external precision better than 140 ppm can be obtained. To measure the 0.1 ng sample with Q (^{143}Nd) >10 $\times 10^{-11}$, enhancement of the ionization efficiency of Nd to at least 1.3% is required.

3.2. Comparison with the conventional dynamic MC-TIMS technique

The data of the JNdi-1 measurements carried out at Nagoya University between July 2004 to May 2006 by conventional

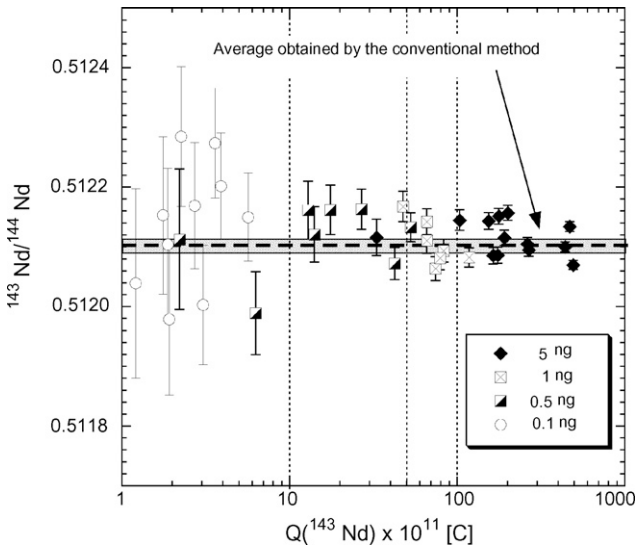

Fig. 2. Results of total evaporation normalization measurements of $^{143}Nd/^{144}Nd$ for samples of 0.1–5 ng JNdi-1. The horizontal axis shows the measured electric charge Q of ^{143}Nd in each run. The horizontal dashed line and the shaded area show the mean value and the reproducibility (0.512101 ± 0.000012 (2S.D.), n = 37) of the large sample measurements of JNdi-1 by conventional dynamic MC-TIMS at Nagoya University.

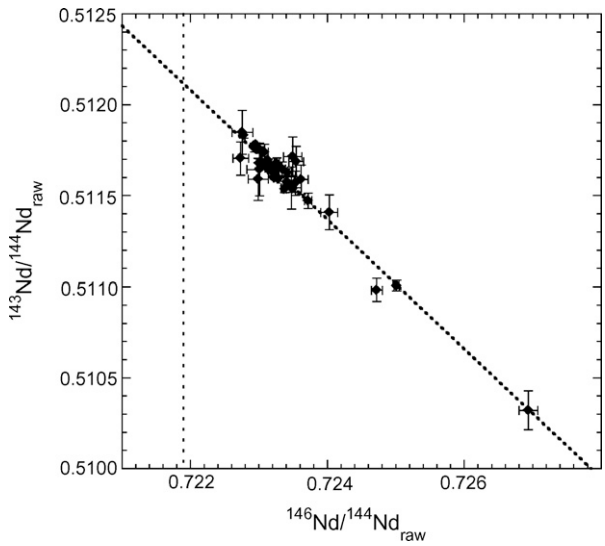

Fig. 3. Correlation plots of the raw $^{146}Nd/^{144}Nd$ and raw $^{143}Nd/^{144}Nd$ ratios of 0.1–5 ng JNdi-1 measurements, showing the remaining mass discrimination of the non-normalized isotope ratios. The diagonal dashed line indicates the theoretical mass fractionation trajectory. The vertical dashed line indicates the normalizing ratio $^{146}Nd/^{144}Nd$ = 0.7219.

Table 5
The $^{143}Nd/^{144}Nd$ ratios of JNdi-1 obtained by dynamic MC-TIMS measurement performed at Nagoya University

^{144}Nd intensity (V)	Ratios[a]	$Q^{143}Nd$[b] $\times 10^{11}$ (C)	$^{143}Nd/^{144}Nd$	2S.D.	2R.S.D. (ppm)	n
0.5	200	1587.5	0.512101	0.000011	22	37
0.25	200	793.8	0.512108	0.000020	40	4
0.1	300	471.1	0.512110	0.000041	81	8
0.05	300	235.6	0.512088	0.000054	105	10
0.01	400	62.5	0.512085	0.000169	329	10
0.005	400	31.2	0.512037	0.000666	1300	9
0.003	400	18.7	0.512450	0.001371	2675	16

[a] Number of ratios taken for a single measurement.
[b] Calculated with the average time of the measurement. Note that the ion beam consumed during the warm-up procedure is not included.

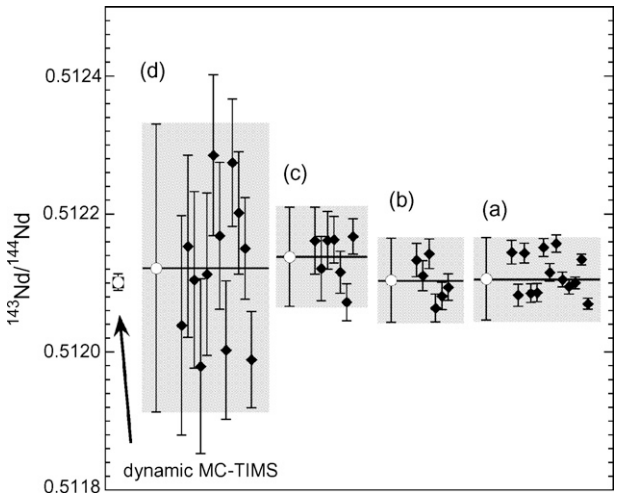

Fig. 4. Mean values (horizontal lines) and external standard deviations (shaded areas) of $^{143}Nd/^{144}Nd$ for four sections: (a) Q (^{143}Nd) = 100–500 $\times 10^{-11}$, (b) Q (^{143}Nd) = 50–100 $\times 10^{-11}$, (c) Q (^{143}Nd) = 10–50 $\times 10^{-11}$ and (d) Q (^{143}Nd) = 1–10 $\times 10^{-11}$. The mean values and 2S.D. of the dynamic MC-TIMS measurements are also plotted.

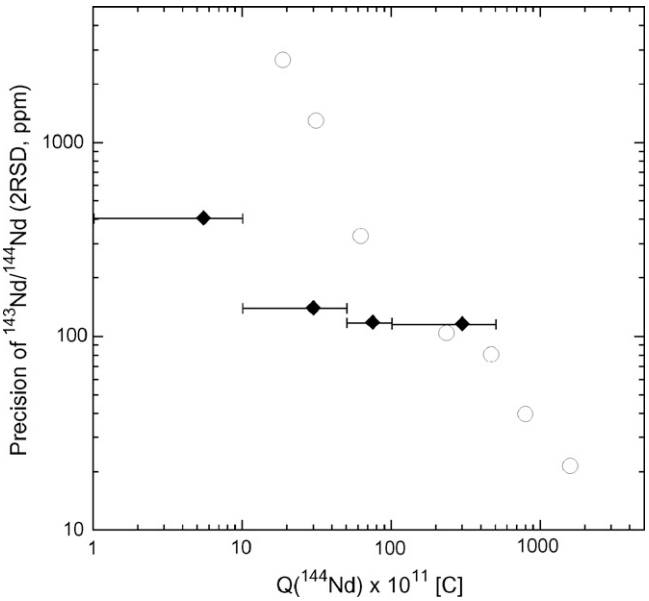

Fig. 5. Relative external standard deviations of the $^{143}Nd/^{144}Nd$ ratio by the total evaporation normalization measurements (diamonds) are compared with those of conventional dynamic MC-TIMS measurements (open circles).

dynamic MC-TIMS using Sector 54-30 were compiled for comparison (Table 5). The measured electric charge Q for the conventional measurements was estimated from the ion current and the average measurement time. Ion beam consumption during the filament warm-up procedure was not taken into consideration in the estimation of Q.

The relative external standard deviation of $^{143}Nd/^{144}Nd$ ratio measurements by dynamic MC-TIMS increased significantly as the measured electric charge decreased (Fig. 5). The increase of the uncertainty is likely to reflect a decrease in the signal-to-noise ratio of the faraday cups and an increase in the random error due to ion counting statistics. Only the measurement with a ^{144}Nd intensity over 0.05 V, which corresponds to Q (^{143}Nd) >236 $\times 10^{-11}$, gives an external precision (2S.D.) of approximately 100 ppm or better.

In contrast, the degradation of the relative external standard deviations by TEN is gradual. The precision of the TEN measurement for Q (^{143}Nd) values of less than 100 $\times 10^{-11}$ is remarkably better than that of the conventional measurement. The external precision of the TEN measurements is better than 140 ppm for Q (^{143}Nd) values as small as 10 $\times 10^{-11}$.

4. Conclusions

The neodymium isotope ratio of very small samples (0.5–5 ng) was measured precisely by the proposed TEN method. The external precision achieved for measurements with Q (^{143}Nd) = 100–500 $\times 10^{-11}$, which corresponds to 5 ng samples, was 116 ppm (2S.D.). Using our proposed method, samples as small as 0.5 ng can be measured with an external precision of 140 ppm (2S.D.). Samples of 0.1 ng Nd can be measured with such precision if the ionization efficiency of Nd is over 1.3%. The precision of the total evaporation normalization method is superior to that of the conventional method for isotope ratio measurements of samples smaller than 5 ng.

Acknowledgements

The authors would like to thank Y. Asahara for comments on the manuscript and for fruitful discussions. This work was supported in part by Research Fellowships for Young Scientists from the Japan Society for the Promotion of Science (JSPS)

and by the 21st Century COE Program G-4 “Dynamics of the Sun-Earth-Life Interactive System”.

References

[1] I.T. Platzner, Modern Isotope Ratio Mass Spectrometry, John Wiley & Sons, Chichester, 1997.
[2] A.E. Cameron, D.H. Smith, R.L. Walker, Anal. Chem. 41 (1969) 525.
[3] J.L. Birck, Chem. Geol. 56 (1986) 73.
[4] M.F. Thirlwall, Chem. Geol. 94 (1991) 13.
[5] M. Romkowski, S. Franzini, L. Koch, Proceedings of 8th Annual ESARDA Symposium, Commission European Comm, London, 1987, p. 12.
[6] E.L. Callis, R.M. Abernathey, Int. J. Mass Spectrom. Ion Processes 103 (1991) 93.
[7] S. Richter, S.A. Goldberg, Int. J. Mass Spectrom. 229 (2003) 181.
[8] J.C. Dubois, G. Retali, J. Cesario, Int. J. Mass Spectrom. Ion Processes 120 (1992) 163.
[9] R.K. O’Nions, P.J. Hamilton, N.M. Evensen, Earth Planet. Sci. Lett. 34 (1977) 13.
[10] T. Tanaka, S. Togashi, H. Kamioka, H. Amakawa, H. Kagami, T. Hamamoto, M. Yuhara, Y. Orihashi, S. Yoneda, H. Shimizu, T. Kunimaru, K. Takahashi, T. Yanagi, T. Nakano, H. Fujimaki, R. Shinjyo, Y. Asahara, M. Tanimizu, C. Dragusanu, Chem. Geol. 168 (2000) 279.
[11] K.L. Ramakumar, R. Fiedler, Int. J. Mass Spectrom. 184 (1999) 109.
[12] M. Tanimizu, T. Hayashi, T. Tanaka, J. Mass Spectrom. Soc. Jpn. 52 (2004) 177.
[13] H. Hidaka, M. Ebihara, M. Shima, Anal. Chem. 67 (1995) 1437.
[14] W.A. Russell, D.A. Papanastassiou, T.A. Tombrello, Geochim. Cosmochim. Acta 42 (1978) 1075.
[15] R.K. O’Nions, S.R. Carter, N.M. Evensen, P.J. Hamilton, Ann. Rev. Earth Planet. Sci. 7 (1979) 11.
[16] G.J. Wasserburg, S.B. Jacobsen, D.J. DePaolo, M.T. McCulloch, T. Wen, Geochim. Cosmochim. Acta 45 (1981) 2311.

参考論文

Single mineral Rb-Sr isochron dating applied to the Nohi Rhyorite and a quartz porphyry dyke, central Japan.

S. Wakaki and T. Tanaka

Geochemical Journal **39**, 21-28 (2005).

（濃飛流紋岩および石英斑岩脈に対する単一鉱物 Rb-Sr アイソクロン年代測定）

Geochemical Journal, Vol. 39, pp. 21 to 28, 2005

Single mineral Rb-Sr isochron dating applied to the Nohi Rhyolite and a quartz porphyry dyke, central Japan

SHIGEYUKI WAKAKI* and TSUYOSHI TANAKA

Department of Earth and Planetary Sciences, Nagoya University, Chikusa, Nagoya 464-8602, Japan

(*Received November 12, 2003; Accepted April 30, 2004*)

Conventional (multi-)mineral Rb-Sr isochron method requires several mineral species. Not all rock-forming minerals, however, provide the same chronological information. The closure temperature and the extent of weathering differ from mineral to mineral. On the other hand, the whole-rock isochron method has ambiguities on the initial Sr isotope equilibrium. In order to eliminate these complications and to date individual events related to each minerals in a given rock sample accurately, single mineral Rb-Sr isochron method was developed and applied to two different types of Cretaceous volcanic rocks in central Japan, Agigawa welded tuff sheet (Nohi Rhyolite Complex) and quartz porphyry (a dyke intruded into the Toki granite). Precise drilling was carried out on single phenocrystic grains of K-feldspar and chlorite (latter from quartz porphyry only) in order to obtain several aliquots from a single mineral grain. The internal difference of parent/daughter isotope ratios is expected fortuitously.

Rb-Sr multi-mineral isochron method failed to yield a precise age from the Agigawa welded tuff sheet, probably because of partial alteration. A single grain K-feldspar age of 72.0 ± 4.1 Ma obtained from the same sample is likely to date annealing of the K-feldspar grain by the intrusion of the Toki granite. In the case of the quartz porphyry dyke, three K-feldspar grains gave the ages of 79.9 ± 6.8 Ma, 71 ± 14 Ma and 82 ± 18 Ma. Combined K-feldspar age for all separates from the three grains is 77.0 ± 4.6 Ma, probably corresponding to the intrusion of the dyke. On the other hand, a combined single mineral isochron age of chlorites (five grains) in the same quartz porphyry dyke is 54.5 ± 4.6 Ma. It seems to date the chlorite formation, which corresponds to the subsequent hydrothermal alteration. Single mineral isochron method proved its effectiveness in the case when Rb-Sr isotope system was partially disturbed between different mineral phases.

Keywords: geochronology, single mineral isochron, Rb-Sr dating, Nohi rhyrolite, isochron by single mineral

INTRODUCTION

The Rb-Sr isotope system is widely used in various geochronological studies. The whole-rock isochron method, in case of the differentiated layers of an intruded rock bodies are the subjects, yields information about the whole rock mass. While the isochron method requires equilibrium of the initial Sr isotope ratios, the fact whether all samples were isotopically equilibrated at the time of the large rock mass formation is a matter of argument in many cases. On the other hand, the multi-mineral isochron method, yields information on the rock hand specimen. In this case, closure temperature (Dodson, 1973) and the extent of weathering differ from one mineral to another. Closure temperature, depends on grain size, shape, cooling rate and mineral compositions (Giletti, 1986; Giletti, 1991). So, even for the same mineral species, changes in a grain size of biotite led to differences in the history of Rb-Sr isotope system and in the apparent ages (Yanagi, 1980). Thus, for the rocks which have experienced complicated thermal history, the mineral isochron could not be obtained precisely.

In order to dispel these uncertainties, several approaches were taken previously utilizing the heterogeneity within a single mineral grain. Vance and O'Nions (1990) and Burton and O'Nions (1991) derived single grain Sm-Nd ages of garnet. Rakovan *et al*. (1997) reported single crystal Sm-Nd apatite ages. Ducea *et al*. (2003) revealed the age difference within a single garnet grain and discussed the cooling rates. However, most of the garnet ages were based on garnet-whole rock isochron.

We have developed a new micro-sampling procedure producing several aliquots from a single mineral grain with potentially different parent/daughter isotope ratios. With the new sampling procedure, Rb-Sr dating of a single mineral grain is possible. In order to obtain sufficient number of aliquots from a single mineral grain, phenocrysts from an igneous rock are advantageous. Thus the potential of the single mineral isochron dating method is shown on the example of two Cretaceous igneous rocks, from central Japan, Agigawa welded tuff sheet (Nohi Rhyolite Complex) and a quartz porphyry dyke (Toki granite pluton) (Fig. 1).

*Corresponding author (e-mail: wakaki@gcl.eps.nagoya-u.ac.jp)

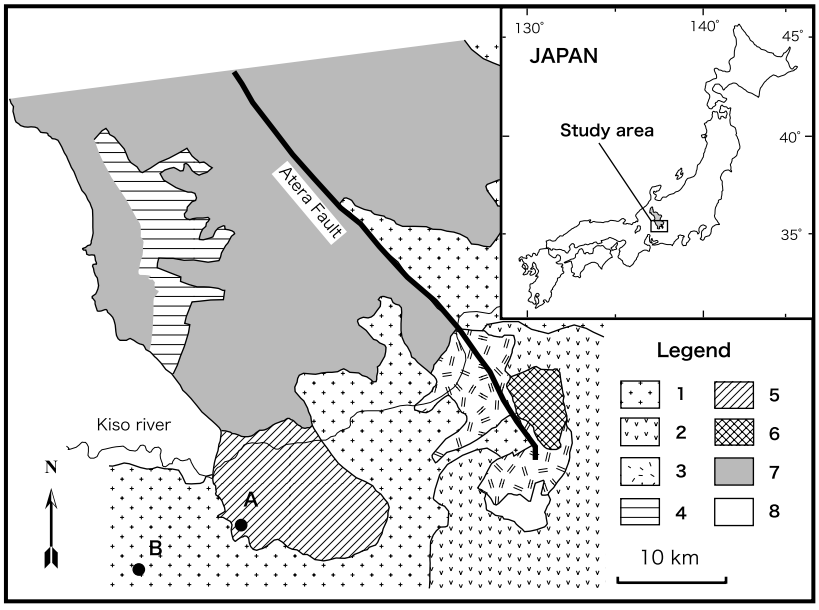

Fig. 1. Simplified geological map of the southern part of the Nohi Rhyolite complex modified after Koido (1991). Sampling locality of Agigawa welded tuff sheet and quartz porphyry dyke are shown as A and B, respectively. Abbreviations: 1-Toki granite, 2-Inagawa granodiorite, 3-Nohi Rhyolite complex (sequence III-VI), 4-Ako welded tuff sheet (sequence II Nohi Rhyolites), 5-Agigawa welded tuff sheet (sequence I Nohi Rhyolites), 6-Fujimidai welded tuff sheet (sequence I Nohi Rhyolites), 7-Other sequence I Nohi Rhyolites, 8-Mesozoic sedimentary rocks.

SAMPLES AND GEOLOGY

The Nohi Rhyolite Complex, consisting mainly of rhyolite to rhyodacite welded tuff sheets, is the largest Late Cretaceous to Paleogene volcanic pile in Central Japan (Fig. 1). It extends for about 100 km in NW-SE direction with the width of 50 km and the thickness of 3000 m (Yamada *et al*., 1992). These rhyolite piles have been classified into 6 volcanic sequences defined by layers of pyroclastic rocks (Volcanic sequences I~VI: Koido, 1991). Fission-track (Yamada *et al*., 1992), CHIME (Suzuki *et al*., 1998) and Rb-Sr whole rock ages (Okamoto *et al*., 1975; Shirahase, 1982) have been reported from every sequence, ranging from 85 Ma (sequence I) to 56 Ma (sequence VI).

Agigawa welded tuff sheet, located in the southern end of the complex, is a member of the oldest volcanic sequence I (Koido, 1991). The rock contains phenocrysts of quartz, biotite, plagioclase and K-feldspar. Average size of the K-feldspar phenocrysts, target of this study, is 5 mm 4 mm on the exposed surface of the cut slab. Matrix is fine-grained and dominated by quartz and plagioclase. Persite structures are observed in K-feldspars. Agigawa welded tuff sheet was intruded by the Inagawa granodiorite and successively by the Toki granite (Yamada, 1966).

CHIME zircon and allanite ages of the Agigawa welded tuff sheet were reported by Suzuki *et al*. (1998) as 85 ± 5 Ma and 86 ± 7 Ma, respectively. There were interpreted as the eruption age. Shirahase (1982) published Rb-Sr whole rock ages of rocks from every volcanic sequence. Fujimidai welded tuff sheet (Volcanic sequence I) showed evidently younger age of 68.8 ± 8.1 Ma compared to the stratigraphically younger Ako welded tuff sheet (Volcanic sequence II: 81.2 ± 4.0 Ma). This inconsistency strongly suggests the resetting of the Rb-Sr isotope system in the sequence I by the intrusion of the granitoids (Yamada, 1966). Since the Fujimidai and Agigawa welded tuff sheet is stratigraphically identical, contemporary disturbance of the Rb-Sr isotope system in the latter unit is to be expected.

The quartz porphyry occurs as a dike several meters wide cutting the Toki granite. Rb-Sr whole rock age of the Toki granite was reported as 72.3 ± 3.9 Ma with the initial Sr ratio of 0.7106 ± 0.0001 (Shibata and Ishihara, 1979). The quartz porphyry contains phenocrysts of quartz, K-feldspar and chlorite. Some of the K-feldspar phenocrysts have inclusions of poikilitic muscovites. Average grain sizes of phenocrysts are 10 mm 5 mm for K-feldspar, 3 mm 3 mm for the largest chlorites and 2 mm 2 mm for the medium sized chlorites on the exposed surface of the cut slab. Matrix consists of fine-grained quartz, plagioclase, K-feldspar and muscovite. The presence of chlorite and sericite suggests that the dyke had suffered a secondary hydrothermal alteration.

Table 1. Rb-Sr isotopic data for the K-feldspar separates of the Agigawa welded tuff sheet

Sample	Sample weight (mg)	Rb (ppm)	Sr (ppm)	$^{87}Rb/^{86}Sr$	$^{87}Sr/^{86}Sr$[(a)]
Kf-11					
11A-02	1.00	218	123	5.13	0.713652 ± 13
11A-03	0.89	268	156	4.98	0.713449 ± 14
11A-04	1.11	242	307	2.28	0.710827 ± 14
11A-05	1.00	216	277	2.25	0.710644 ± 14
11A-06	1.57	248	197	3.64	0.711916 ± 14
11A-07	2.10	304	116	7.56	0.716136 ± 14
11A-08	2.36	286	205	4.05	0.712384 ± 17
11A-09	1.99	245	314	2.26	0.710674 ± 16
11B-11	1.45	318	253	3.63	0.712082 ± 16
11B-12	0.94	252	273	2.67	0.711061 ± 16
11B-13	1.18	242	265	2.65	0.711012 ± 13
Kf-12					
12H-01	0.92	344	172	5.80	0.714310 ± 16

[(a)]Errors refer to last two digits and are 2 standard errors of the mean of mass spectrometry.

EXPERIMENTAL PROCEDURE

Samples were sliced into slabs 5 mm thick to expose a fresh surface. Target mineral grain was drilled from the surface of one section to obtain a mineral separates. A striker with a tungsten carbide needle was used for the drilling. The drilling was continued until sufficient amount of the separate was sampled. The drill hole was about 0.5 mm deep and about 1–1.5 mm in diameter for 1–2 mg of K-feldspar separates. Texture-related drilling is possible within this precision. Thin section for EPMA analysis was obtained from the opposite side of the slab, involving the identical mineral grain.

Investigated were two K-feldspar grains (Kf-11 and Kf-12) from the Agigawa welded tuff sheet, as well as three K-feldspar grains (Kf-01, Kf-02 and Kf-10) and five chlorite grains (Ch-06, Ch-08, Ch-09, Ch-51 and Ch-52). Chlorite grains Ch-08, Ch-09, Ch-51 and Ch-52 were analyzed as single fractions individually. Two matrix separates of the quartz porphyry dyke were also obtained with the precise drilling. Moreover, conventional mineral separation was performed for the Agigawa welded tuff sheet in order to obtain a multi-mineral isochron. Mineral fraction, which easily extracted with a hand magnet referred as magnetic fraction. Biotite was separated with isodynamic separator and K-feldspar and quartz-plagioclase fraction with heavy liquid. Fraction, which have intermediate density between K-feldspar and quartz-plagioclase fraction referred as matrix fraction.

Mineral separates were dissolved in $HClO_4$-HF mixture. Rb and Sr were separated using conventional column chemistry with cation exchange resin. Total amount of HCl used in the column chemistry of the Agigawa welded tuff sheet mineral separates differed from that of quartz porphyry mineral separates resulting in the difference of total blanks on Rb and Sr.

Sr isotope ratios were measured in dynamic mode with a VG Sector 54-30 thermal ionization mass spectrometer at Nagoya University. The mass fractionation during the measurement was corrected to $^{86}Sr/^{88}Sr = 0.1194$. Average value for the NIST SRM 987 Sr standard was 0.710237 ± 0.000017 (2). In the case of small Sr samples (Sr < 40 ng), a Ta emitter solution (Birck, 1986) was used to load Sr onto single Re filament. Other samples were loaded onto single Ta filament with 2M-H_3PO_4.

Concentrations of Rb and Sr were determined on aliquots of the sample solution with the isotope dilution mass spectrometry (ID-MS) on a thermal ionization quadrupole mass spectrometer, Finnigan MAT Thermoquad THQ. The spike was enriched with ^{87}Rb and ^{84}Sr. Total procedure blanks for the Agigawa welded tuff sheet mineral separates were 0.07 ng for Rb and 0.2 ng for Sr. Total procedure blanks for the quartz porphyry dyke mineral separates were 0.08 ng for Rb and 0.6 ng for Sr. Sr blank correction was carried out on seven chlorite separate and one K-feldspar separates of quartz porphyry dyke, in which blank/sample ratio was higher than 2%. Contributions of Rb and Sr blanks to the rest of the samples were under analytical precision and have not been corrected for. The reproducibility of $^{87}Rb/^{86}Sr$ ratios are estimated as 1.5%, from repeated analysis of the reference rock JB-1a. In the case of the chlorites in quartz porphyry, analytical error of the Rb and Sr concentrations was up to 7%, owing to the low contents of these elements. The decay constant of ^{87}Rb used in this study is $_{^{87}Rb} = 1.42 \times 10^{-11}$ y^{-1} (Steiger and Jäger, 1977). Isochron fitting and

error calculation are perfomed with ISOPLOT (Ludwig, 1991).

Results and Discussion

Sample I: Agigawa welded tuff sheet

Rb-Sr isotopic results on the Agigawa welded tuff sheet, for both mineral separates obtained by precise drilling and conventional mineral separation, are presented in Tables 1 and 2, respectively.

The spread in $^{87}Rb/^{86}Sr$ ratios of the single grain K-feldspar mineral separates (from 2.25 to 7.56) is sufficient for the isochron regression (Table 1). Rb concentration varies between 216 to 350 ppm, and Sr between 116 to 314 ppm, respectively (Table 1). No correlation was found between Rb and Sr concentrations (or the $^{87}Rb/^{86}Sr$ ratios) and the location in the mineral grain. Examined K-feldspar grain shows a perthite texture (Fig. 2). As a result of micro-sampling, each K-feldspar separates probably includes different proportion of albite lamellas leading to the wide spread in $^{87}Rb/^{86}Sr$ ratio.

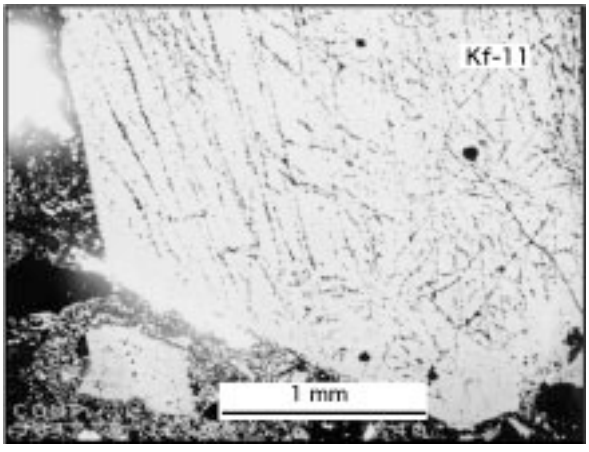

Fig. 2. Back-scattered electron image of Agigawa welded tuff K-feldspar (Kf-11) showing exsolution lamellae of albite (dark).

Isochron plot of K-feldspar separates is shown in Fig. 3. Eleven fractions from a single K-feldspar grain Kf-11, clearly give a single mineral isochron. This isochron yields an age of 72.0 ± 4.1 Ma with an initial $^{87}Sr/^{86}Sr$ ratio of 0.70834 ± 0.00022 (MSWD = 0.40). Another separate from a different K-feldspar grain Kf-12 is in harmony with this single mineral isochron.

The newly obtained Rb-Sr K-feldspar age is clearly younger than the previously reported CHIME zircon age 85±5 Ma (Suzuki *et al.*, 1998) as well as the Rb-Sr whole rock age for stratigraphically younger Ako welded tuff sheet (81.2 ± 4.0 Ma: Shirahase, 1982). Since the K-feldspar age is concordant with Rb-Sr whole rock age of 72.3 ± 3.9 Ma (Shibata and Ishihara, 1979) for the adjacent Toki granite, it is reasonable to consider it as reflecting resetting caused by the Toki granite intrusion.

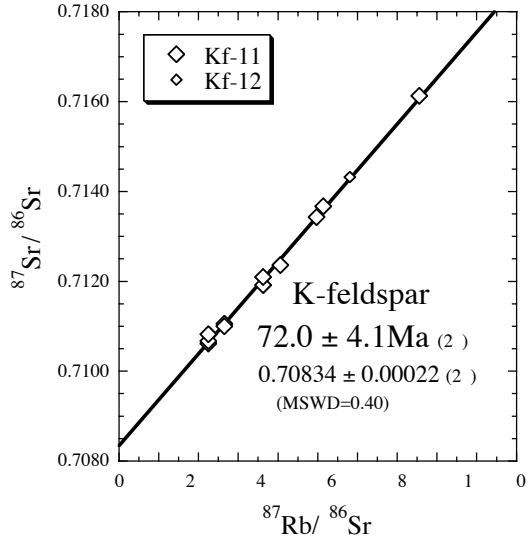

Fig. 3. Rb-Sr isochron plot showing single mineral isochron of a K-feldspar grain Kf-11 in the Agigawa welded tuff sheet. Smaller diamond is a separate from another K-feldspar grain Kf-12 excluded from the isochron regression.

Table 2. Rb-Sr isotopic data for the mineral fractions of the Agigawa welded tuff sheet

Sample	Sample weight (mg)	Rb (ppm)	Sr (ppm)	$^{87}Rb/^{86}Sr$	$^{87}Sr/^{86}Sr$[(a)]
whole rock	3.99	217	105	5.98	0.714784 ± 14
biotite	52.80	838	8.1	306	1.010133 ± 18
quartz and plagioclase	688.82	2.30	14.2	0.47	0.709015 ± 14
K-feldspar	1.84	379	144	7.59	0.716238 ± 14
matrix fraction[(b)]	228.16	177	113	4.53	0.713684 ± 16
magnetic fraction[(b)]	41.57	20.4	12.8	4.62	0.713749 ± 23

[(a)]Errors refer to last two digits and are 2 standard errors of the mean of mass spectrometry.
[(b)]See text.

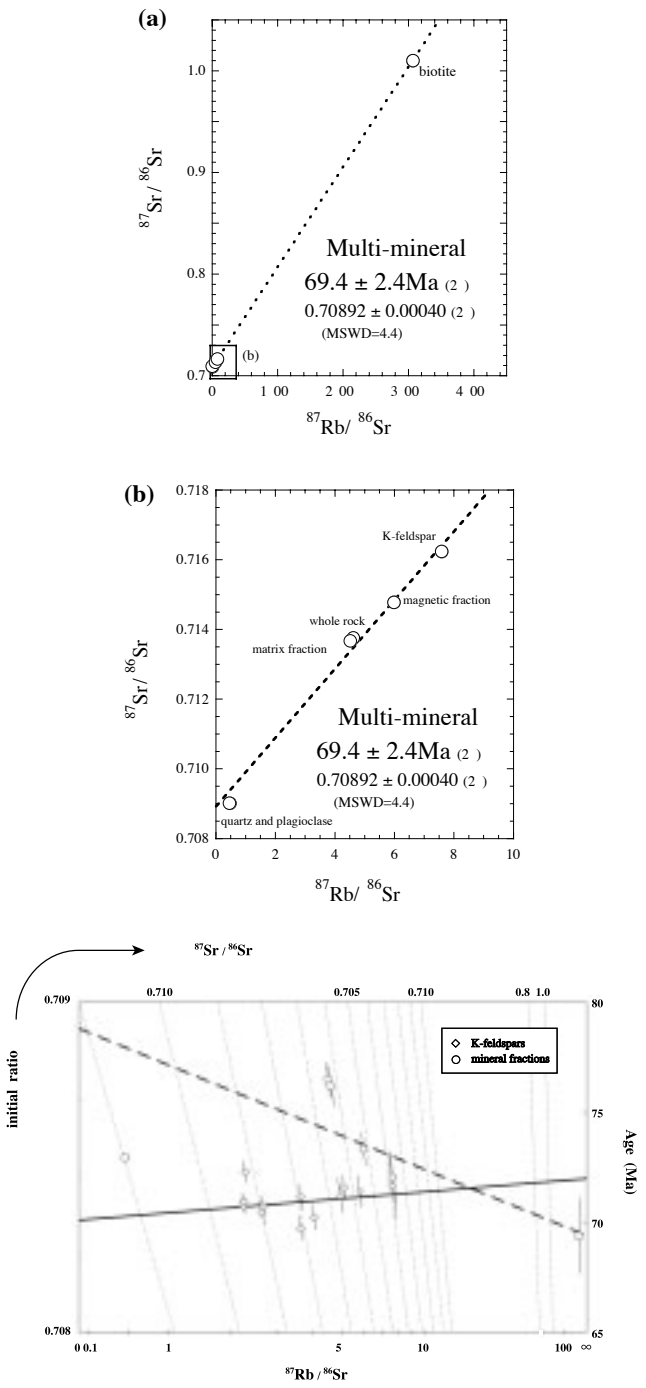

Fig. 4. (a), (b) Conventional mineral isochrons of the Agigawa welded tuff sheet. (c) Single mineral K-feldspar isochron and conventional mineral isochron of the Agigawa welded tuff sheet are comparatively shown in an alternative isochron diagram (Provost, 1990). The dotted oblique lines are constant $^{87}Sr/^{86}Sr$ lines. Constant $^{87}Rb/^{86}Sr$ is vertical to the abscissa. Ages are shown in the right-hand border. The error bars in symbols are the same as Figs. 1 and 2(a). Errors for $^{87}Sr/^{86}Sr$ are in the size of the symbols. An isochron is shown as a line connecting initial $^{87}Sr/^{86}Sr$ in the left-hand border and age in the right-hand border. In this diagram, large scatter of the data points in the conventional mineral isochron is clearly shown.

The case of the conventional multi-mineral isochron (Figs. 4(a) and (b)) is somewhat different. The range of the $^{87}Rb/^{86}Sr$ ratios is 0.47 to 306, i.e., greater than that of the single mineral K-feldspar separates by two orders of magnitude, owing to the presence of the biotite fraction. The multi-mineral isochron regression yields 69.4 ± 2.4 Ma with an initial $^{87}Sr/^{86}Sr$ ratio of 0.70892 ± 0.00040 (MSWD = 4.4). The age and the initial Sr ratio seem to be indistinguishable from those of the single mineral K-feldspar separates within the errors. The large variation in the $^{87}Rb/^{86}Sr$ ratio resulted in the apparently precise age data (small errors). However, the scatter of the data points from the isochron regression, indicated by the MSWD value 4.4, is decidedly large (Fig. 4(c)) showing that the resetting of Rb-Sr isotope system was incomplete even on a hand specimen scale. The diffusional resetting of the Rb-Sr isotope system seems to be more sensitive in the single mineral isochron of K-feldspar than in the multi-mineral isochron, owing to the small sample scales (mm size) and to the relatively low closure temperature of K-feldspar.

Sample II: Quartz porphyry dyke

The analytical results of the quartz porphyry dyke mineral separates are presented in Table 3. Seven separates of the Kf-01 were taken from three sections, and separates of the Kf-02 and Kf-10 from a single cross section, respectively. Rb concentration varies between 262 to 495 ppm, and Sr between 94 to 177 ppm (Table 3). The $^{87}Rb/^{86}Sr$ ratio of twenty-one K-feldspar separates from these three grains varies from 5.61 to 9.99.

Isochron plot of three K-feldspars in the quartz porphyry dyke are shown in Figs. 5(a), (b) and (c). Separates of Kf-01 and Kf-10 give isochron age of 79.9 ± 6.8 Ma with a initial $^{87}Sr/^{86}Sr$ ratio of 0.70945 ± 0.00070 (MSWD = 1.3) and 82 ± 18 Ma with a initial $^{87}Sr/^{86}Sr$ ratio of 0.7090 ± 0.0022 (MSWD = 0.52), respectively (Figs. 5(a) and (b)).

The separates of Kf-02 did not give a collinear regression (Fig. 5(c)), owing to the scatter of some data points suggesting a disturbance of the Rb-Sr system (Rb gain and/or Sr loss). From the observation of thin sections, considerable amount of micro-inclusions mainly consisting of muscovite are found in the vicinity of the grain boundary. Even though we have paid attention to avoid obvious inclusions during the drilling procedure, much smaller inclusions had possibly contaminated some of the mineral separates. Such a contamination would result in apparent Rb gain and/or Sr loss. Excluding the three particularly scattered points (02E-01, 02E-02 and 02E-08), the regression line yields an isochron age of 71 ± 14 Ma with an initial $^{87}Sr/^{86}Sr$ ratio of 0.7105 ± 0.0017 (MSWD = 0.84) (Fig. 5(c)). All three ages and initial $^{87}Sr/^{86}Sr$ ratios from the three K-feldspar grains are indistin-

Table 3. Rb-Sr isotopic data for the mineral separates of quartz porphyry dyke

Sample	Sample weight (mg)	Rb (ppm)	Sr (ppm)	$^{87}Rb/^{86}Sr$	$^{87}Sr/^{86}Sr$[(a)]
K-feldspar					
Kf-01					
01D-02	2.35	362	113	9.27	0.720090 ± 14
01D-03	9.67	344	177	5.61	0.715833 ± 16
01D-04	2.95	412	146	8.17	0.718595 ± 26
01E-05	12.29	359	163	6.39	0.716865 ± 14
01D-06	13.23	361	152	6.88	0.717244 ± 16
01D-07	0.69	308	121[(d)]	7.36	0.717353 ± 16
Kf-02					
02E-01	1.87	330	112	8.51	0.718619 ± 14
02E-02	2.41	320	105	8.79	0.718805 ± 17
02E-03	2.37	384	137	8.11	0.718614 ± 16
02E-04	2.91	353	105	9.77	0.720270 ± 16
02E-05	2.72	396	125	9.19	0.720015 ± 16
02E-06	2.44	370	124	8.65	0.719250 ± 14
02E-07	2.07	351	128	7.94	0.718598 ± 16
02E-08	1.95	386	127	8.78	0.718593 ± 16
Kf-10					
10T-01	1.76	262	94	8.1	0.718177 ± 16
10T-02	1.56	272	106	7.43	0.717698 ± 14
10T-03	0.57	366	118	8.99	0.719432 ± 24
10T-51	0.81	437	139	9.10	0.719638 ± 14
10T-52	0.44	495	145[(d)]	9.99	0.720079 ± 20
10T-53	0.69	330	103	9.29	0.719651 ± 17
10T-54	0.81	476	158	8.73	0.719191 ± 19
Matrix separates					
mt04E-01	2.74	147	83	5.1	0.715796 ± 16
mt05E-01	2.49	166	72	6.7	0.717147 ± 16
Chlorites					
06G-02	5.30	25	5.4[(d)]	14	0.721184 ± 110[(b)]
06G-03	4.08	53	8.2[(d)]	19	0.725471 ± 55[(b)]
08F-02	11.99	31	13.6[(d)]	6.60	0.716171 ± 17
09D-01	2.59	15.9	11.4[(d)]	4.05	0.713772 ± 16
Ch51F-01[(c)]	4.18	49	12.4	11	0.719079 ± 19
Ch52G-01[(c)]	4.34	22	8.30	7.5	0.716348 ± 36[(b)]

[(a)]Errors refer to last two digits and are 2 standard errors of the mean of mass spectrometry.
[(b)]Large errors are due to small Sr sample size.
[(c)]Procedure of column chemistry and blank values are identical with those for the Nohi Rhyorite minerals (see text).
[(d)]Blank corrected value.

guishable within the error.

Relatively large errors on ages and initial Sr ratios of Kf-02 and Kf-10 are due to the limited variation of the $^{87}Rb/^{86}Sr$ ratios. Combining the data of several grains and increasing the number of samples from a single grain are the ways to reduce the error.

In the former case, the initial Sr isotope equilibrium required for the age determination must be expanded to several grains in hand specimen scale. As shown in the three K-feldspar grains (Table 3), combination of multiple grains will possibly expand the variation of the $^{87}Rb/^{86}Sr$ ratios. Combining the data of three K-feldspar grains, with the exception of the three particularly scattered points in Kf-02, more precise isochron age of 77.0 ± 4.6 Ma with an initial $^{87}Sr/^{86}Sr$ ratio of 0.70970 ± 0.00052 (MSWD = 1.18) is obtained (Fig. 6).

The latter also improves the regression of the isochron. Excluding the samples, which have $^{87}Rb/^{86}Sr$ ratios greater or smaller than that of Kf-01 (5.7–9.3), isochron age of the three grains only changes to 79.0 ± 5.2 Ma. This may implies that analyzing more samples (from a single grain) is effective in this case. Moreover, reduction of the sampling scale has a potential to arise heterogeneity in a mineral grain more clearly.

The low Sr concentration in the chlorites requires relatively large sample amounts for the analysis. Thus, sin-

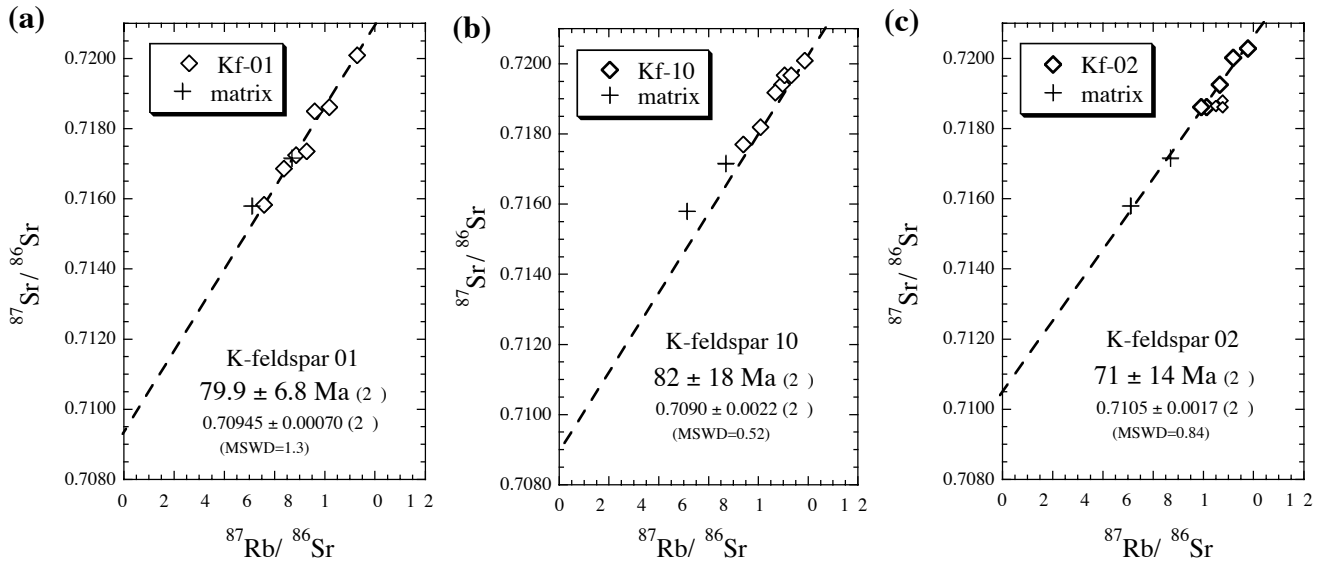

Fig. 5. Rb-Sr isochron plots for the quartz porphyry dyke. Diamonds: K-feldspar separates, Crosses: matrix separates from the same rock. In (c), three particularly scattered points 02E-01, 02E-02 and 02E-08 excluded from the isochron regression (see text) are shown by smaller symbols. The three isochrons show no difference beyond the errors.

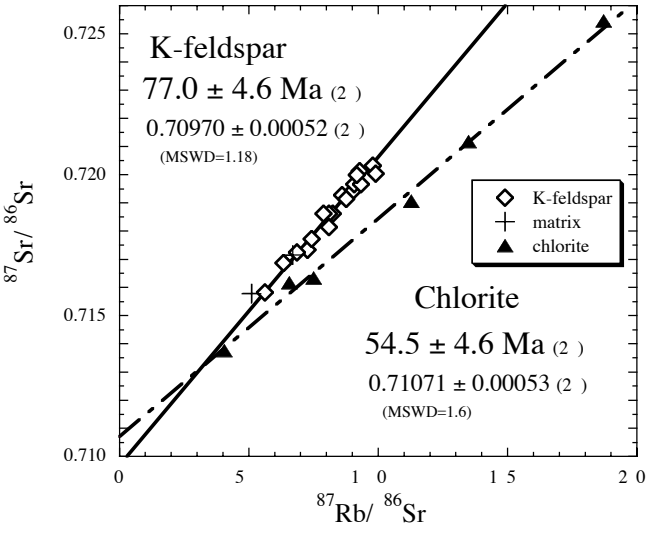

Fig. 6. Rb-Sr isochron plot of the K-feldspar and chlorite separates from the quartz porphyry dyke.

gle chlorite grain was hardly able to split into fractions and most of the chlorites were analyzed as whole grain separates. Combining the data of multiple grains is also required in such case. Combination of six fractions separated from five chlorite grains, yield an age of 54.5 ± 4.6 Ma with an initial $^{87}Sr/^{86}Sr$ ratio of 0.71071 ± 0.00053 (MSWD = 1.6) (Fig. 6). The chlorite age is younger than the K-feldspar age of the same rock specimen. The relatively large scatter of the chlorite separates around the regression line probably suggests an incomplete equilibration of the Sr isotopes among the grains. Since the chlorites are considered as a hydrothermal origin, the chlorite age 54.5 ± 4.6 Ma probably dates a hydrothermal alteration.

K-feldspar age, on the other hand, dates chronologically distinguishable event older than the alteration. The Rb-Sr age of K-feldspar, 77.0 ± 4.6 Ma, is likely to indicate the formation age of the quartz porphyry dyke. Two matrix separates obviously show affinity to the K-feldspar isochrons, and indicate the simultaneous formation of K-feldspars grains and the matrix. No significant difference is found between the K-feldspar age of the quartz porphyry dyke and the reported age of the Toki granite (72.3 ± 3.9 Ma). The obtained K-feldspar age, together with field observations, suggests successive intrusion of the Toki granite and the quartz porphyry dyke. The hydrothermal event did not seem to affect the K-feldspar itself seriously.

CONCLUSIONS

The capability of the single mineral isochron dating method was shown by two case studies. The method can date distinctive events related to each mineral within a single rock even if it has been exposed to some secondary processes. The internal difference of parent/daughter isotope ratio in a single mineral grain is sufficient for the isochron regression, even with a random sampling.

In the case of the Agigawa welded tuff sheet, the conventional Rb-Sr mineral isochron method has failed to yield a precise age, suggesting a disturbance of the Rb-Sr isotope system among different mineral phases. However, the single mineral isochron method applied to a single K-feldspar grain has successfully obtained an accurate Rb-Sr K-feldspar age of 72.0 ± 4.1 Ma, which is likely to date an annealing age of the single K-feldspar grain by the intrusion of the Toki granite.

The quartz porphyry dyke shows Rb-Sr K-feldspar age of 77.0 ± 4.6 Ma and chlorite age of 54.5 ± 4.6 Ma. These correspond to the formation and the age of hydrothermal alteration, respectively. The single mineral isochron method has clearly distinguished two chronologically different events preserved in different minerals from a single rock.

Acknowledgments—We would like to express our thanks to Prof. K. Suzuki for information on the sampling locality and for helpful discussion about CHIME dating, to S. Yogo for technical assistance in thin section, to M. Tsuboi for his help with EPMA analysis and to Prof. K. Shibata and Dr. Y. Asahara for comments on the manuscript. We are grateful to Prof. I. Kaneoka and Dr. V. Janousek for their critical and helpful reviews.

REFERENCES

Birck, J. L. (1986) Precision K-Rb-Sr isotopic analysis: Application to Rb-Sr chronology. *Chem. Geol.* **56**, 73–83.

Burton, K. W. and O'Nions, R. K. (1991) High-resolution garnet chronometry and the rates of metamorphic processes. *Earth Planet. Sci. Lett.* **107**, 649–671.

Dodson, M. H. (1973) Closure temperature in cooling geochronological and petrological systems. *Contr. Mineral. Petrral.* **40**, 259–274.

Ducea, M. N., Ganguly, J., Rosenberg, E. J., Patchett, P. J., Cheng, W. and Isachsen, C. (2003) Sm-Nd dating of spatially controlled domains of garnet single crystals: a new method of high-temperature thermochronology. *Earth Planet. Sci. Lett.* **213**, 31–42.

Giletti, B. J. (1986) Diffusion effects on oxygen isotope temperatures of slowly cooled igneous and metamorphic rocks. *Earth Planet. Sci. Lett.* **77**, 218–228.

Giletti, B. J. (1991) Rb and Sr diffusion in alkali feldspars, with implication for cooling histories of rocks. *Geochem. Cosmochem. Acta* **55**, 1331–1343.

Koido, Y. (1991) A Late Cretaceous-Paleogene cauldron cluster: the Nohi Rhyolite, central Japan. *Bull. Volcanol.* **53**, 132–146.

Ludwig, K. R. (1991) ISOPLOT: A Plotting and Regression Program for Radio-Isotope Data. U.S. Geol. Survey Open-File Report 91-445. 39 pp.

Okamoto, K., Nohda, S., Masuda, Y. and Matsumoto, T. (1975) Significance of Cs/Rb ratios in volcanic rocks as exemplified by the Nohi Rhyolite complex, central Japan. *Geochem. J.* **9**, 201–210.

Provost, A. (1990) Animproved diagram for isochron data. *Chem. Geol.* (*Isot. Geosci. Sect.*) **80**, 85–99.

Rakovan, J., McDaniel, D. K. and Reeder, R. J. (1997) Use of surface-controlled REE sectoral zoning in apatite from Llallagua, Bolivia, to determine a single-crystal Sm-Nd age. *Earth Planet. Sci. Lett.* **146**, 329–336.

Shibata, K. and Ishihara, S. (1979) Rb-Sr whole-rock and K-Ar mineral ages of granitic rocks in Japan. *Geochem. J.* **13**, 113–119.

Shirahase, T. (1982) Rubidium-strontium ages and strontium isotope ratios of the late Cretaceous felsic volcanic rocks in Central Japan (abstract). *5th Intern. Conf. Geochronol. Cosmochronol. Isotope Geol.*, 348.

Steiger, R. H. and Jäger, E. (1977) Subcommission on geochronology: convention on the use of decay constants in geo- and cosmochronology. *Earth Planet. Sci. Lett.* **36**, 359–362.

Suzuki, K., Nakazaki, M. and Adachi, M. (1998) An 85 ± 5 Ma age for the Agigawa welded tuff sheet in the oldest volcanic sequence of the Nohi Rhyolite, central Japan. *J. Earth Planet. Sci. Nagoya Univ.* **45**, 17–27.

Vance, D. and O'Nions, R. K. (1990) Isotopic chronometry of zoned garnets: growth kinetics and metamorphic histories. *Earth Planet. Sci. Lett.* **97**, 227–240.

Yamada, N. (1966) Presence of Ryoke Granite intruding into the Nohi Rhyorite and its geologic significance. *Jour. Geol. Soc. Japan* **72**, 355–358.

Yamada, N., Shibata, K., Tsukada, E., Uchiumi, S., Matsumoto, T., Takagi, H. and Akahane, H. (1992) Radiometric ages of igneous rocks around the Atera Fault, central Japan, with special reference to the age of activity of the Atera Fault. *Bull. Geol. Surv. Japan* **43**, 759–779.

Yanagi, T. (1980) Rb-Sr ages, grain sizes, and mineral inclusions of biotite in a granite. *Sci. Repts. Dept. Geol. Kyushu Univ.* **13**, 155–162.